ABSTRACT OF DISSERTATION

Peng Yuan

The Graduate School
University of Kentucky
2005

MODELING, SIMULATION AND ANALYSIS OF MULTI-BARGE FLOTILLAS IMPACTING BRIDGE PIERS

ABSTRACT OF DISSERTATION

A dissertation submitted in partial fulfillment of the requirements for the degree of Doctor of Philosophy in the College of Engineering at the University of Kentucky

By
Peng Yuan

Lexington, Kentucky

Director: Dr. Issam E. Harik, Professor of Civil Engineering

University of Kentucky

Lexington, Kentucky

2005

ABSTRACT OF DISSERTATION

MODELING, SIMULATION AND ANALYSIS OF MULTI-BARGE FLOTILLAS IMPACTING BRIDGE PIERS

The current design code governing bridge structure resistance to vessel impact loads in the U.S. is the American Association of State Highway and Transportation Officials' (AASHTO) *Guide Specification and Commentary for Vessel Collision Design of Highway Bridges*. The code stipulated method, based on Meir-Dornberg's equivalent static load method, is usually not warranted because of insufficient data on the impact load histories and wide scatter of the impact force values. The AASHTO load equations ignore certain fundamental factors that affect the determination of impact forces and bridge dynamic responses. Some examples of factors that are omitted during standard impact force analysis are: impact duration, pier geometry, barge-barge and barge-pier interactions, and structural characteristics of bridges.

The purpose of this research is to develop new methods and models for predicting barge impact forces on piers. In order to generate research information and produce more realistic flotilla impact data, extensive finite element simulations are conducted. A set of regression formulas to calculate the impact force and time duration are derived from the

simulation results. Also, a parametric study is performed systematically to reveal the dynamic features of barge-bridge collisions. A method to determine the quasi upper bound of the average impact force under any given scenarios is proposed. Based on the upper bounds of the average impact forces, an impact spectrum procedure to determine the dynamic response of piers is developed. These analytical techniques transform the complex dynamics of barge-pier impact into simple problems that can be solved through hand calculations or design charts. Furthermore, the dependency of the impact forces on barge-barge and barge-pier interactions are discussed in detail. An elastoplastic model for the analysis of multi-barge flotillas impacting on bridge piers is presented. The barge flotilla impact model generates impact force time-histories for various simulation cases in a matter of minutes. The results from the proposed model are compatible with the respective impact time-histories produced by an exhaustive finite element simulation.

All of the proposed methods and loading functions in this study are illustrated through design examples. Accordingly, the research results may help engineers to enhance bridge resistance to barge impacts and also lead to economic savings in bridge protection design.

KEYWORDS: Barge Modeling, Flotilla Impact Force, Bridge Pier, Finite Element Simulation, Dynamic Response

Peng Yuan

March 21, 2005

MODELING, SIMULATION AND ANALYSIS OF MULTI-BARGE FLOTILLAS IMPACTING BRIDGE PIERS

By

Peng Yuan

Dr. Issam E. Harik

Director of Dissertation

Dr. Kamyar Mahboub

Director of Graduate Studies

March 21, 2005

RULES FOR THE USE OF DISSERTATIONS

Unpublished dissertations submitted for the Doctor's degree and deposited in the University of Kentucky Library are as a rule open for inspections, but are to be used only with due regard to the rights of the authors. Bibliographical references may be noted, but quotations or summaries of parts may be published only with the permission of the author, and with the usual scholarly acknowledgments.

Extensive copying or publication of the dissertation in whole or in part also requires the consent of the Dean or the Graduate School of the University of Kentucky.

DISSERTATION

Peng Yuan

The Graduate School

University of Kentucky

2005

MODELING, SIMULATION AND ANALYSIS OF MULTI-BARGE FLOTILLAS IMPACTING BRIDGE PIERS

DISSERTATION

A dissertation submitted in partial fulfillment of the requirements for the degree of Doctor of Philosophy in the College of Engineering at the University of Kentucky

By
Peng Yuan

Lexington, Kentucky

Director: Dr. Issam E. Harik, Professor of Civil Engineering

University of Kentucky

Lexington, Kentucky

2005

I dedicate this dissertation to my great mother, Xia Jian-Guo.

ACKNOWLEDGEMENT

I am especially grateful to Professor Issam E. Harik, my supervisor, for his sustained support of my studies, for his mentoring, for being a great source of inspiration, for his guidance and encouragement throughout my graduate studies, for providing an excellent research environment for me.

I would like to express my deep appreciation to the members of my doctorial dissertation committee for reading the drafts of my dissertation and providing insightful technical and editorial advice, and making this thesis possible. It is a great honor to be one of their students. Thanks to Professor George E. Blandford for his professional guidance and courteous assistance and friendship. Thanks to Professor Hans Gesund for his influence on my research philosophy and many kindnesses to me. Thanks to Professor Tingwen Wu for serving on my committee and for his valuable courses I attended.

I would like to thank the complete staff of the Department of Civil Engineering for their hospitality, help and cooperation. The working environment I experienced at the Department of Civil Engineering was highly motivating and encouraging.

Finally, I would like to dedicate this work to my mother, my wife, and daughter half a world away. It is their unwavering support, love, understanding, and sacrifices that make all my accomplishment possible.

Table of Contents

List of Tables

List of Figures

List of Files

[1] Dissertation_Yuan.pdf

Chapter 1 Introduction

1.1 General Remarks and Motivation for Research

On 15 September 2001, a 4-barge tow collided into the Queen Isabella Causeway, Texas, as shown in Figure 1.1. When the bridge collapsed, eight people perished and the lives of thousands were affected [1]. On 26 May 2002, a barge hit an I-40 highway bridge over the Arkansas River in Oklahoma, as shown in Figure 1.2 [2], collapsing the bridge and sending 15 vehicles into the water with people trapped inside [3]. These are only two examples of many accidents caused by barge collisions recently in the United States. Although the I-40 bridge had pier protection cells inside the navigation channel, the accident occurred outside the navigation channel. According to Peters [2], most bridges over navigable water can be struck either within or outside the regular navigation channel by barge tows and individual commercial vessels, thus increasing the complexity of appropriate bridge protection.

Figure 1.1 Four loaded barges crashed into the Queen Isabella Causeway, Texas, September 15, 2001, destroying a 73.2m (240 ft) section of the bridge

Figure 1.2 Barge-Impacted I-40 Bridge, Oklahoma, May 26, 2002

Approximately 26,000 dry cargo barges, 3,000 tanker barges, and 1,200 towboats operate today on 40234 km (25000 miles) inland waterways in the United States [4]. A barge tow (flotilla), consisting of one tug and fifteen attached barges, has a 22500-ton or 800000-bushel capacity, the equivalent of 225 train cars or 870 semi trucks. The 365.85 m (1200 ft) long barge tow carries as much coal or grain as 4.4 km (2.75 miles) of trains or 34.5 miles of semi-trucks. Inland barge flotillas, as shown in Figure 1.3, carry approximately 15 percent of the nation's freight [5].

Figure 1.3 Inland barge tows

During the period from 1965 to 2002, an average of one catastrophic accident per year involving vessel-bridge collisions was recorded worldwide. More than half of these occurred in the United States. Between 1992 and 2001, there were 2692 incidents nationwide where barges collided with bridges, resulting in human deaths, injuries and economic losses, according to a U.S. Coast Guard and American Waterways Operators report [6]. In general, any bridge accessible by a barge tow is probably hit at least once during its service life [7]. Furthermore, barge tow traffic is expected to increase by 150 percent in the next 50 years [5]. Protecting highway bridges from barge impact has become crucial due to the heavy barge traffic passing underneath. The high frequency and serious consequence of barge-bridge collisions necessitate the development of regulations and requirements for structural design and bridge evaluation.

Although vessel-bridge collisions have drawn considerable attention in the past twenty years, no significant research has been committed toward multi-barge flotilla collisions. Despite high frequencies of barge-bridge collisions, vessel impact studies published in technical literature focus more intensely on ship collisions. However, while similar in many respects, barge vessels and ship vessels differ in some fundamental ways. Significant differences exist between the speeds, shapes, and structures of oceanic ship vessels and barge vessels using inland waterways [8].

At present, design specifications used both domestically and internationally employ empirical equations as a part of codified procedures for computing equivalent static design loads due to vessel impacts. The current design code for bridge structures to resist vessel impact loads in the United States is the American Association of State Highway and Transportation Officials' (AASHTO) *Guide Specification and Commentary*

for Vessel Collision Design of Highway Bridges [9]. The empirical crush model provided by the AASHTO guide specifications represents the state-of-the art on the subject of barge-bridge collisions. However, as indicated by the authors of the AASHTO guide specifications, the use of dynamic analysis for the design of barge-bridge collision protection is usually not warranted because of insufficient data on the impact load histories and wide scatter of the impact force values. Moreover, the vessel impact design requirements have not been updated for more than a decade, although there have been damaging vessel collisions throughout this period. To date, neither the collision mechanics nor the prediction of impact forces between a barge and a bridge has been well established. Many potential fallibilities of the code stipulated method remain uninvestigated. Most practical questions revolve around the accuracy of the AASHTO formulas, local impact damage, multi-barge flotilla impact forces, and dynamic barge-bridge interaction. Recent studies at the Kentucky Transportation Center have shown that AASHTO considerably overestimates the multi-barge flotilla impact forces [10]. Consequently, the cost of bridge substructures is unnecessarily high. On one bridge alone, savings could reach millions of dollars if accurate prediction of flotilla forces can be made.

Vessel impact is one of the most significant design considerations for bridges that span navigable waterways. The quantification of barge impact loads, used for bridge protection design, is the motivation of this research.

1.2 Objectives of the Dissertation

The overall goal of this research is to study the characteristics of barge-pier collisions and develop new methods for predicting the impact loads on bridge piers. Specifically, the major tasks to be undertaken in order to achieve these objectives are:

1) Conduct a literature survey;
2) Develop finite element (FE) models for typical barges;
3) Perform dynamic simulations of single barges impacting bridge piers;
4) Perform dynamic simulations of multi-barge flotillas impacting bridge piers;
5) Propose new methods for calculating the barge impact loads on bridge piers;
6) Demonstrate the developed methods for the analysis of bridges.

1.3 Organization of the Dissertation

The remainder of the dissertation is composed as follows.

Chapter 2 presents a state of the art overview of the vessel-bridge collision topic and a concise sketch of prior developments on the subject.

In Chapter 3, descriptions of the methods used to model a hopper barge and bridge piers are given. The chapter ends with a discussion of the assumptions and limitations associated with modeling barges.

Chapter 4 consists of a systematic parametric study of single-barges impacting rigid piers. The fundamental characteristics of barge-pier collisions are discussed in this chapter. Also, a set of impact load functions are developed.

Chapter 5 discusses the influence of pier flexibility on barge-pier impact dynamics. Criteria are provided with regard to how rigidity affects the impact forces and dynamic response of bridge piers and when such effects become significant.

Chapter 6 describes simulations of collisions between multi-barge flotillas and bridge piers. Time-histories of the impact forces caused by multi-barge flotillas are generated, and the dynamic interaction between barges in a flotilla is discussed. This chapter concludes with the presentation of a set of load functions for a column of barges.

Chapter 7 is comprised of a numerical and analytical study concerning the determination of single barge impact loads on bridges and the dynamic response of piers subjected to barge impact. The upper bounds of the barge impact forces and a conservative method to predict barge impact loads, which accounts for pier shape and size, are provided.

In Chapter 8, a formulation for dynamic system identification is addressed for a barge impacting a pier. This system identification determines a simple mathematical representation that delineates the crushing behavior of a barge under a collision-loading environment. A single-degree-of-freedom (SDOF) system to represent a crushed barge is developed in the displacement domain using the elastoplastic-collapse concept.

Chapter 9 describes an elastoplastic spring-mass model to analyze multi-barge flotillas impacting bridge piers. It accounts for the essential factors pertaining to such impacts, such as pier geometry, stiffness, and dynamic interaction.

Chapter 10 demonstrates the application of the barge impact forces developed previously through case studies. In addition, this chapter evaluates the dynamic response of two real bridges subjected to barge impact loads.

Chapter 11, the final chapter, contains conclusions of this dissertation and recommendations for future study.

1.4 Units of the Dissertation

Even though the barge weight, dimension, and velocity are traditionally in English units, and AAHSTO uses the English system of units, this dissertation will primarily use the International System of Units (SI). However, both English and SI values will be provided when an English unit is necessary. Table 1.1 shows some quantities typically used in this study in both English and SI units as well as conversion factors for transforming from English units to SI units.

Table 1.1 System of units

Quantity	English system	SI system	Conversion factor
Length	foot (ft) inch (in)	meter (m) meter (m)	0.3048 0.0254
Force	kip (1000 lb)	Newton (N)	4448.2
Mass	slug (lb-sec^2/ft) short ton	kilogram (kg) metric ton (t)	14.59 0.9072
Velocity	ft/sec knot	m/s m/s	0.3048 0.51
Energy	kip-ft	Joule (J)	1355.82

Chapter 2 Review of Literature

A state of the art overview of barge-bridge collisions as well as the most important historical research that has been conducted in this area is discussed in this chapter. It should be noted that the focus of this study is to develop improved methods for predicting barge impact forces on piers, more specifically; this study focuses on the contact forces generated during collision accidents. Therefore, the following discussion does not include topics such as inland waterway traffic control and vessel-bridge collision probabilities although these topics are very important.

2.1 The AASHTO Guide Specifications

The most influential study regarding barge impact loads was performed by Meir-Dornberg [11], and the equations prescribed in the AASHTO Guide Specifications [9] were created by him. The experimental and theoretical studies performed by Meir-Dornberg concerned the relationship between the crushing force and barge deformation when a barge collides with a lock entrance structure or a bridge pier. Meir-Dornberg's study included the dynamic loading of three 1:4.5 barge bottom models by means of a pendulum hammer, the static loading of a 1:6 bottom model, and numerical computations. No significant difference was found between the static and dynamic forces measured during his study. The resulting relationship of the barge deformation and impacting loading is shown in Figure 2.1 [8]. Using the test data, Meir-Dornberg developed the following equations for the barge deformation and impact force during a collision event.

$$a_B = 3.1(\sqrt{1 + 0.13E_B} - 1) \tag{2.1}$$

$$P_B = \begin{cases} 60a_B & a_B < 0.1 \\ 6+1.6a_B & a_B \geq 0.1 \end{cases} \tag{2.2}$$

where the barge deformation a_B is in meters; the initial kinetic energy of the barge E_B is in $\text{MN} \cdot \text{m}$; and the impact force P_B is in MN.

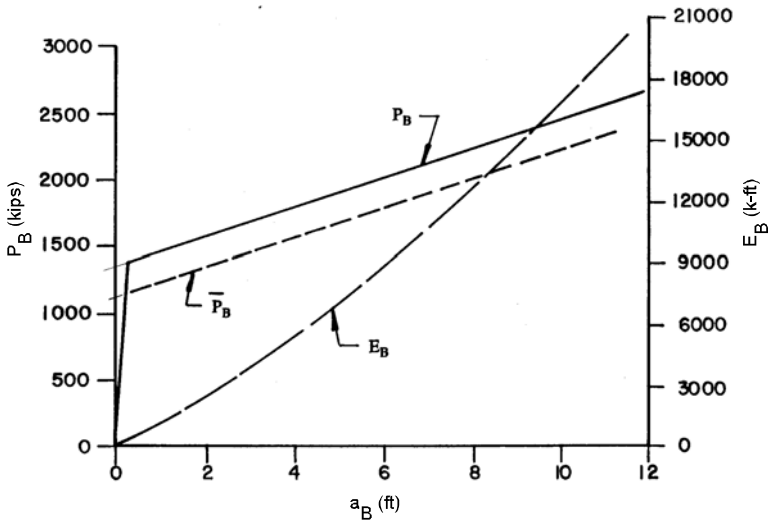

Figure 2.1 Barge impact force P_B and deformation energy E_B versus damage length a_B for European barges Types II and IIa

The AASHTO Guide Specifications adopted the above equations to calculate barge impact loads imparted to a given bridge pier. By introducing two modification factors and converting the above equations into the U.S. customary units, AASHTO gives the following equations to calculate barge damage depth a_B and barge impact force P_B.

$$a_B = 10.2\left(\sqrt{1+\frac{C_H \cdot E_B}{5672}}-1\right)\cdot\frac{1}{R_B} \tag{2.3}$$

$$P_B = \begin{cases} 4112a_B R_B, & a_B < 0.34 \\ (1349+110a_B)R_B, & a_B \geq 0.34 \end{cases} \tag{2.4}$$

$$R_B = \frac{1}{35}B \tag{2.5}$$

where E_B is in k-ft; a_B is in ft; the barge width B is in ft; P_B is in kips; R_B is a modification factor to correct the impact force for a barge whose width is not 10.7 m (35 ft); C_H is a hydrodynamic mass coefficient to account for the surrounding water upon the moving vessel.

The above equations provide a simple load determination method for barge-bridge collisions, but several important physical aspects of general barge impacts are not addressed. First, the impact forces from Meir-Dornberg's method are entirely independent of impacted bridge piers. As pointed out by Pedersen et al. [12], in case of collision against a pier with limited width or with a step or recess, the collision load may need to be adjusted. Consolazio et al. [13] also found that both pier shape and pier size affect the impact forces. Second, as an equivalent static method, the Meir-Dornberg method does not address dynamic effects of the impact loadings. Under some circumstances, barge-pier collisions can induce a significant dynamic response of bridges. The term "equivalent static load" is not properly defined because of ignorance of bridge structural characteristics. A dynamic analysis should always be carried out for important structures, in particular, if transient or permanent deflections or movements of the bridge structure and/or the fender or buffer system are introduced in the analysis [8]. Thirdly, the pendulum hammer used in Meir-Dornberg's study acted as a rigid object as compared to the barge model, because his focus was on the reaction forces of the barge models and not the reaction forces of real bridge piers. However, when a vessel collides with a deformable bridge pier, the impact may not be analogous to rigid body impact. Energy dissipation arises due to the crushing of the impacting vessel, but also due to the deformation of the impacted bridge pier and displacement of the soil surrounding the

bridge foundation [13]. Eqs. (2.1) and (2.2) may predict much larger impact forces than those actually produced in barge collisions because of the assumption that barge-pier impact was idealized as rigid-body impact. Finally, barges nearly always travel in a group (flotilla), not separately. Therefore, it is more significant to quantify the impact force for a multi-barge flotilla than for a single barge. According to Whitney and Harik [10], Eq. (2.4) overestimates the impact forces for multi-barge flotillas. The flexibility of the cable connectivity between barges in a flotilla is incompatible with the assumption that the entire flotilla acts as a single rigid body on the pier. A portion of the impact energy will be dissipated through the interaction among barges in the flotilla.

Although the Meir-Dornberg method has a number of shortcomings, it forms an excellent beginning for the comprehension and quantification of barge impact forces.

2.2 The Whitney and Harik Model

Whitney and Harik [10] developed a statistical procedure to analyze and transform barge traffic data into a component of bridge design in conjunction with the current AASHTO specifications. Aside from identifying typical flotilla velocities and elevations on the Ohio River, U.S.A., they derived barge-loading functions for bridge piers. This is the only published work that can be found to include an analysis of multi-barge flotillas impacting bridges. Three basic assumptions are made in Whitney and Harik's collision models:

1) The dynamic stiffness of a barge during collision is described by Meir-Dornberg's impact force and crushing distance relationship, i.e., Eqs. (2.1) and (2.2).

2) The barge can be divided into a non-linear crushing zone and an elastic compression zone. In addition, the mass of the crushed parts can be discarded.

3) Only one column in a multi-barge flotilla produces the impact forces.

The first assumption is critical to the described models because it simplifies the procedures for determining the interaction between the barge and the pier during impact. Consequently, this underlying assumption rests the models on Meir-Dornberg's formulas.

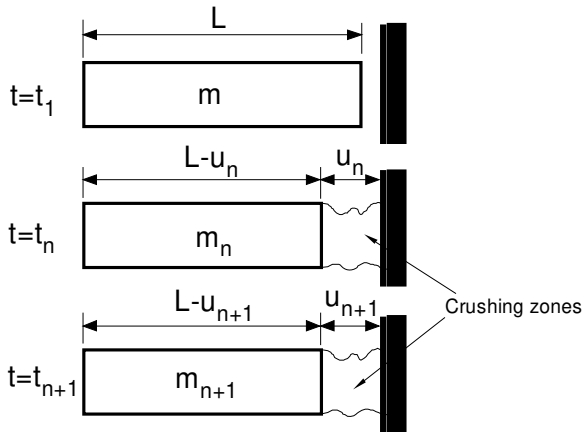

Figure 2.2 Simplified barge impact model by Whitney and Harik

Based on the three assumptions, the momentum of a barge, as shown in Figure 2.2, at times t_n and t_{n+1} can be expressed as, respectively

$$I_n = m_n \dot{x}_n , \tag{2.6}$$

$$I_{n+1} = (m_n - dm)(\dot{x} - d\dot{x}) \tag{2.7}$$

where m_n is the uncrushed mass at time t_n, dm is the crushed mass at time t_{n+1}, and $\dot{x}$ is the velocity of the uncrushed mass at time t_n.

Thus, by Newton's second law the barge impact force F can be written as

$$F = \frac{dI}{dt} \tag{2.8}$$

or

$$F = m_n \frac{d\dot{x}}{dt} + \dot{x}\frac{dm}{dt} - d\dot{x}\frac{dm}{dt}. \tag{2.9}$$

The last term of Eq. (2.9) is small compared to other terms and thus it can be neglected, the equation becomes

$$F = m_n \frac{d\dot{x}}{dt} + \dot{x}\frac{dm}{dt} \tag{2.10}$$

Letting $\frac{dm}{dt} = d(\bar{m}L)/dt = \bar{m}\dot{x}$ and $m_n \frac{d\dot{x}}{dt} = f(x)$ in Eq. (2.10), yields

$$F = f(x) + \bar{m}\dot{x}^2 \tag{2.11}$$

where $\bar{m}$ is the mass per unit length of the barge, *f(x)* is the barge impact force function given by Eq. (2.2), and *x* is the barge crushing distance.

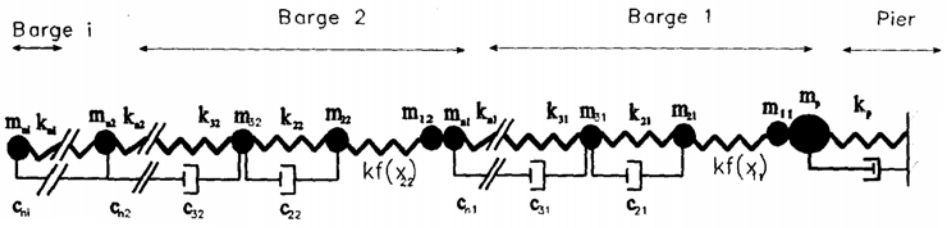

Figure 2.3 Multi-Barge non-linear lumped mass impact model by Whitney and Harik

From Eq. (2.11), the impact forces for single barges can be obtained by integration with respect to time. Figure 2.3 shows the multi-barge impact model where each barge is discretized into several elements. The first element of each barge is the crushing element, which is assigned the ASSHTO bilinear load deformation relationship, Eq. (2.4). The axial barge element stiffness of other elements was calculated from the

cross-sectional properties of a Jumbo Hopper (see section 3.1 for details). A computer program was written to evaluate the multi-barge impact loads.

For a single barge, this model agrees with the AASHTO method very well. In fact, this result can be expected from Eq. (2.11) since the second term of Eq. (2.11) is much smaller than the first one for single barges. Regarding multi-barge flotilla impacts, the impact forces generated by the Whitney and Harik model are significantly smaller than those generated by the AASHTO method. One apparent factor leading to this result is the interaction between barges in a flotilla.

Based on past barge-bridge collision investigations, AASHTO suggests that only the barges in a single column of a multi-column flotilla be used to generate impact loading [10]. This recommendation is based on the assumption that the barges in adjacent columns are lashed together with ropes that will break during a collision event. However, whether the connections between barge columns are broken or not during a collision event, the initial impact forces are produced by the intact flotilla, not by a single column of barges. Most probably, there is not enough time for the barges to separate before a large part of the kinetic impact energy is dissipated. Therefore, it may be inappropriate to make such an assumption.

Whitney and Harik concluded that it is conservative to neglect the effect that the pier flexibility has on the impact forces. For a majority of cases, the determination of barge impact forces may be regarded as independent of pier stiffness.

2.3 Finite Element Simulations

The finite element (FE) method, in general, is based on the representation of a given structure as an assembly of small elements that produces an approximate numerical

solution. In more and more engineering problems today, it is sufficient to obtain approximate numerical solutions to problems rather than exact closed form solutions.

Currently, computers contain sufficient computational power to allow the use of a new generation of crash analysis codes to simulate the nonlinear, dynamic response of bridge structures subjected to barge impacts. Popular FE simulation codes, such as LS-DYNA [14] and MSC.Dytran [15], use an explicit solver that eliminates the need to repetitively decompose large global stiffness matrices as is required by implicit codes. The explicit finite element solution is advanced in time, without solving any equations, by the central difference method:

$$\dot{u}^{n+1/2} = \dot{u}^{n-1/2} + \Delta t \cdot M^{-1}(F^{external} - \int B^T \sigma dV) \tag{2.12}$$

$$\dot{u}^{n+1} = \dot{u}^{n-1} + \Delta t \cdot \dot{u}^{n+1/2} \tag{2.13}$$

where $F^{external}$ is the vector of applied forces associated with the boundary conditions and body forces, M is the diagonal mass matrix, B is the discrete gradient operator, and σ is the stress.

The explicit methodology is more suitable for the analysis of a collision accident involving high non-linearity, contact, friction, and rupture. The required calculation efforts are fewer than those associated with the commonly used implicit methods. Furthermore, the convergence of calculations is much easier to realize when the explicit method is used. The program LS-DYNA has been developed for analyzing the dynamic response of 3-D structures, and it possesses many features that are critical for efficient and accurate analysis of crashes [16]. LS-DYNA is based on the public domain DYNA-3D code and is already widely used by industry.

The complexity of flotilla-bridge collisions inhibits the creation of reliable conclusions from small-scale model tests alone. In addition, performing full-scale field-testing is not economically feasible. Since the 1990s, FE simulations, which accurately evaluate traditionally non-testable scenarios, have succeeded as a supplement to experimental testing in crashworthiness studies. FE models can be built as accurately as the respective prototypes in the real world. Nonlinear and large displacement FE simulation can produce detailed information that is difficult to observe or measure in physical experiments. In addition, various collision scenarios, even non-testable scenarios, may be simulated.

Recently, Consolazio et al. [13, 17, 18] used FE simulation techniques to analyze a single barge impacting a bridge pier. In their studies, FE models of a JH and an existing bridge pier were developed using the program LS-DYNA. The main concluding remarks of their published works are as follows:

1) The loads predicted by the FE simulations for light to moderate impact conditions (barge deformation < 64 mm) are larger than those predicted by AASHTO. Moreover, such loads act on the pier for a short time with significant oscillation.

2) Under severe impact conditions (barge deformation > 64mm), the equivalent static load from the AASHTO method appears reasonable since the time-varying load histories produced from impact simulations are sustained for a relatively longer duration. However, the load values predicted by AASHTO are considerably larger than those from FE simulations.

3) The pier stiffness as well as the pier geometry has significant influence on the barge impact force.

4) The FE simulations correlated with results from AASHTO design codes in barge deformations.

The determination of the impact loads is intricate. It is not viable to solve this problem analytically with an exact mathematical model. Presently, FE simulations are almost the only effective means for calculating the barge impact forces as the only feasible alternative to highly simplified formulas.

Nevertheless, FE simulations are prohibitively expensive regarding the time required for both model generation and computation, and currently, are only employed in research purposes. Challenges involved in analyzing such a non-linear problem include structural contact, criteria for the material's rupture, and crack propagation. For the time being, only a limited group of researchers have acquired the ability to solve such a problem.

2.4 Barge Impact Experiments

In April 2004, Florida engineers conducted the first-ever planned collision between a barge and a real bridge, the St. George Island Causeway Bridge spanning the bay from the small town of East Point to St. George's Island (see Figure 2.4 [6,53]). The bridge and the barge were fitted with more than 150 sensors to provide a microsecond-by-microsecond record of the impact load as the barge hit the bridge at increasingly faster speeds. The objectives of the experiment included:

1) To obtain experimental data about the magnitudes of loads generated, the durations of time over which these loads persist during an impact, and the manner in which the loads are shared by multiple piers, which are connected via the bridge deck (the roadway on top of the piers).

2) To measure soil response during the impact test.

(a)

(b)

(c)

Figure 2.4 Barge impact experiment: (a) St. George's Island Causeway Bridge, FL; (b) a bridge pier with impact blocks and data acquisition system installed; (c) push boat and test barge with payload

According to Consolazio et al. [53], full-scale barge impact tests conducted on the stiffer pier generated a maximum impact load of approximately 4.7 MN (1056 kips) and significant levels of damage to the test barge. Comparisons between measured barge deformation (as shown in Figure 2.5) and corresponding deformations predicted using the AASHTO barge impact design provisions indicated favorable agreement. However, most of the dynamic impact loads measured during testing of this pier fell well below the equivalent static load values predicted by the AASHTO provisions. Dynamic loads measured during barge impact tests were all bounded at the upper end by an apparent plastic load capacity of the barge bow. This plastic load capacity was considerably less that that predicted by the AASHTO provisions. Tests conducted on the more flexible pier were performed at lower impact speeds, used a smaller barge weight, and produced deformations of the barge bow that remained in the elastic range. Comparisons between peak measured dynamic loads and corresponding AASHTO equivalent static loads demonstrated that the peak dynamic loads typically exceeded the AASHTO loads.

However, when a time averaging process was used to compute effective dynamic impact forces, the experimental data and AASHTO provisions were found to be in much better agreement.

Figure 2.5 Barge bow deformation [53]

While this physical test program yielded valuable impact data, interpretations of the results have limitations due to the pre-testing conditions of the piers impacted by the barges. The bridge employed an old design that is no longer used by highway departments and its piers were different from the piers of most current bridges. Such slender piers are not common in modern practice.

In December 1999, the Army Corps of Engineers Waterways Experiment Station conducted an experiment of similar proportions by purposely crashing a barge flotilla into a lock chamber wall in order to measure barge impact loads [19]. The tests utilized a fifteen-barge tow impacting the lock wall structures at low velocities and various oblique angles. The intent of the testing program was to determine the impact loading history imparted to the lock wall and the interaction between the individual barges in the tow during the impact. An empirical correlation was derived that determines the maximum impact force (normal to the wall) as a function of the linear momentum normal to the wall:

$$F_{\max} = 0.435mv\sin\theta \tag{2.14}$$

where θ is the flotilla impacting angle with the lock wall shown in Figure 2.6, the flotilla mass m is in k-sec^2/ft, the flotilla velocity v is in ft/sec, and the maximum force $F_{\max}$ is in kips.

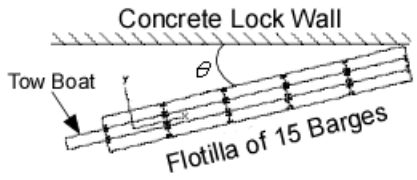

Figure 2.6 Plan view of the barge-wall collision tests conducted by the Army Corps of Engineers Waterways Experiment Station

It should be noted that the majority of the impacts made by barge flotillas, while transiting such locks, do not result in damage to the barge structure or to the chamber walls. This type of impact may be described as glancing with large oblique angles, as opposed to a direct impact. Because both the barge corner and wall approximately act as rigid objects under low impact speed conditions, the tests are not appropriate for correlation to direct impacts with bridge piers. Furthermore, the shallow impact angles used in the concrete lock wall tests are not representative of most barge collisions with concrete bridge piers in which maximum loads are typically generated at nearly head-on impact angles, not shallow oblique angles [53].

2.5 Ship Collision Force on Piers

An extensive amount of literature regarding ship-ship or ship-platform collisions exist in contrast to the scant amount of literature that may be complied from various barge-pier collision studies. Most literature that pertains to vessel collision only examines the nature of forces involved in a head-on bow collision accident. Various

analysis models have been derived for estimation of the global loads involved in head-on bow collision events. The models have been based on:

1) Investigation of ship/ship collision cases;

2) Dynamic collision model tests;

3) Quasi-static bow indentation model tests;

4) Direct calculation of crushing resistance;

5) Or, some combination of the above.

2.6 The Minorsky Method

Based on an investigation of twenty-six ship-ship collisions, Minorsky [20] proposed an empirical correlation between the resistance to penetration and the energy absorbed in ship-ship collision. This approach has been widely used, and subsequently modified by many researchers. The linear correlation between the damaged volume of ship structure and absorbed energy (see Figure 2.7 [22]) was found to be:

$$E_T = 47.2R_T + 32.7 \tag{2.15}$$

where E_T is the energy absorbed in collision (MJ), and R_T is the damaged volume of ship structural steel (m^3).

Reardon and Sprung [21] revalidated Minorsky's function Eq. (2.15) by separately investigating sixteen collisions. They proposed the following relationship:

$$E_T = \left(47.1 \pm 8.8\right) R_T + 28.4 \tag{2.16}$$

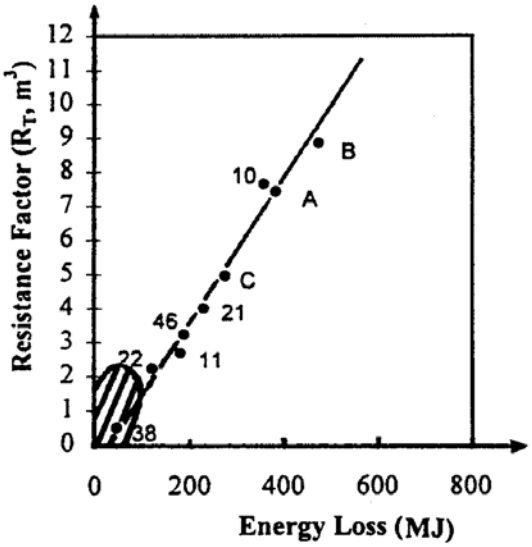

Figure 2.7 Minorsky's original correlation

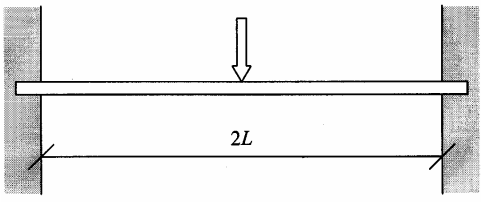

Figure 2.8 Jones' beam model

As Reardon and Sprung stated, the intercept term of Minorsky's correlation, 28.4 MJ in Eq. (2.16), is the energy expended from puncturing and tearing through the shell of the struck ship. However, this single value approach is not accurate in low-energy collisions without rupture of the side shell. To correct the limitation under low energy conditions, a simplified procedure introduced by Jones [22] extended the Minorsky correlation by modeling the ship's side shell as a clamped beam subjected to a concentrated load at mid span as shown in Figure 2.8. It is also assumed that membrane

behavior occurs from the beginning of deformation. This results in the following equations for predicting the low energy structural response.

$$E_T = 0.030288\sigma_y \left(\frac{w}{L}\right)^2 R_T \tag{2.17}$$

$$R_T = \frac{2LB_e t}{144} \tag{2.18}$$

where σ_y is the yielding strength of the beam (psi); w is the deformation of the beam at mid-span (in); L is one half of unsupported span of the beam (in); B_e is the breadth of beam (in); and t is the thickness of the beam (in).

Based on a study of McDermott, Van Mater [23] extended Jones' analysis to off-center striking (ref. Figure 2.9) and derived the maximum deflection of the side panel based on a rupture strain of 0.1.

$$E_{(a,b)} = E_{CL}\frac{a}{b} \tag{2.19}$$

$$w_m = 0.453a \tag{2.20}$$

where $E_{(a,b)}$ is the absorbed energy when the striking point is away from the mid-span (ton-knots^2); E_{CL} is the absorbed energy derived by Jones (ton-knots^2); a is the distance from the striking point to the close support (in); b is the distance from the striking point to the far support (in); w_m is the maximum deformation of the side panel (in).

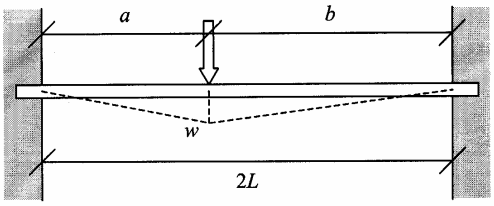

Figure 2.9 Van Mater's beam model

Based on measurements of lengthening of the broken side shell to the membrane stress, Woisin [24] also proposed an alternative to the intercept term in Minorsky's correlation. He suggested that the energy absorbed by the ruptured shell could be calculated as follows:

$$b = 0.5\sum Ht_s^2 \tag{2.21}$$

where b is the absorbed energy by ruptured side shell and longitudinal bulkheads (MJ); H is the height of broken or heavily deformed side shell and bulkheads (m); t_s is the thickness of the side shell and longitudinal bulkheads (cm).

With these improvements, the Minorsky equation has been transformed into an effective method that estimates the extent of vessel average collision forces in a more general way. There are several similar analysis schemes available today. Each of them decomposes the struck structure into simple substructures or components, such as plates, stiffeners, web frames, and panels, etc. The energy absorbed in each substructure during the collision process is calculated separately. The total absorbed energy up to rupture of the ship boundary is obtained through the summation of the absorbed energy for all components. Nearly all of the calculation procedures developed by previous and current research in collision analysis determine the lost kinetic energy in an uncoupled solution of the external problem, and then calculate the deformation energy of the colliding structures with increasing penetration. Finally, such procedures find the maximum penetration by matching the deformation energy to the lost kinetic energy. This approach relies on the solution of final velocities of struck and striking ships by an external model. This general uncoupled solution procedure requires significant simplifying assumptions, and/or restrictions of the degrees of freedom of the system. This form of analysis may

also be performed in a time domain with a fully coupled time-stepping solution similar to Hutchison [25] and Crake [26]. Starting with the initial external condition, impact forces are calculated based on internal structural mechanics at each time step and applied to the struck and striking ships in the external model until the residual energy equals to zero.

2.7 The Woisin Method

The AASHTO formulas [9] for ship collision forces on bridges were primarily developed from research conducted by Woisin [27] to generate collision data to protect reactors of nuclear powered ships with other impacting ships. Accurate collision force-time histories were not obtained in Woisin's tests due to electronic measuring difficulties in the instrumentation and induced vibrations in the model test setup. Woisin computed the average impact force $\overline{P}$ by dividing the kinetic energy loss by the bow damage depth. Based on theoretical and model test results, Woisin proposed the following relationship between the mean impact force averaged over time, $\overline{P}(t)$, and the mean impact force averaged over the damage depth, $\overline{P}(a)$:

$$\overline{P}(t) = 1.25\overline{P}(a) \tag{2.22}$$

The major factors that affected the mean impact force arranged in order of decreasing importance by Woisin [8] were:

1) Ship size (DWT);
2) Type of ship;
3) Shape and structure of the bow;
4) Amount of ballast water in the bow;

5) Impact speed.

Based on Woisin's data, AASHTO proposed the following relationship for bulk carriers traveling at the speed of 8 to 16 knots.

$$P_s = 220(DWT)^{1/2}\left(\frac{V}{27}\right) \tag{2.23}$$

where DWT is the dead weight tonnage in metric tones, V is the vessel velocity in ft per second, and P_s is the mean impact force in kips.

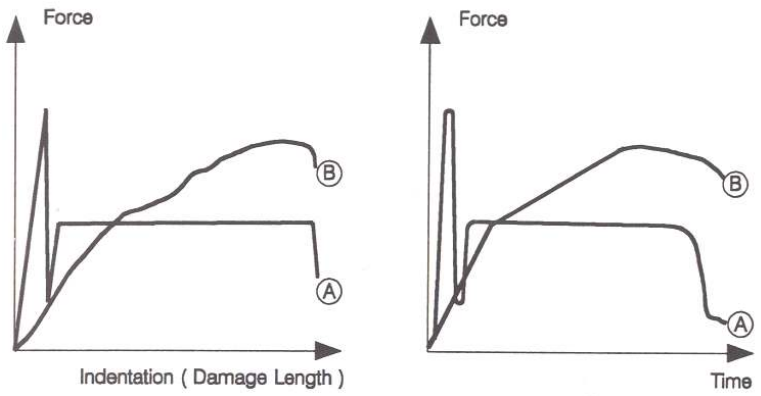

Figure 2.10 Schematic representations of impact force dynamics

Two representative force-indentation relationship curves are shown in Figure 2.10, together with the corresponding force history curves [8]. The curves, designated A, indicate drastic fluctuation of the force during a very short (0.1 - 0.2 sec) initial phase of the collision event followed by a more or less constant force during the remaining time [28, 29]. The time duration of the maximum force, which has been estimated at twice the constant average force during the remaining collision time, is normally considered to be too brief to leave any influence on a relatively robust bridge structure. The curves of Figure 2.10, designated B, indicate a gradually increasing impact force during the course of the collision accident. This may not involve a higher average force, but the longer

duration of the relatively high force level during the last phase of the collision event implies that the maximum force rather than the average force should be used in design when based on static force analysis [30].

2.8 Other Empirical Formulas

Based on the Minorsky relationship, Woisin et al. [28] developed an equation giving the average collision force for bridge design:

$$P_0 = \frac{V^{2/3} L^2}{1100} \tag{2.24}$$

where P_0 is the average collision impact load in MN, V is the vessel velocity in m/sec, and L is the vessel's length (m).

Eq. (2.24) was used in the design of the Bahrain Causeway and Faroe Bridges [8]. Based on studies performed for the newest Sunshine Skyway Bridge in Tampa Bay, Florida, Knott and Bonyun [31] proposed an alternative equation for a vessel traveling in a partially loaded, ballasted, or light (empty) condition as:

$$P_{\max} = 0.88(DWT)^{1/2} \left(\frac{V}{8}\right)^{2/3} \left(\frac{D_{act}}{D_{\max}}\right)^{1/3} \tag{2.25}$$

where V is the vessel velocity at the time of impact (m/sec); D_{act} is the vessel displacement at the time of impact (tonnes); D_{max} is the maximum (fully loaded) displacement of the vessel (tonnes).

The Norwegian Public Roads Administration [32] prescribes the following vessel collision loads for bridges and ferry ramps in the public road system:

$$P = 0.5\left(DWT\right)^{1/2} \tag{2.26}$$

where P is the static equivalent collision force (MN).

Detailed and comprehensive vessel collision load regulations have been established for the Great Belt Bridge project in Denmark in 1991 based on the work of Frandsen et al. [33] and Pedersen et al. [30]. These researches purported that the maximum impact forces rather than the average forces should be used as the design force for design on the basis of equivalent static analysis. Maximum impact forces have been established for vessels between 500 DWT and 30,000 DWT. Different impact speeds and loading conditions were considered. The following equations are the result of this work.

$$P_{bow} = 210\left[EL^2 + \left(5.0 - L\right) L^{2.6} \right]^{1/2} \text{ for } E \geq L^{2.6} \tag{2.27}$$

$$P_{bow} = 210\left(5.0EL\right)^{1/2} \text{ for } E < L^{2.6} \tag{2.28}$$

$$L = \frac{L_{pp}}{275} \tag{2.29}$$

$$E = \frac{E_{imp}}{1425} \tag{2.30}$$

where P_{bow} is the maximum bow collision load (MN), L_{pp} is the length of the vessel (m), and E_{imp} is the kinetic energy of the vessel (MNm).

Eqs. (2.27) through (2.30) account for the effect of strain rate, impact speed, vessel loading conditions, and vessel size. For large vessels, the formulas produce higher impact forces for static design than others.

2.9 Summary

A review of the current state of practice in vessel-bridge collision engineering shows that no significant research has been committed toward multi-barge flotilla collision issues. No current research has been found to focus on collisions between

multi-barge flotillas and bridges. Despite high frequencies of barge-bridge collisions, vessel impact studies published in technical literature focus more intensively on ship collisions. Despite many research efforts, as tabulated in Table 2.1, important questions remain to be answered about barge-bridge collisions.

Table 2.1. General information regarding past studies on vessel impact forces

Research Approaches					Researchers	Date	Objectives
Experiment	Statistic method	Numerical simulation	Analytical method	Bridge Project			
	√				Minorsky [20]	1959	Ship-ship collisions
		√			Amdahl [45]	1983	Ship-platform impacts
√					Woisin [27]	1976	Ship impact forces on bridges
√					Nagasawa [46]	1981	Small vessel - rigid pier collisions
				√	Knott et al. [31]	1983	Ship impact forces on bridges
√		√			Meir-Dornberg [11]	1983	Barge impact forces on bridges
				√	Modjeski &Masters [42]	1985	Vessel impact forces on bridges
√					Ohnishi [47]	1983	Tanker-pier collisions
		√		√	Frandsen et al.[33]	1991	Ship-bridge impacts
√			√		Pedersen et al. [12]	1993	Ship impact forces
			√		Jagnannathan and Gray [48]	1995	Barge impact forces on walls
	√		√		Whitney and Harik [10]	1996	Barge flotilla impact forces on bridges
			√		Zhang [50]	1999	Vessel collision mechanics
√		√			Consolazio et al. [17]	2003	Barge impact forces on bridges
	√				Ghosn and Moss [49]	2003	Extreme loads on bridges
√					Patev et al. [19]	2003	Barge flotilla impact forces on walls

Chapter 3 Development of Barge Finite Element Model

This chapter discusses the development of a finite element (FE) model for a typical barge using the ANSYS Parametric Design Language (APDL) [34]. The APDL is particularly useful when FE simulations are to be performed for a wide range of scenarios.

A correct and efficient FE model is critical to the generation of accurate, yet manageable, FE simulations. In this context, "correct" means that the model accurately represents the objects in the real world; "efficient" signifies that the application of the model takes less computation time. Since a typical time step for a collision simulation would be on the order of a microsecond, the simulation of a multi-barge flotilla colliding with a pier for several seconds could require several days of computer computation time. Therefore, a high-quality FE model is necessary for the feasible conduction of barge-pier collision studies.

3.1 Barge Characteristics

Barges of numerous designs are used for every imaginable purpose on inland waterways (rivers). However, the Jumbo Hopper (JH) barge is the most common and standardized type of barge. Also, the JH is one of the most versatile types of barges, as it can transport a wide range of products. Barges are often towed or pushed in groups of two or more. Therefore, the dimensions and drafts of barges tend to be standard in order to provide hydrodynamic efficiency. In addition, standard barge dimensions facilitate the establishment of tow configurations through locks on river systems [9].

JHs, as shown in Figure 3.1, are the baseline of the AASHTO Guide Specifications, and are the most widely used barges in the U.S. The configurations of a

typical JH are shown in Figure 3.2 [9]. In this study, the development of a JH model is based on the respective blueprints and specifications provided by a barge manufacturer. The difference in dimensions between the AASHTO's barge configurations and barge blueprints are presented in Table 3.1. For the purpose of this study, these minute differences for such a huge structure are not significant and are therefore ignored.

Figure 3.1 Jumbo hopper barges

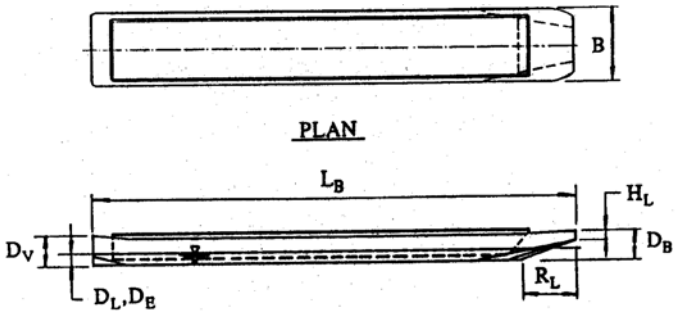

L_B	=	length (feet)	195
B_M	=	width (feet)	35
D_V	=	depth of vessel (feet)	12
D_E	=	empty [light] draft (feet)	1.7
D_L	=	loaded draft (feet)	8.7
D_B	=	depth of bow (feet)	13
R_L	=	bow rake length	20
H_L	=	head log height (feet)	2-3
C_C	=	cargo capacity (tons)	1700
W_E	=	empth displacement (tons)	200
W_L	=	loaded displacement (tons)	1900

Figure 3.2 Characteristics of Jumbo Hoppers

Table 3.1. JH dimensions for present barge model

Symbols	ASSHTO (1991)	This study[a]
L_B = length (ft)	195	200
B_M = width (ft)	35	35
R_L = bow rake length (ft)	20	27.5
D_B = depth of bow (ft)	13	14
D_V = depth of vessel (ft)	12	12
H_L = head log height (ft)	2 - 3	2.25

Note: a. Barge plans from Jeffboat LLC, U.S.A.

Jumbo Hoppers are constructed of mild steel in the form of standard structural shapes. The skin of a JH, supported by trusses, is made from steel plates with thicknesses 0.01 m to 0.013 m (3/8 to ½ in). The raked bow and stern are comprised of fourteen and thirteen trusses at equal spaces, respectively. Each side box has 24 trusses at a space of 2.06 m (81 in). To support the bottom there are 73 floor beams spaced at 0.69 m (2.25 ft) in the translational direction. The beams and trusses of a JH are depicted in Figure 3.3.

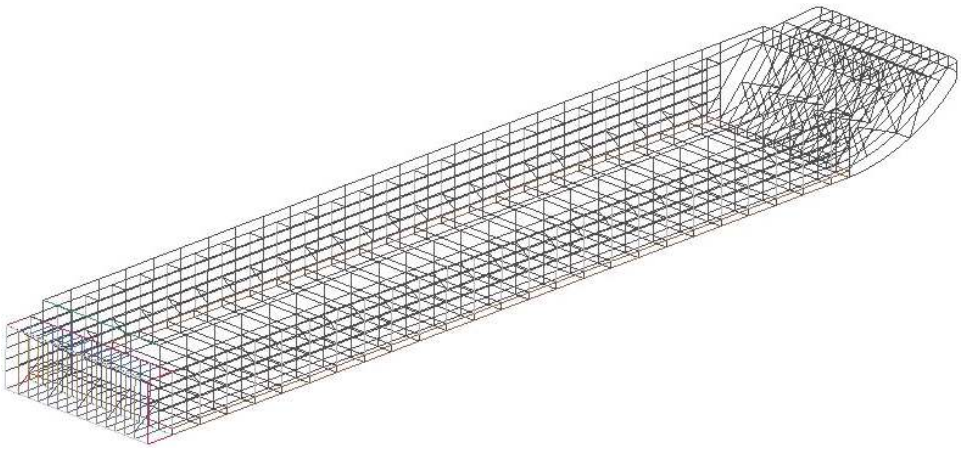

Figure 3.3 Beams and trusses in a Jumbo Hopper

3.2 Barge Divisions

The FE model of such a complicated object as a JH contains elements that vary greatly in sizes. Also, elements are assigned different properties depending on their

respective location within the structure. For modeling purposes, the barge is divided into three zones as shown in Figure 3.4: the bow portion (Zone-1), the hopper portion (Zone-2), and the stern portion (Zone-3). The zones are distinguished by using different elements and material models due to the differences in behavior exhibited during impact.

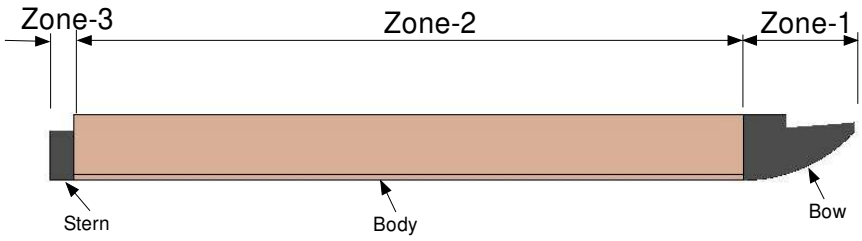

Figure 3.4 Three zones of the barge model

A head-on collision occurs when a barge-bow contacts a bridge pier directly. In such an event, a major part of the kinetic impact energy is dissipated through the deformation of Zone-1. Therefore, it is essential to model Zone-1 accurately so its structural characteristics can be correctly represented in the numerical model. In the model, fine elements and nonlinear inelastic material models are assigned to the structural elements of Zone-1.

The length of a barge is approximately 5.7 times as long as its width and the total mass of the barge is distributed longitudinally. Because plastic deformation is not expected in the barge body during impact, Zone-2 is modeled in a relatively coarse fashion using larger elements and elastic material models.

Zone-3 of the model may experience contact with other barges in a multi-barge flotilla. Although no large deformation in this region, the contact structural members are modeled using smaller elements than those of Zone-2.

3.3 Element Types and Material Models

The FE model of a JH consists of 4-node shell, 3-node beam, 2-node discrete spring, 2-node damper, 1-node point mass, 8-node brick, and 2-node link elements. In addition, four types of material models are used in the numerical model. The material and element descriptions included in the model are summarized in Table 3.2.

Table 3.2. Summary of element types and material models used for the JH model

Object	Part	Element type (LS-DYNA)	Material model
Zone 1	Plate	Shell (SHELL163)	Piecewise linear plasticity
	Truss	Beam (BEAM161)	Piecewise linear plasticity
Zone-2 & Zone-3	Plate	Shell (SHELL163)	Isotropic elastic
	Truss	Beam (BEAM161)	Isotropic elastic
Target	Pier	Solid (SOLID164)	Rigid
	Mass	Point (MASS166)	Isotropic elastic
	Spring	Spring (COMBI165)	Linear elastic
	Damper	Spring (COMBI165)	Linear viscosity
Lashing cable	Cable	Cable (LINK167)	Isotropic elastic

The FE model of a JH and a pier is shown in Fig 3.4, which is composed of 18,930 shell, 9,000 beam, and 2,300 brick elements. During a preliminary modeling attempt, the barge was modeled using only shell elements. The consequential CPU time expense was too large to continue using a model composed entirely of shell elements. It was determined that all of the internal truss members and stiffeners should be modeled using beam elements with angle or channel sections. The shell elements are only used for the skin of the barge model.

Special care was taken to accurately represent the true stiffness of the barge. During the construction process for an actual hopper barge, the various steel plates that make up the head log, the bow, and the internal angles are placed together and welded to each other in an overlapping fashion. This overlapping effectively increases the stiffness

of the barge bow [13]. To achieve this effect in the finite element model, structural members are attached to each other using a type of constraint in LS-DYNA, *CONSTRAINED_SPOTWELD. This constraint can represent a spot weld between two or more nodes. The spot weld constraint is a modification of the nodal rigid body that incorporates the ability to impose a failure criterion to the weld. Due to the small element size used in Zone-1, the use of spot weld constraints at each node would provide a good representation of a continuous weld. The welds used in the model are specified to have infinite strength, thus no failure criterion was specified.

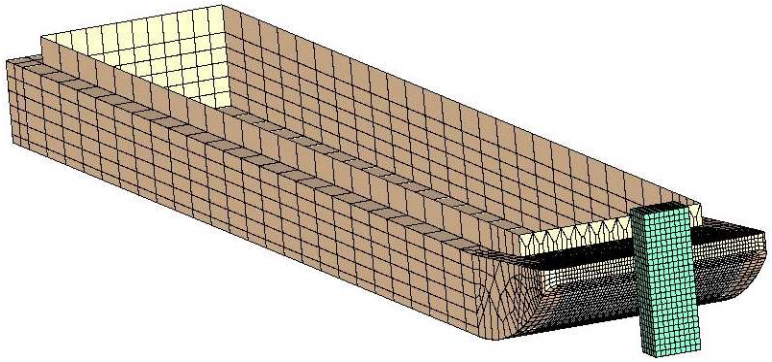

Figure 3.5 FE model of a Jumbo Hopper

3.3.1 Properties of Elements

3.3.1.1 The Belytschko-Lin-Tsay Shell Element (SHELL163)

The Belytschko-Lin-Tsay shell [16, 34] is a 4-node element with both bending and membrane capabilities. Both in-plane and normal-to-plane loads are permitted. The formulation of this element is based on the Mindlin-Reissner assumption, so transverse shear is included. The formulation has a higher computational efficiency than the Hughes-Liu shell element which requires five times more mathematical operations to be computed relative to the Belytschko-Lin-Tsay element. On the other hand, the Belytschko-Lin-Tsay shell element does not support warpage of the element since it is

based on a perfectly flat geometry. To correct this problem in the present model, the Belytschko-Lin-Tsay shell element with Belytschko-Wong-Chiang improvement is adopted, but the efficiency is decreased by 25%. The geometry of the element is shown in Figure 3.6.

The element has six degrees of freedom at each node: translations in the nodal *x*, y, and *z* directions and rotations about the nodal x, y, and z-axes. The nodes of the element are numbered counterclockwise, and the normal of the element is obtained by:

$$\hat{e}_3 = \frac{s_3}{\|s_3\|} \tag{3.1}$$

$$s_3 = r_{31} \times r_{42} \tag{3.2}$$

$$\|s_3\| = \sqrt{s_{31}^2 + s_{32}^2 + s_{33}^2} \tag{3.3}$$

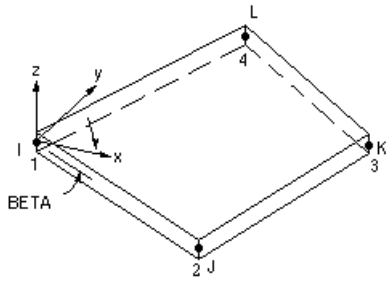

Figure 3.6 SHELL163 geometry

It is important to know the orientation of a given element in problems involving contact, because the contact algorithms require the input of the orientation of such elements. Two integration points are sufficient for linear elastic materials, while more points are required for nonlinear materials.

3.3.1.2 The Hughes-Liu Beam Element (BEAM161)

The Hughes-Liu beam [16] is computationally efficient and robust. A cross-section integration rule can be specified to model arbitrary cross-sections. Since the

beam generates a constant moment along its length, the corresponding element meshes require reasonable fineness to achieve adequate accuracy. The geometry of the element is shown in Figure 3.7.

The element with 12 degrees of freedom is defined by nodes I and J in the global coordinate system. The node K is used only to initially orient the element.

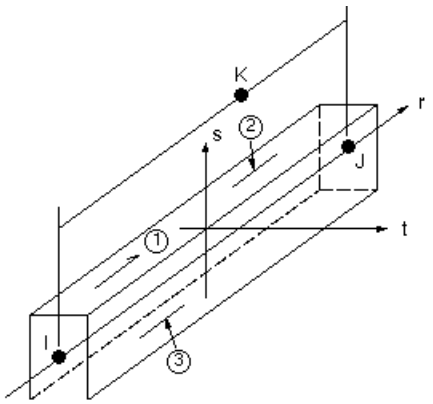

Figure 3.7 BEAM161 geometry

3.3.1.3 The SOLID164 Element

The SOLID164 element [16] is an 8-node brick element with three translational degrees of freedom at each node. By default, this element uses reduced (one point) integration and viscous hourglass control for faster element formulation. One-point integration is advantageous because it requires a small amount of computer calculation time, while simultaneously it adds robustness to the model in cases of large deformations. A fully integrated solid formulation is also available, but it is approximately four times more costly in terms of CPU computation time.

Wedge, pyramid, and tetrahedral shaped SOLID164 elements are simply degenerate bricks (i.e. some of the nodes are repeated). These shapes are often too stiff

in bending and create various difficulties in certain cases. Therefore, these degenerate shapes are avoided. The geometry of the element is shown in Figure 3.8.

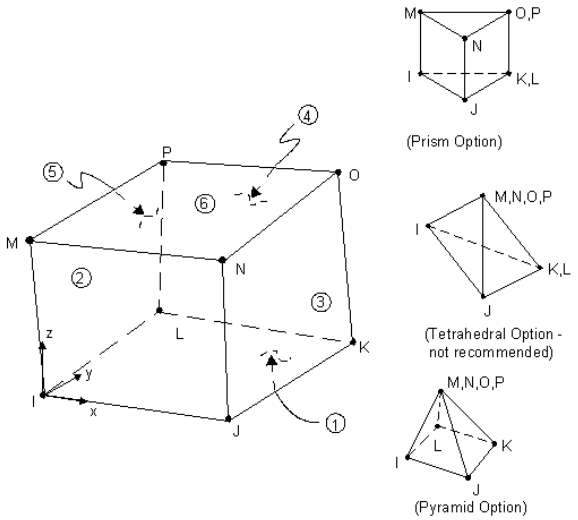

Figure 3.8 SOLID164 geometry

3.3.1.4 The Spring and Damper Element (COMBI165)

The COMBI165 [16] is a 2-node, 1-D element. It provides a variety of discrete element formulations that can be used individually or in combination to model complex force-displacement relations. A COMBI165 element can be overlaid and attached to any of the other explicit elements. The geometry of the element is shown in Figure 3.9.

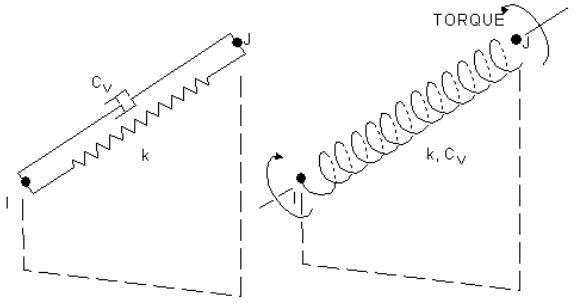

Figure 3.9 COMB165 geometry

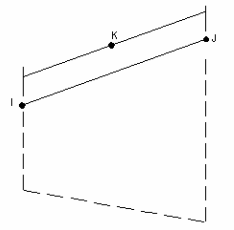

Figure 3.10 LINK167 geometry

3.3.1.5 The Cable Element (LINK167)

The geometry of the LINK167 element [16, 34] is shown in Figure 3.10. This element is defined by nodes I and J in the global coordinate system. The node K is used only to initially orient the element. The element has three translational degrees of freedom at each node. The force, *F*, generated by the link is nonzero only if the link is in tension. *F* is given by:

$$F = k \cdot \max(\Delta L, 0) \tag{3.4}$$

where ΔL is the change in length and *k* is the cable stiffness. An initial tensile force is realized by using a positive offset for the cable.

3.3.1.6 The MASS166 Element

The MASS166 element [16, 34] is defined by a single node with concentrated mass components. The geometry of the element is shown in Figure 3.11.

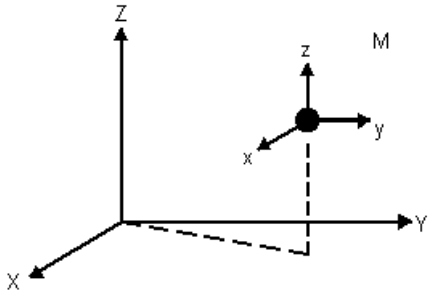

Figure 3.11 MASS166 geometry

3.3.2 The Material Models

A major advantage of the 3D finite element method of structural analysis is that it enables the incorporation of specialized models that accurately reflect material behavior. The program LS-DYNA accepts a wide range of material and equation of state models. Four material models are used in the present JH model.

In the material formulation used in this study, the failure process is modeled by erosive elements. When the effective plastic strain of an element reaches a critical strain value, this element is deleted from the calculation.

3.3.2.1 The Piecewise Linear Plasticity Model

The material used in the JH model is normal mild steel (A36). The material-hardening characteristics have a significant influence on the dynamic collapse mechanisms, so that approximations for the stress-strain relationship closely resemble the actual stress-strain curve. In the crushing regions, the Piecewise Linear Isotropic Plasticity model is applied, which allows stress versus strain curve input and strain rate dependency.

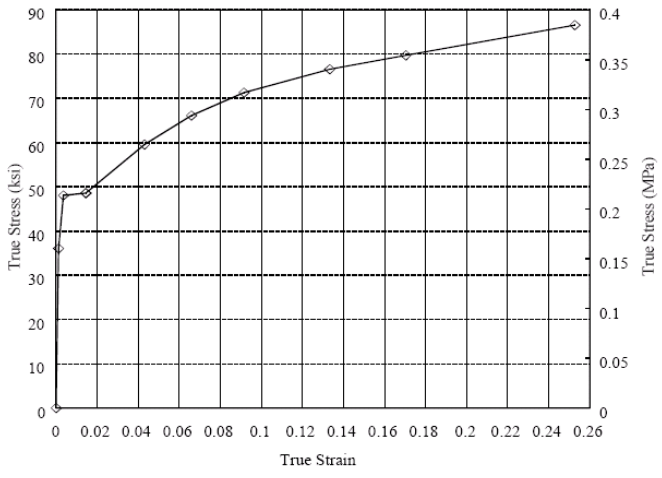

Figure 3.12 True stress vs. true strain curve for A36 structural steel

The parameters are determined from the tests conducted at the University of Florida on a standard 18-inch tension coupon [13]. A plot of the stress vs. strain curve used is shown in Figure 3.12. The impact velocity and material stain-hardening properties also influence the transition conditions for dynamic progressive bucking or global bending collapse [35]. To account for the strain rate, the model makes use of the Cowper-Symonds law given by:

$$\frac{\sigma}{\sigma_{\mathrm{y}}} = 1 + \left(\frac{\dot{\varepsilon}}{40.4} \right)^{1/5} \tag{3.5}$$

where σ is the dynamic yield stress; σ_y is the static yield stress; and $\dot{\varepsilon}$ is the effective strain rate;

Eq. (3.5) is a commonly used plasticity law, especially for steel.

3.3.2.2 The Isotropic Elastic Model

Except for the materials of Zone-1, the Isotropic Elastic Model [14] is applied. The properties of the A36 grade steel are presented in Table 3.3. It should be noted that the material density of Zone-2 is adjusted by the following formula to match the real weight of a barge:

$$\rho_{adj} = \frac{M_b - (M_1 + M_3)}{M_2} \rho_s \tag{3.6}$$

where ρ_{adj} is the used density for Zone-2; M_b is the self weight of barge; M_1, M_2 and M_3 are the weights of Zone-1, Zone-2 and Zone-3, respectively; and ρ_s is the steel density.

Table 3.3. Mechanical properties of steel and reinforced concrete

Material	Density Kg/m^3 ($Sec^2 \cdot lb/in^4$)	Poisson's ratio	Elastic modulus Pa (lb/in^2)	Yield stress Pa (lb/in^2)
A36 steel	7.91×10^3 (7.4×10^{-4})	0.33	2.07×10^{11} (3.0×10^7)	2.48×10^8 (3.6×10^4)
Reinforced concrete	2.34×10^3 (2.2×10^{-4})	0.20	2.28×10^{10} (3.3×10^6)	

3.3.2.3 The Rigid Material Model

A rigid material type (Type 20) in the LS-DYNA code is used to define the perfectly rigid body that remains so for the duration of the analysis [14]. Since the rigid elements are bypassed in the element processing and no storage is allocated for storing history variables, the material type is very efficient in terms of CPU computation time. Realistic values of Young's modulus and Poisson's ratio are required to determine sliding interface parameters when the rigid body interacts in the context of contact. Unrealistic values may contribute to numerical problems in contact analyses. In the present model, the rigid material model is only applied to rigid piers, so the properties of reinforced concrete, which are also tabulated in Table 3.3, are used.

3.4 Contact Definition

Contact treatment is an integral part of crash research. Accurate modeling of contact interfaces between bodies is crucial to a successful collision simulation. The dynamic simulation software, LS-DYNA, is well equipped to handle contact problems. In the LS-DYNA program, contact is defined by identifying parts, part sets, segment sets, or node sets.

Since deformations are much larger in crash modeling, accurately modeling the stresses within a structure is not sufficient. One must describe the inter-part contact between different parts of the model as well as intra-part contact when a part buckles in upon itself. For a complicated model with many parts, such as a barge flotilla model, the automatic contact algorithm is preferred. At the start of program execution, LS-DYNA checks the spacing between parts and activates contact between nearby neighbors. As the structure collapses, the contact table is periodically updated. If an expected contact is missed by the automatic routine, it can be set explicitly by the user.

3.4.1 Contact between the Barge and the Pier

Since Surface-to-Surface contact (STS) [14] is very efficient for bodies that experience large amounts of relative sliding with friction, such as a block sliding on a plane, STS is used to define the contact between the barge and pier. The barge is treated as the slave surface, and the pier is treated as the master surface. The resultant contact forces for the slave and master sides of each contact interface are output directly by LS-DYNA in the global coordinate system.

3.4.2 Contact inside the Barge

In the barge-bridge collision analysis, the barge deformations may be very large, and predetermination of where and how contact takes place inside the barge bow may be difficult or even impossible. Some elements in Zone-1 deflect enough to contact with one another, consequently increasing the secondary stiffness of the barge structure. For this reason, automatic single surface contact (ASSC) [14] is adopted. Unlike implicit modeling, where over-defining contact will significantly increase computation time, using single surface contact in an explicit analysis will cause only minor increases in

CPU computation time. By implementing AASC, the slave surface is defined as a list of part IDs, and LS-DYNA automatically determines which surfaces within this list may come into contact. Therefore, no contact or target surface definitions are required for ASSC.

Large initial penetrations can cause the local stresses to exceed the material's yield stress. In these cases, the initial node positions must be readjusted manually. Often this situation can be detected by running sub-models of each part in a static, load-free situation to see if the part breaks apart or exhibits large, spontaneous deformations.

3.4.3 Contact between Barges in a Flotilla

During a collision event, the barges in a multi-barge flotilla collide with one another. These internal contacts between the barges are realized by defining ASSC [14]. Because the deformation can be expected to be very small without penetration, only the interfaces need to be included in the contact part list. The problem is that no contact force data is written for single surface contacts as all of the contact forces originate from the slave side, and thus, the net contact forces are zero. To obtain the resultant contact forces, appropriate force transducers are introduced into the mode via the *CONTACT_FORCE_TRANSDUCER_PENALTY command. A force transducer measures contact forces produced by other contact interfaces defined in the model, and does not affect the results of the simulation. By assigning a subset of the parts defined in a single surface contact to the slave side of a force transducer, the impact forces can be extracted for the subset of the parts.

3.4.4 Friction Definition

During impact, a portion of the collision energy is dissipated by the sliding friction between the barge and pier. More important, friction should be included in the simulation because it will stabilize the model. In the LS-DYNA program, friction is invoked by inputting non-zero values for the static and dynamic friction coefficients, *FS* and *FD*, respectively.

$$\mu_c = FD + (FS - FD) \cdot e^{-DC \cdot V_{rel}} \tag{3.7}$$

where μ_c is the friction coefficient; *DC* is the exponential decay coefficient, and V_{rel} is relative velocity of the surfaces in contact.

In practice, it is difficult to determine the parameters DC and V_{rel}. After checking the sensitivity of the parameters in Eq. (3.7), $FD = FS = 0.35$ is used for steel to concrete, and $FD = FS = 0.21$ for steel to steel.

3.5 Other Considerations

3.5.1 Mass Scaling

For extensive simulations of multi-barge flotillas impacting bridge piers, the required computing time is an important matter. As stated in Chapter 2, explicit methods are computationally fast and conditionally stable. The maximum time step depends on the time that a wave needs to travel through an element in the shortest direction ($l_{\min}$) because, when the step is larger, it is possible for nonlinear phenomena to occur within this time step. The time step Δt_{cr} is determined using the Courant-Friedrich-Levy criterion as it applies to shell elements:

$$\Delta t_{cr} = \frac{l_{\min}}{c} \tag{3.8}$$

$$c = \sqrt{\frac{E}{(1-\nu^2)\rho}} \tag{3.9}$$

where v is the Poisson' ratio; ρ is the specific mass density; E is Young's Modulus.

In order to increase Δt_{cr}, an efficient approach is to use mass scaling. In LS-DYNA when mass scaling is requested, density ρ_i of element i is adjusted to achieve a user specified time step size Δt_{spc}:

$$\rho_i = \frac{E \cdot \Delta t_{spc}^2}{l_i^2 (1-\nu^2)} \tag{4.0}$$

Note that mass scaling is applied only to elements with a calculated time step size Δt_{cr} smaller in magnitude than Δt_{spc}. Although proper use of mass scaling will add a small amount of mass to the model and slightly change the given structure's center of mass, the benefit of the computation time reduction achieved far outweighs the minor errors introduced. The reduction in computer calculation time is greater than 50% for most cases, as compared to an analysis without mass scaling.

Table 3.4. Examination of mass scaling

Barge	**Simulation time (sec)**	Δt_{cr} ($\times 10^{-5}$ **sec**)	Δt_{spc} ($\times 10^{-5}$ **sec**)	**CPU time (hours)**	**Added mass (%)**
Single barge	1.0	3.85	3.85	7	0
			5	2	2.1
Two-barge flotilla	1.0	3.85	3.85	11	0
			5	4	1.4

For example, Table 3.4 compares four simulations with the identical input, except that two of the simulations contain mass scaling and two do not. Test runs show that

mass scaling does not affect the results, and can be used safely. To save time, mass scaling is applied in the simulations of this study.

3.5.2 Hourglass Control

In the preliminary FE simulations, it was observed that hourglass control can be ignored without significantly affecting the behavior of the model. Because hourglass control prolongs a given simulation, in order to reduce CPU computation time hourglass control is applied only to the elements in Zone-1.

3.5.3 Mesh Convergence

It is well known that a finite element crash analysis is very sensitive to the size of the mesh. Choice of mesh size must be balanced with the cost of computation time. Different meshes were created and examined to investigate mesh convergence in trial simulations. The final mesh was chosen based upon solution convergence and CPU usage. The present barge model behaves very well with respect to the two criteria.

3.5.4 FE Simulation Simplifications

The mechanisms involved in a barge-pier collision are complex and include both structural and hydrodynamic components. The structural mechanisms undergone by the steel components comprising the vessel structure include bending, stretching, compression, scraping (friction), buckling, crushing, folding, fracture, and tearing. The hydrodynamic mechanisms include rigid body motions with attendant changes in added mass. Comprehensive modeling of a given collision is quite complex and involves the coupled effects of:

1) the 3-D motion of the barge and the pier;

2) hydrodynamic forces from the surrounding water;

3) friction between the contact surfaces;

4) large plastic deformation of the involved structures;

5) fracture and propagation of cracks in the structure.

Depending on the level of detail, each of these effects may be too complex to model and predict theoretically. It is common practice in FE analysis to make simplifying assumptions. One can think of the real world as having all analysis "options" turned on all the time, but in FE analysis, these options must be activated one by one. Therefore, it is significant to carefully simplify the modeling as much as possible with due consideration to the desired level of accuracy.

Water not only adds kinetic impact energy but also absorbs impact energy. For simplicity, water involvement (such as viscosity and flow) is excluded in this study. The neglect of water minimally influences the present work due to the short duration of barge-pier collision processes. Moreover, the water effect may be alternatively considered as an added mass to the barge to produce a conservative result.

As stated in Chapter 2, the impact forces and ensuing damage during barge-pier impacts are maximized by considering head-on encounters. Since a major concern of this study is the determination of impact loads on the isolated piers, only frontal impact scenarios will be examined herein. Nevertheless, it should be noted that different impact angles are an important consideration in the study of bridge structure responses.

For simplicity of analysis, it is assumed that the ship under consideration moves in the horizontal plane, with no pitching or heaving movements. The dynamics of the whole barge vessel, therefore, is considered only in a simplified manner in this research.

3.6 Summary

A FE model of a typical barge was developed using the APDL Language, which closely replicates all of the components of a JH according to the respective blueprints and specifications. The model is applicable to a variety of FE simulation scenarios as either a single barge or a part of a multi-barge flotilla.

Chapter 4 Single Barge Impact Study

Examining the topic of single-barge collisions with bridge piers is very valuable because the insight gained from such studies may be used to clarify the more general problem of flotilla-bridge collisions. During barge-bridge collision events, a major part of the kinetic impact energy is dissipated through the deformation and damage of the barge contacting with the pier. The impact force is tantamount to the crushing resistance of the bow structure. In general, the collision problems brought about by multi-barge flotillas are merely an extension of the single-barge collision.

In this chapter, several important factors involved in the determination of barge impact forces on bridge piers, such as the velocity, mass and kinetic energy of barges, and the geometry of piers, are systematically investigated. Based on the numerical simulation results, loading functions to predict single-barge impact forces are developed.

Pier flexibility tends to obscure the effect of other parameters influencing barge-pier collisions. Hence, in order to demonstrate how other important parameters affect barge-pier collision, the analysis presented in this chapter concentrates on rigid piers, and a more thorough exploration of pier flexibility is deferred to Chapter 5.

4.1 Impact Velocity and Barge Mass

Two important factors that affect barge impact forces are barge mass and velocity at impact. Per AASHTO terminology, barge flotilla velocity is the speed a flotilla can achieve if the river velocity is zero. Whitney et al. [10] compiled vast amounts of data in order produce comprehensive statistics regarding the traveling velocity of barge flotillas.

The average barge velocity on inland waters is 2.06 m/s (4 knots), and the maximum is 3.09 m/s (6 knots). As for the barge mass, it is defined in Chapter 3. The empty displacement (self-weight) and loaded displacement (fully loaded) of a Jumbo Hopper (JH) are 200 short tons (181.4 metric tons) and 1900 short tons (1723.7 metric tons), respectively.

4.2 Elasticity of Collision

Elasticity is a measure of how much of the kinetic energy of the colliding objects before the collision remains as kinetic energy of the objects after the collision. The coefficient of restitution is used as a measure of the elasticity of barge-bridge collisions.

The restitution condition expresses the ratio between the velocities at which the contact objects approach and depart. For head-on impacts on rigid piers, the coefficient of restitution is defined as:

$$e = \frac{V_{t_d}}{V_i} \tag{4.1}$$

where V_i and V_{t_d} are the velocities of the barge before impact and after impact (the impact forces drop to zero), respectively.

The value of *e* is equal to 1 and 0 for a perfectly elastic and a completely inelastic collision, respectively. According to the impulse-momentum law, the global velocity of the barge at time *t* is given by:

$$V(t) = V_i - \frac{\int_0^t P(t)dt}{m_B} \tag{4.2}$$

where m_B is the mass of barge, and $P(t)$ is the impact force function.

Substituting Eq. (4.1) into Eq (4.2) yields:

$$\begin{aligned} e &= \frac{V_{t_d}}{V_i} \\ &= 1 - \frac{\int_0^{t_d} P(t)dt}{I_i} \\ &= 1 - \frac{A_{t_d}}{I_i} < 1 \end{aligned} \tag{4.3}$$

where A_{t_d} is the area under the force curve $P(t)$, and $I_i = m_B V_i$ is the initial momentum of the barge.

From Eq. (4.3), it can be seen that *e* cannot be greater than unity as this would reflect an increase in the mechanical energy of the bodies by effect of the impact. Several values of *e*, resulting from the FE simulations of barges impacting square and circular piers, are presented in Tables 4.1 and 4.2, respectively. In general, the coefficient of restitution is small in high-energy impacts, and it approaches a relatively larger value in low-energy impacts. Moreover, the coefficient of restitution is a stable indicator of impact extent because it varies only slightly with a change in the impact velocity or the pier size.

Only circular and square piers are investigated herein because of the ubiquitous use of these pier-types in bridge construction. To study the effect of pier sizes, the parameter α, barge to pier width ratio, is introduced here. Essentially, α describes the contact area between the barge and pier. A flat wall ($\alpha \geq 1.0$) is merely a special case of square piers. The conjunction of barge damage depth, a_B and the ratio, α, describes the damaged material volume of the bow structure. As shown in Chapter 2, the Minorsky

approach [20] correlates the resistance and damaged volume of the ship structural steel in a collision event.

From Tables 4.1 and 4.2, when the impact velocity $V_i \geq 1.54$ m/s (3 knots), most of the coefficients $e < 0.3$. The area under the pulse curve may be calculated by Eq. (4.3) as:

$$A_{t_d} = (1-e)I_i > 0.7I_i \tag{4.4}$$

thus, the average impact force over the impact time duration t_d is:

$$\overline{P} > \frac{0.7I_i}{t_d} = \frac{0.7m_B V_i}{t_d} \tag{4.5}$$

The minimum value of e in Tables 4.1 and 4.2 is 0.15. Hence, the average impact force is obtained as

$$\overline{P} < \frac{0.85I_i}{t_d} = \frac{0.85m_B V_i}{t_d} \tag{4.6}$$

combining Eqs. (4.5) with (4.6) yields:

$$0.85I_i \geq I_{t_d} \geq 0.7I_i \quad \text{for } V_i \geq 1.54 \text{ m/s} \tag{4.7}$$

where $I_{t_d} = \overline{P}t_d$ is the impulse caused by the collision.

Eq. (4.7) is valid for most collision cases. Regarding the cases that produce a large value of e, for example, when $e > 0.5$, the barge rebounds back from the pier with little plastic deformation. The pulse shape of such cases (e is large) resembles a triangle and contains a sharp peak; whereas the pulse shape of cases with a small e contains an apparent plateau. Corresponding to the plastic deformation, the resistance of the barge stays nearly constant.

Table 4.1. Coefficient of restitution for a single-barge impacting square piers

m_B (ton)	V_i (m/s)	Coefficient of restitution e			
		$\alpha = 0.1$	$\alpha = 0.3$	$\alpha = 0.5$	$\alpha = 0.7$
1723.7 (fully loaded)	0.51	0.34	0.32	0.51	0.57
	1.03	0.30	0.24	0.22	0.21
	1.54	0.23	0.24	0.24	0.18
	2.06	0.21	0.20	0.19	0.21
	2.57	0.18	0.17	0.15	0.15
	3.09	0.17	0.17	0.15	0.15
861.8 (half loaded)	0.51	0.44	0.53	0.66	0.65
	1.03	0.29	0.28	0.23	0.43
	1.54	0.29	0.24	0.22	0.20
	2.06	0.25	0.27	0.24	0.19
	2.57	0.23	0.20	0.22	0.22
	3.09	0.21	0.20	0.20	0.19
430.9 (quarterly loaded)	0.51	0.53	0.67	0.68	0.67
	1.03	0.37	0.41	0.59	0.60
	1.54	0.30	0.27	0.24	0.42
	2.06	0.31	0.25	0.21	0.22
	2.57	0.27	0.26	0.21	0.18
	3.09	0.24	0.26	0.24	0.19

Table 4.2. Coefficient of restitution for a single-barge impacting circular piers

m_B (ton)	V_i (m/s)	Coefficient of restitution e			
		$\alpha = 0.1$	$\alpha = 0.3$	$\alpha = 0.5$	$\alpha = 0.7$
1723.7 (fully loaded)	0.51	0.35	0.35	0.34	0.35
	1.03	0.26	0.28	0.28	0.27
	1.54	0.22	0.24	0.24	0.24
	2.06	0.21	0.22	0.22	0.22
	2.57	0.20	0.20	0.19	0.20
	3.09	0.19	0.19	0.19	0.19
861.8 (half loaded)	0.51	0.42	0.44	0.42	0.44
	1.03	0.30	0.29	0.29	0.29
	1.54	0.27	0.28	0.28	0.28
	2.06	0.24	0.25	0.25	0.26
	2.57	0.22	0.23	0.22	0.22
	3.09	0.22	0.23	0.23	0.23
430.9 (quarterly loaded)	0.51	0.50	0.54	0.51	0.55
	1.03	0.37	0.36	0.35	0.35
	1.54	0.30	0.30	0.29	0.30
	2.06	0.28	0.29	0.29	0.29
	2.57	0.27	0.26	0.26	0.28
	3.09	0.23	0.23	0.26	0.25

The following regression formulas, which calculate coefficient e, are the result of more than 100 FE simulations.

For $0.05 \le \alpha \le 1.0$ square piers:

$$e = 0.279 + 0.040\alpha - (0.081 + 0.042\alpha)\ln E_i \tag{4.8}$$

and for $0.05 \le \alpha \le 1.0$ circular piers:

$$e = 0.061 + 0.057\alpha - (0.155 - 0.008\alpha)\ln E_i \text{ for } 0 < E_i \le 0.114 \tag{4.9}$$

$$e = 0.273 + 0.005\alpha - (0.046 + 0.001\alpha)\ln E_i \text{ for } E_i > 0.114 \tag{4.10}$$

where E_i is the initial kinetic energy of the barge in MJ; α is the pier to barge width ratio.

4.3 Simulation of Pier Shape and Size

The AASHTO method [9] assumes that barge-impact forces are independent of pier geometry. However, pier shape and size are important design factors that ensure protection to bridges from vessel or wave impacts. For example, after being destroyed by a freight ship, the Bowen Bridge [36] in Hobart, Australia, was rebuilt with pointed pier ends to deflect or tear impacting vessels. Also, recent studies [13, 17] have shown that the impact forces are significantly dependent on pier geometry.

4.3.1 Square Piers

The time histories of the barge crushing distance $\delta(t)$ and impact force $P(t)$, as shown in Figure 4.1, are obtained by allowing a fully loaded barge, with an initial velocity $V_i = 2.06$ m/s (4 knots), to collide with a rigid square pier. From Figure 4.1, it can be seen that the ratio α significantly affects the impact process. A wider pier produces a larger impact force, shorter time duration, and smaller barge damage distance. This result is reasonable because the contact force between the barge and pier is roughly proportional to the width ratio α, and the deformation of a barge absorbs energy that is closely related to the volume of deformed steel in the crushed area [20].

Table 4.3 presents the simulation results for the scenarios that $V_i = 1.8$ m/s (3.5 knots) and $\alpha = 0.1$ to 1.0. From this table, it is clear that the impact characteristics of a barge are strongly related to pier sizes. As α increases, the maximum force $P_{\max}$ increases, and both the barge damage depth a_B and impact duration t_d decrease. Although the ratios $\overline{P}_{1/2} / P_{\max}$ and $\overline{P} / P_{\max}$, and the coefficient of restitution e oscillate, the gaps are insignificant. When α is small, the yielding strength of the bow structure is overcome by the local crushing. The larger α becomes, the stiffer the barge, because more trusses in the bow take part in the resistance to crushing. When $\alpha \geq 1.0$, the barge bow has no local crushing, but instead, it undergoes overall buckling.

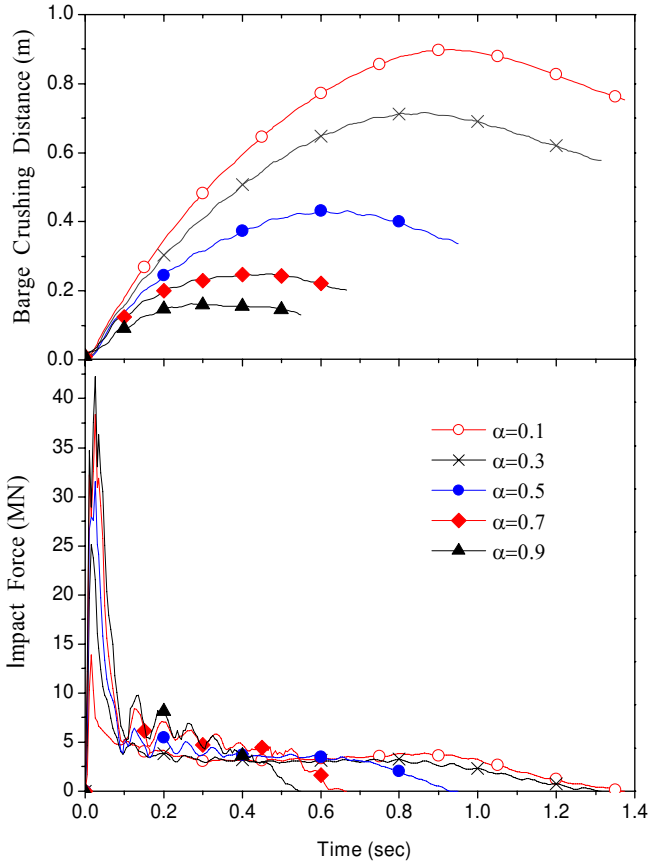

Figure 4.1 Impact force and crushing distance time-histories for a fully loaded barge impacting a series of square piers with a velocity of V_i = 2.06 m/s (4 knots)

By careful inspection of Table 4.3 several important conclusions may be made. For example, the impact duration, t_d, is dependent on the pier size. The impact duration can be calculated using the regression function, $t_d \approx 1.433 - 1.168\alpha$, for the cases in the table. As aforementioned, the time duration of impact t_d apparently decreases as α increases. In addition, the dissipated energy is approximately equal for all of the impacts due to the nearly constant value of *e*, which fluctuates above and below 0.2. It should be noted that the influence of α upon impact forces is also velocity dependent. This assertion is made because α indicates how many structural members participate in crushing resistance directly, and V_i indicates how quickly the structure members act.

Table 4.3. Summary of a fully loaded barge impacting square piers with a velocity of V_i = 1.8 m/s (3.5 knots)

Ratio α	Impact force (MN)			Coefficient of restitution e	Duration t_d (s)	Damage depth a_B (m)
	$P_{\max}$	$\bar{P}_{1/2} / P_{\max}$	$\bar{P} / P_{\max}$			
0.10	12.91	0.28	0.20	0.22	1.435	0.568
0.20	19.19	0.21	0.15	0.21	1.295	0.473
0.30	22.96	0.21	0.15	0.20	1.080	0.369
0.40	26.14	0.23	0.16	0.22	0.875	0.280
0.50	29.72	0.26	0.18	0.23	0.715	0.204
0.60	33.25	0.27	0.19	0.23	0.615	0.166
0.70	36.21	0.30	0.19	0.22	0.535	0.136
0.80	38.83	0.32	0.19	0.19	0.505	0.102
0.90	40.01	0.33	0.18	0.19	0.500	0.070
1.00	40.52	0.39	0.25	0.16	0.355	0.000

4.3.2 Circular Piers

The circular shape is another common geometry used for bridge piers. It has been found that the impact force patterns for circular piers and for square piers are not the same [17].

The time histories of the barge crushing distance $\delta(t)$ and the impact force $P(t)$, as shown in Figure 4.2, are obtained by allowing a barge to collide into a rigid circular

pier with an initial velocity $V_i = 2.06$ m/s (4 knots). All the curves in Figure 4.2 are very similar in shape for each value of α. Although the ratio, α, affects the impact force and barge crushing distance of circular piers, the influence is not as significant as that on square piers. In addition, the maximum impact force of a circular pier is much smaller than that of a square pier with the same α, due to a gradually increasing contact area for the circular pier.

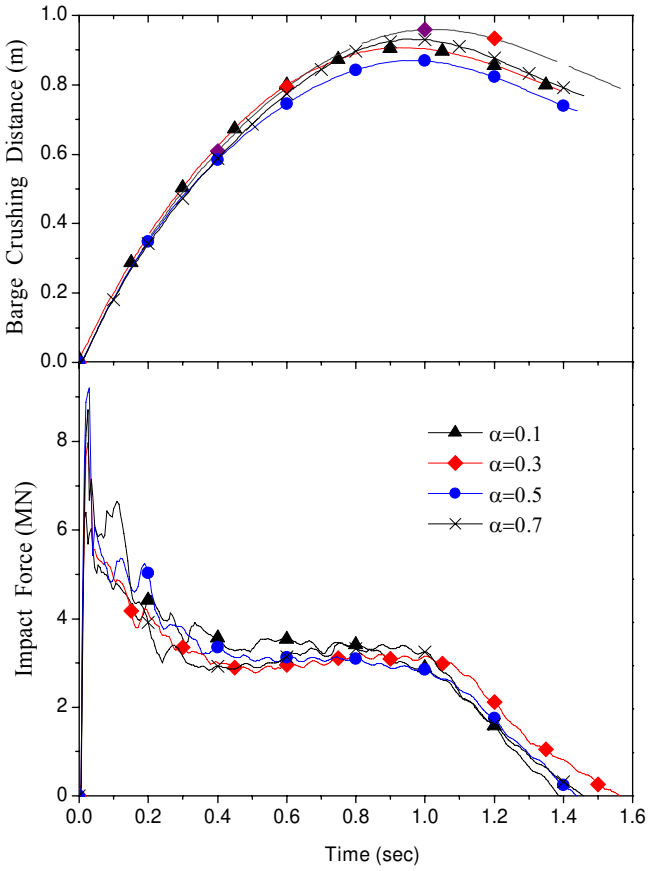

Figure 4.2 Impact force and crushing distance time-histories of a fully loaded barge impacting a series of circular piers with a velocity of $V_i = 2.06$ m/s (4 knots)

Tables 4.4 and 4.5 compare the impact cases with different barge velocities. When the impact velocity is low, the influence of ratio α becomes slightly larger due to

the higher elastic resistance involved. The impact force time-history curves tend to approach the same values as the impact velocity increases. Regarding the cases with a large impact velocity, the plastic deformation of the barge mainly controls the impact processes. As for the cases that have apparent plateaus in impact force time histories, the average impact forces over the first quarter of the impact period, $P_{1/2}$, may be used as an indicator of the impact force level. Moreover, the damage depths of barges for circular piers correlate with the damage depths calculated by AASHTO methods, but the impact forces are smaller than those predicted by the AASHTO analysis.

Table 4.4. Summary of a fully loaded barge impacting circular piers with a velocity of V_i = 1.54 m/s (3.0 knots)

Ratio α	Impact Force (MN)			Coefficient of restitution e	Duration t_d (s)	Damage depth a_B (m)
	$P_{\max}$	$\bar{P}_{1/2} / P_{\max}$	$\bar{P} / P_{\max}$			
0.10	6.10	0.62	0.52	0.22	1.02	0.42
0.20	6.37	0.62	0.52	0.22	0.98	0.41
0.30	6.93	0.50	0.41	0.24	1.15	0.42
0.40	8.00	0.51	0.43	0.24	0.96	0.38
0.50	8.79	0.46	0.39	0.24	0.96	0.36
0.60	7.22	0.50	0.41	0.24	1.10	0.38
0.70	7.16	0.51	0.42	0.24	1.08	0.37
0.80	7.41	0.59	0.50	0.24	0.89	0.35
0.90	8.01	0.46	0.39	0.24	1.06	0.37
1.00	8.48	0.44	0.37	0.24	1.06	0.36

Table 4.5. Summary of a fully loaded barge impacting circular piers with a velocity of V_i = 2.57 m/s (5.0 knots)

Ratio α	Impact force (MN)			Coefficient of restitution e	Duration t_d (s)	Damage depth a_B (m)
	$P_{\max}$	$\bar{P}_{1/2} / P_{\max}$	$\bar{P} / P_{\max}$			
0.10	6.68	0.58	0.49	0.20	1.63	1.18
0.20	7.99	0.52	0.44	0.20	1.52	1.14
0.30	9.48	0.47	0.39	0.20	1.43	1.13
0.40	9.80	0.44	0.36	0.20	1.49	1.10
0.50	10.25	0.41	0.33	0.19	1.56	1.08
0.60	9.21	0.47	0.38	0.20	1.50	1.11
0.70	9.55	0.46	0.38	0.20	1.45	1.11
0.80	9.32	0.46	0.38	0.20	1.51	1.07
0.90	9.64	0.48	0.39	0.20	1.42	1.06
1.00	10.13	0.50	0.40	0.19	1.30	0.92

4.4 Energy Dissipation

Neither the momentum nor the energy of the barge is conserved during a collision event. In addition to the deformation and resisting force time-history, it is important to know how the kinetic impact energy dissipates during an impact. The kinetic energy of the barge at time *t* is given by:

$$E(t) = \frac{1}{2} m V^2(t) \tag{4.11}$$

and the work at deformation by:

$$W(t) = \int_0^t P(t) d\delta \tag{4.12}$$

Due to other energy dissipation mechanisms such as damping and friction, the kinetic energy of the barge at time *t* is:

$$E(t) = E_i - W(t) - E_a(t) \tag{4.13}$$

where $E_i = 0.5 m_B V_i^2$ is the initial kinetic impact energy of barge, and E_a is the energy dissipated due to other factors.

The coefficient of restitution is usually used as a measure of the mechanical energy lost during the collision process. The kinetic energy lost during impact is expressed in terms of *e* as:

$$\Delta E(t) = E_i - E(t) = \left(1 - e^2\right) E_i \tag{4.14}$$

thus, the energy dissipation efficiency can be written as:

$$\xi = \frac{\Delta E(t_d)}{E_i} = 1 - e^2 \tag{4.15}$$

where t_d is the impact duration.

Therefore, the amount of the kinetic energy left at the instant of t_d is:

$$E_{t_d} = (1-\xi)E_i \tag{4.16}$$

From the discussion in the previous section, for $0.15 \le e \le 0.7$, and for initial velocities $V_i \ge 1.54$ m/s (3 knots), the total energy loss $\Delta E(t_d)$ is in the following range:

$$0.51E_i \le \Delta E(t_d) \le 0.98E_i \tag{4.17}$$

i.e.,

$$0.51 \le \xi \le 0.98 \tag{4.18}$$

Figures 4.3.a and 4.3.b demonstrate the relationships between $E(t)$, $W(t)$, and $E_a(t)$ for $V_i = 0.26$ m/s (0.5 knots) and 1.8 m/s (3.5 knots), respectively. It can be seen from the two figures that $E_a(t)$ occupies a relatively large portion of the total kinetic impact energy for the low energy impact (Figure 4.3.a) and a very small portion of the total kinetic impact energy for the high energy impact (Figure 4.4.b). Therefore, it may be assumed that the work done by the impact force against the barge crushing distance equals the energy losses during impact if the impact energy is not very small, namely:

$$\Delta E(t) \approx E_i - W(t) \tag{4.19}$$

Substituting Eq. (4.11) and Eq. (4.12) into Eq. (4.19) yields:

$$\overline{P} \cdot a_B \approx \xi E_i \tag{4.20}$$

where a_B is the final damage depth of the barge.

Acknowledging that $0.51 \le \xi \le 0.98$ when the barge velocity $V_i \ge 1.54$ m/s (3 knots), the average impact force during a barge-bridge collision event may be estimated by:

$$\overline{P} \approx \xi \cdot \frac{E_i}{a_B} \le \frac{0.98 m_B V_i^2}{a_B} \tag{4.21}$$

and

$$\overline{P} \approx \xi \cdot \frac{E_i}{a_B} \ge \frac{0.51 m_B V_i^2}{a_B} \tag{4.22}$$

Because most of the barges in the United States travel at speeds between 1.54 m/s (3.0 knots) and 2.57 m/s (6.0 knots), Eqs. (4.21) and (4.22) may be used to investigate barge-bridge collision accidents when the damage depth a_B is known. Eqs. (4.5), (4.6), (4.21), and (4.22) bound the average impact forces in terms of the impact time duration t_d or the barge damage depth a_B.

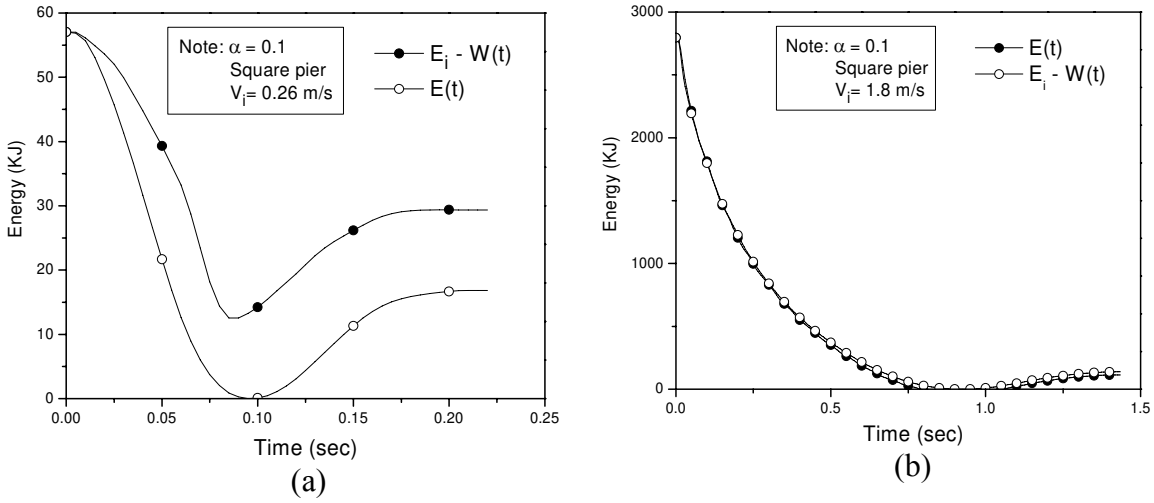

Figure 4.3 Energy vs. time for a fully loaded barge impacting a rigid square pier: (a) low impact energy; (b) high impact energy

4.5 Impact Force versus Kinetic Impact Energy

As discussed in Chapter 2, Meir-Dornberg developed the following equations:

$$E_i = \frac{1}{2} m_B V_i^2 \tag{4.23}$$

$$a_B = 3.1\left(\sqrt{1+0.13E_i}-1\right) \tag{4.24}$$

$$P = \begin{cases} 60a_B & \mathrm{a_B} < 0.1 \\ 6+1.6a_B & \mathrm{a_B} \geq 0.1 \end{cases} \tag{4.25}$$

where the barge damage length a_B is in meters, the initial kinetic energy of the barge E_i is in MJ, and the impact force P is in MN.

Substituting Eq. (4.24) into Eq. (4.25), the equation of impact force, Eq. (4.25), can be rewritten as:

$$P = \begin{cases} 186\left(\sqrt{1+0.13E_i}-1\right) & E_i < 0.5 \\ 1.04+4.96\sqrt{1+0.13E_i} & E_i \geq 0.5 \end{cases} \tag{4.26}$$

where the impact force P is in MN, and the initial kinetic energy E_i is in MJ.

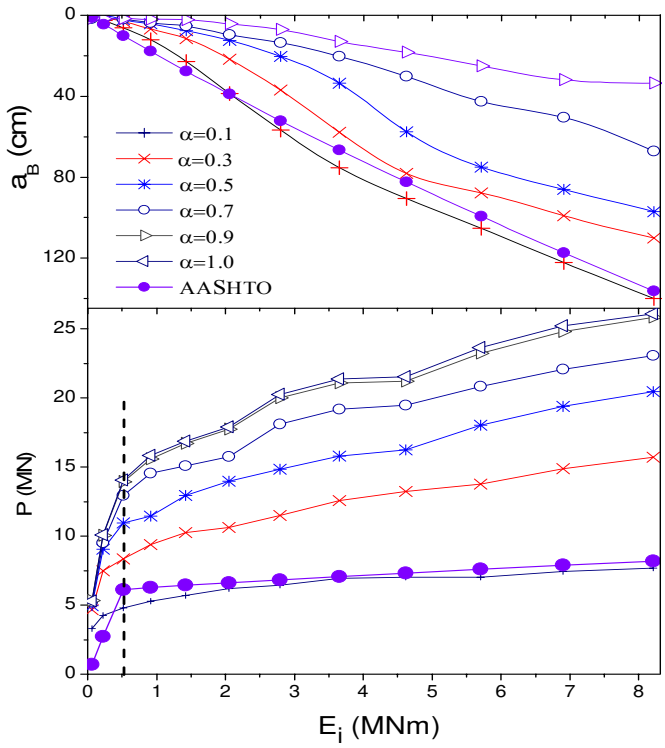

Figure 4.4 Maximum impact force $P_{\max}$ and barge crushing depth a_B vs. initial kinetic energy E_i for a fully loaded barge impacting square piers with different sizes

Eq. (4.26) is a two-segment function with a separating value of $E_i = 0.5\,\text{MJ}$, which is a pivotal point that divides two forms of barge crushing. The elastic behavior dominates the crushing process until the kinetic impact energy is larger than this value. The threshold value $E_i = 0.5\,\text{MJ}$ has also been verified by multiple FE simulations, as shown in Figure 4.4. Prior to the aforementioned turning point, the impact force increases rapidly as the impact energy increases. After the turning point, the slope of the $P(E_i)$ curves become less steep. For a fully-loaded barge (1900 tons) and a half-loaded barge (950 tons), $E_i = 0.5\,\text{MJ}$ corresponds to a barge velocity of 1.5 knots and 2.1 knots, respectively. Therefore, the kinetic impact energy of a single barge or a multi-barge flotilla is larger than 0.5MJ for most cases. It should be noted that the separating energy value is smaller than 0.5 MJ for circular piers, as shown in Figure 4.5. For that reason, the value 0.5 MJ may be used to distinguish different types of barge impacts in general.

As shown in Figure 4.6, the pattern of impact forces is related to the magnitude of impact energy E_i. For example, when $V_i = 0.26$ m/s (0.5 knots), the impact force curve appears to be a triangle, containing a sharp peak with steep sides. The barge deformation is not only small, but also elastic. Plastic deformation develops as the velocity becomes larger. For example, when $V_i = 1.9\,\text{m/s}$ (3.5 knots), the kinetic energy of the barge exceeds the maximum elastic strain energy that can be absorbed by the bow structure, and the maximum impact forces decrease quickly as the pier entry deepens. Moreover, the impact force curve of this case has an apparent plateau.

A further increase of the impact energy causes more structural members to be damaged at the beginning of impact. Figure 4.7 compares the maximum impact forces generated by the same barge and pier with different velocities. As shown in Figure 4.7,

the larger the impact energy, the faster the maximum force plummets. This is because more structural members are damaged instantaneously, which causes the elastic resistance of the barge to diminish.

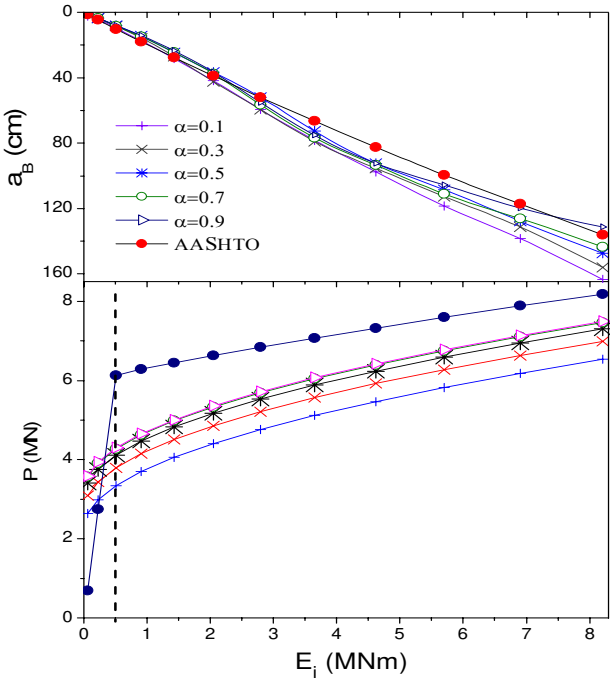

Figure 4.5 Maximum impact force $P_{\max}$ and barge crushing depth a_B vs. initial impact energy E_i for a fully load barge impacting circular piers with different sizes

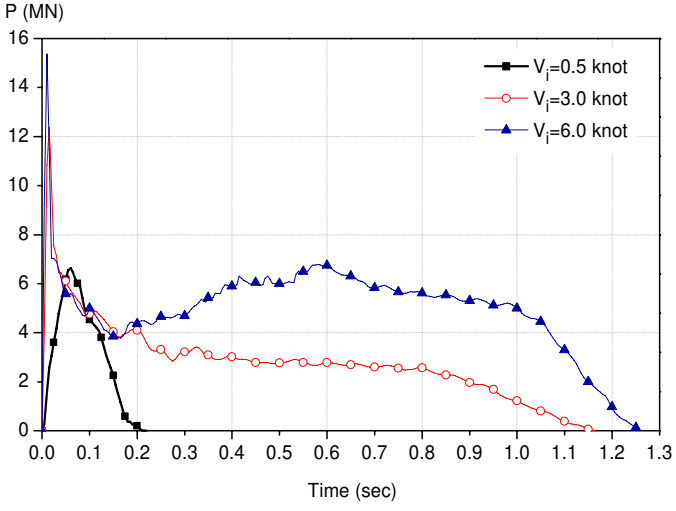

Figure 4.6 Impact force time histories generated by a fully loaded barge impacting a square pier ($\alpha = 0.1$) with different initial velocities

In most cases, the longitudinal truss fails, and the top and bottom plate bulges and folds in front of the intruding pier. During this stage, the resistance force remains more or less constant after reaching the maximum value, which allows a large amount of energy absorption during the pier penetration. Finally, as the motion of the barge begins to changes directions (retreat), the crushing depth reaches its ultimate value and then the impact force begins to decrease.

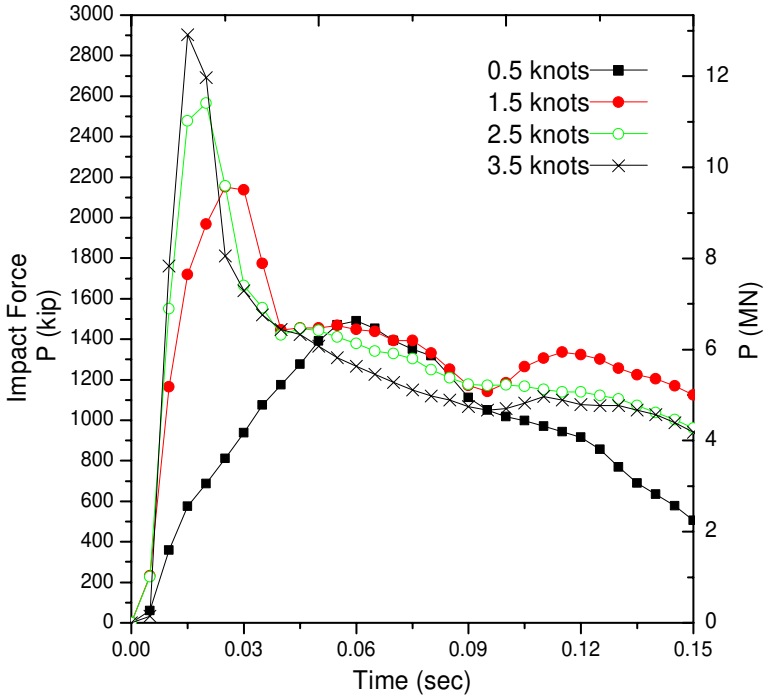

Figure 4.7 Comparison between maximum impact forces generated by a fully loaded barge impacting a square pier ($\alpha = 0.1$)

4.6 Impact Loading Function

The maximum impact force P_{max} is sensitive to the sampling rate in both numerical analyses and experiments. During Woisin's ship collision experiments, the exact values of P_{max} were difficult to obtain due to electronic measuring difficulties [27]. Woisin estimated that the maximum magnitude was, roughly, twice the mean value of the impact

force. In the FE simulations of this study, the sampling frequency is 200 Hz. Figure 4.8 compares the force time-histories generated by different data filters of the program Taurus [37].

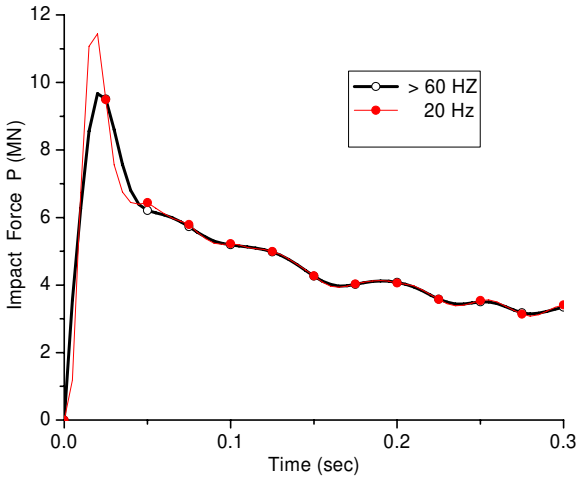

Figure 4.8 The impact forces obtained using different data sampling rate

As mentioned in the previous section, barge flotillas usually travel at a speed between 1.03 and 3.09 m/s (2.0 to 6.0 knots). Within the practical velocity range, the equations of the maximum force, average impact force and impact time duration for square piers, developed by means of multivariable polynomial regressions, are:

$$P_{\max} = -5.04 + 52.78\alpha - 23.59\alpha^2 + 2.71I_i + 3.33V_i \tag{4.27}$$

$$\overline{P} = 4.57 + 5.15\alpha + 3.12\alpha^2 - 0.57I_i - 0.24V_i \tag{4.28}$$

$$t_d = 0.332 - 0.586\alpha + 0.216I_i \tag{4.29}$$

For circular piers, the corresponding regression formulas are:

$$P_{\max} = 2.85 + 4.30\alpha - 2.60\alpha^2 + 0.51I_i + 1.09V_i \tag{4.30}$$

$$\overline{P} = P_{\max}(0.543 - 0.063\alpha - 0.028I_i) \tag{4.31}$$

$$t_d = 0.118 - 0.048\alpha + 0.323I_i \tag{4.32}$$

where the initial momentum I_i is in MN, the approaching velocity of barge V_i is in m/s and the pier to barge width ratio $\alpha = 0.1 - 1.0$.

The above equations correlate very well with the FE simulations. They may be used for a rapid estimation of the impact force generated by a single barge. Finally, the impact duration t_d is satisfied with:

$$\frac{I_i}{\overline{P}} = \frac{m_B V_i}{\overline{P}} \le t_d \le \frac{2I_i}{\overline{P}} = \frac{2m_B V_i}{\overline{P}}. \tag{4.33}$$

4.7 Comparison between Different Methods

According to Woisin's study [27], the average impact force $\overline{P}$ is equal to $0.5P_{\max}$. Based on the FE simulations, it may be asserted that $\overline{P} \approx 0.5P_{\max}$ and $0.7P_{\max}$ for square and circular piers, respectively.

Compared to the FE simulations, the AASHTO formulas generate a larger damage depth but a smaller impact force for wide square piers ($\alpha \ge 0.3$). Regarding circular piers, the FE simulations and the AASHTO method agree well in prediction of barge damage depth, but the AASHTO method overestimates the impact forces.

4.8 Summary

In this chapter, the common characteristics of barge-pier collisions were identified. Both the pier size and shape, which are ignored by the AASHTO specifications, greatly affect barge-pier impact processes. The influence of α is more significant on square piers than on circular piers. Since the kinetic impact energy of barges is greater than 0.5 MJ for most cases, the impact force drops to a much smaller level in a short time interval, and therefore, a major part of the impact energy is dissipated through the plastic

deformation of the barge bow structure. This feature indicates that the impact forces do not increase infinitely as the kinetic impact energy increases. In fact, the average impact forces vary only in a narrow range, which will be further exhibited in the following chapters.

A set of regression formulas have been developed to predict the maximum impact forces, the average impact forces, and the impact time duration for single barges. All of the analytical derivations correlate well with the FE simulations. In chapter 7, an analytical method for predicting the average impact forces of single barges is provided.

Chapter 5 Influence of Pier Flexibility

Chapter 4 discussed the impact forces generated by barges impacting rigid piers. While infinite rigidity cannot be achieved in practice, such assumptions are justified in many instances. However, there is little guidance provided in technical literature concerning the effects of rigidity on the impact forces and dynamic response of bridge piers. There is not a practical method to justify the assumption of infinite rigidity for a given pier. Also, no such guidance exists that establishes the stage(s) of impact at which such effects become significant.

This chapter delineates the influence of pier flexibility on barge-pier collisions, and special emphasis is placed on the effects that pier flexibility has upon the impact force and energy dissipation. The main objective of this research is to provide design techniques to ensure that the barge fails rather than the bridge pier during a collision event. Therefore, the events in which a barge breaks the bridge piers are not considered herein.

5.1 Energy Distribution in a Simple Mass-Spring System

Other variations of the general barge-pier collision model, which are discussed later in this chapter, provide insight into the overall characteristics of barge-pier collisions. For example, a 2-DOF spring-mass system, as shown in Figure 5.1, is studied without considering the energy loss. This highly idealized model provides a simplified medium for observing the nature of the energy distribution of the barge-pier impact system. Although the 2-DOF spring-mass system is not consistent with the impact

mechanics between barges and piers, it is useful for obtaining insight into the energy distribution during a barge-pier collision event.

Suppose the spring-mass system of Figure 5.1 has two rigid masses m_1 and m_2, and two weightless springs with stiffness coefficients k_1 and k_2, respectively. The two generalized coordinates that completely define the motion of the system are x_1 and x_2. Therefore, there will be two Lagrangian equations:

$$\frac{d}{dt}\left(\frac{\partial k_e}{\partial \dot{x}_i}\right) - \frac{\partial k_e}{\partial x_i} + \frac{\partial p_e}{\partial x_i} = 0\,, \quad i = 1,2 \tag{5.1}$$

$$k_e = \frac{1}{2} m_1 \dot{x}_1^2 + \frac{1}{2} m_2 \dot{x}_2^2 \tag{5.2}$$

$$p_e = \frac{1}{2} k_1 \left(x_1 - x_2\right)^2 + \frac{1}{2} k_2 x_2^2 \tag{5.3}$$

where k_e and p_e are the kinetic energy and the potential energy of the system, respectively.

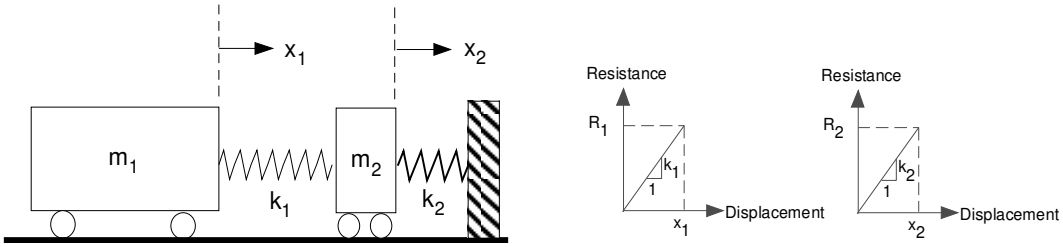

Figure 5.1 2-DOF system with linear springs

The equation of motion for the independent variables x_1 and x_2 are obtained by substituting the expressions given by Eqs. (5.2) and (5.3) into Eq. (5.1) results in:

$$\begin{pmatrix} m_1 & 0 \\ 0 & m_2 \end{pmatrix} \begin{Bmatrix} \ddot{x}_1 \\ \ddot{x}_2 \end{Bmatrix} + \begin{pmatrix} k_1 & -k_1 \\ -k_1 & k_1 + k_2 \end{pmatrix} \begin{Bmatrix} x_1 \\ x_2 \end{Bmatrix} = 0 \tag{5.4}$$

It follows that the characteristic determinant is given by:

$$\begin{vmatrix} k_1 - m_1\lambda & -k_1 \\ -k_1 & k_1 + k_2 - m_2\lambda \end{vmatrix} = 0, \tag{5.5}$$

or

$$m_1 m_2 \lambda^2 - \left[m_1 \left(k_1 + k_2 \right) + m_2 k_1 \right] \lambda + k_1 k_2 = 0. \tag{5.6}$$

Thus, the roots (eigenvalues) are given by:

$$\lambda_{1,2} = \frac{m_1(k_1 + k_2) + m_2 k_1 \mp \sqrt{\left[m_1(k_1 + k_2) + m_2 k_1 \right]^2 - 4 m_1 m_2 k_1 k_2}}{2 m_1 m_2} \tag{5.7}$$

Corresponding to each eigenvalue λ_i is an eigenvector $\{A\}_i$, representing the displacement configuration of the system for the *i*th mode. However only one eigenvector is of interest herein, such that $x_1 / x_2 > 0$, and:

$$\frac{A_1}{A_2} = \frac{k_1}{k_1 - m_1 \lambda_1} \tag{5.8}$$

Letting $\xi = k_1 / k_2$ and $\eta = m_1 / m_2$, the expansion of Eq. (5.8) yields:

$$\frac{A_1}{A_2} = \frac{2}{1 - \eta\left(1 + \frac{1}{\xi} \right) + \sqrt{\left[\eta\left(1 + \frac{1}{\xi} \right) + 1 \right]^2 - 4\frac{\eta}{\xi}}} \tag{5.9}$$

The ratio of the net displacements of the two masses is given by:

$$\frac{\Delta_1}{\Delta_2} = \frac{A_1 - A_2}{A_2} = \frac{2}{1 - \eta\left(1 + \frac{1}{\xi} \right) + \sqrt{\left[\eta\left(1 + \frac{1}{\xi} \right) - 1 \right]^2 + 4\frac{\eta}{\xi}}} - 1 \tag{5.10}$$

and the ratio of the energy stored by the two springs is given by:

$$\frac{E_1}{E_2}=\frac{k_1\Delta_1^2}{k_2\Delta_1^2}=\zeta\left[\frac{2}{1-\eta\left(1+\frac{1}{\xi}\right)+\sqrt{\left[\eta\left(1+\frac{1}{\xi}\right)-1\right]^2+4\frac{\eta}{\xi}}}-1\right]^2 \tag{5.11}$$

Figure 5.2 contains the plots of the ratios defined in Eqs. (5.10) and (5.11) as functions of the mass ratio η and stiffness ratio ξ. It is apparent that the mass ratio η is not as influential as the stiffness ratio ξ, and the difference between the curves, primarily due to η, is negligible when $\eta > 5$. The energy-partitioning pattern heavily depends on the stiffness coefficients rather than the masses. Most of the kinetic energy is absorbed by the weaker spring if the stiffness ratio $\xi \le 0.1$, and the corresponding oscillator has a much larger deformation. In practice, piers of highway bridges are much stiffer than steel barges, and the respective stiffness ratios ξ are usually less than 1/10 (barge / bridge).

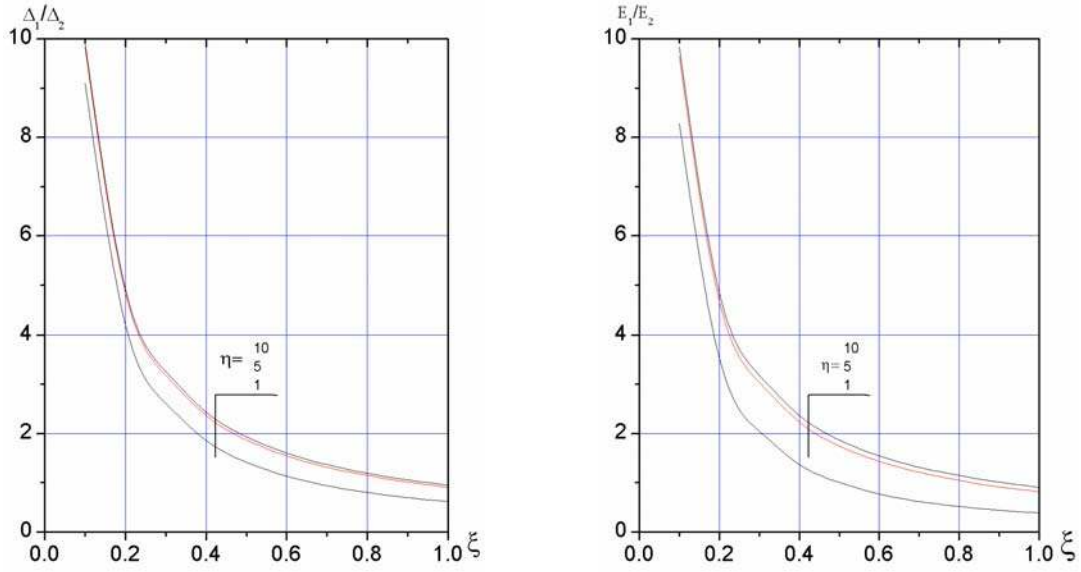

(a) (b)

Figure 5.2 Displacement ratio and energy partition ratio vs. stiffness ratio ξ for the 2-D system: (a) displacement; (b) energy partition

Through experimentation, Meir-Dornberg [11] derived the following force-displacement relationship for barges:

$$P(a_B) = \begin{cases} 60a_B, & a_B < 0.1 \\ 6 + 1.6a_B, & a_B \geq 0.1 \end{cases} \tag{5.12}$$

where the barge damage length a_B is in meters, and the impact force P is in MN.

In order to describe a more general barge crushing problem, the spring stiffness k_1 in Fig 5.1 is replaced with Meir-Dornberg's bilinear equation Eq. (5.12). That is, the system response can be viewed as linear in different stages.

The energy absorbed by the barge during impact can be expressed as:

$$W = \int_0^{a_B} P(x)dx \tag{5.13}$$

Assuming the barge damage depth $a_B \geq 0.1$ m and substituting Eq. (5.12) into Eq. (5.13) results in the following expression:

$$W = 6a_B + 0.8a_B^2 - 0.578 \tag{5.14}$$

where W is in MJ, and a_B is in meters.

According to Hooke's law, the displacement of spring 2 (pier stiffness) is given by:

$$x_2 = \frac{P(\Delta)}{k_2} \tag{5.15}$$

so that, the energy absorbed by spring 2 is:

$$E_2 = \frac{1}{2}\frac{P^2(\Delta)}{k_2} \tag{5.16}$$

Dividing Eq. (5.14) by Eq. (5.16), the energy ratio can be expressed as:

$$\frac{W}{E_2} = \frac{12a_B + 1.6a_B^2 - 1.156}{\left(1 + 1.6a_B\right)^2} \times 10^{-6} k_2 \tag{5.17}$$

where the ratio W / E_2 is dimensionless, the barge damage depth a_B is in meters, and the spring stiffness k_2 is in N/m.

For further physical interpretation of the above results, consider an example of barge-pier collisions.

Example: An actual reinforced concrete pier is idealized as a vertical beam with three different support conditions, as shown in Figure 5.3. The values of stiffness *k* are presented in Table 5.1.

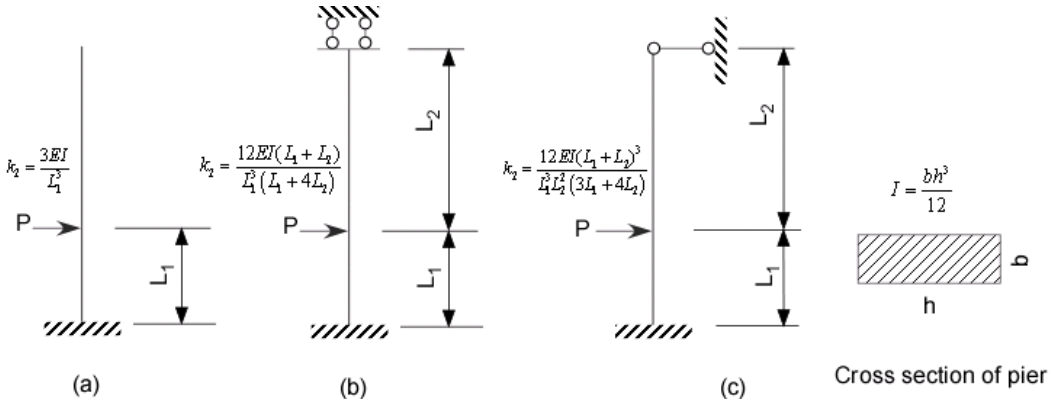

Figure 5.3 Idealized pier models with different boundatry conditions

Table 5.1. Pier dimensions and stiffness coefficients corresponding to the boundary conditions shown in Figure 5.3

L_1 (m)	L_2 (m)	b (m)	h (m)	Pier type	k_2 (N/m)
14	16	2	6	(a)	9.77×10^8
				(b)	1.50×10^9
				(c)	3.89×10^9

Solution: Substitution of the known parameters into Eq. (5.17) results in a plot of the energy ratio W / E_2 versus the barge damage length a_B, as shown in Figure 5.4.

Compared with piers in reality, the piers in this example are only moderately stiff. Figure 5.4 confirms that most of the impact energy is dissipated by the barge in all three cases. Therefore, barges may be regarded as absorbing all of the impact energy during a barge-pier collision event unless the impacted pier is very slender.

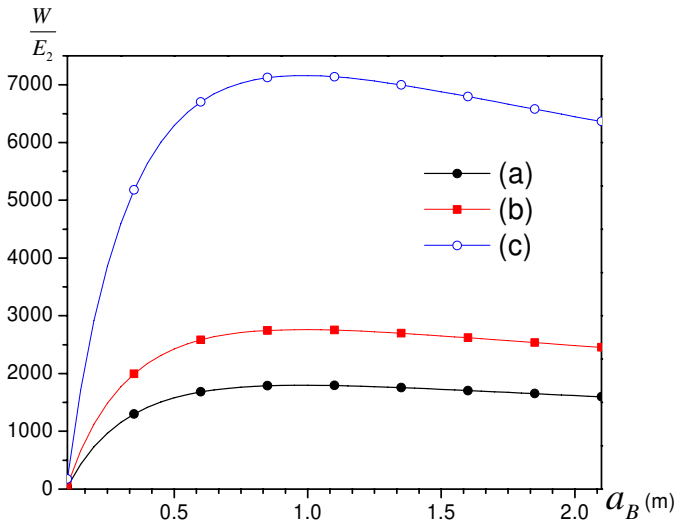

Figure 5.4 Energy distribution ratio vs. barge damage depth for the ideal piers

5.2 Impact Force Dependency on Pier Stiffness

In this section, the influence of pier flexibility on impact forces is investigated using FE simulations. The deformation of the pier shown in Figure 5.5 may be regarded as being composed of three parts: displacements of the contact point, pier-top, and pier-foundation. The structural interaction between the soil and the pier is not addressed in detail in this chapter, but Chapter 10 provides an example that includes the soil properties.

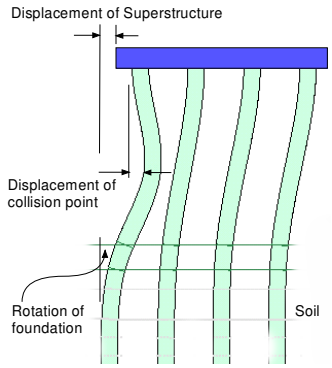

Figure 5.5 Deformation shape of a pier subjected to barge impact

Because the interaction between a barge and a pier during impact occurs only at the contact area, the relative stiffness of the pier affects the impact force as well as the time duration of the impact. In order to simplify the discussion, an idealized barge-pier collision system is used. As shown in Figure 5.6, the system consists of a fully loaded barge and an impacting body with a spring. The simulations have only two variables: barge velocity V_i and spring constant k. For brevity, the pier width is assumed as a constant, 1.07 m ($\alpha = 0.1$). As pointed out in Chapter 4, the size of the contact area affects the impact forces during a barge-pier collision event. A detailed discussion of the barge stiffness is deferred to Chapter 7.

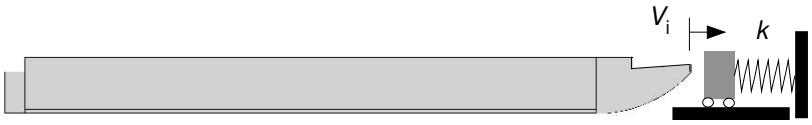

Figure 5.6 Simplified barge-pier collision model

The impact simulation results are presented in Table 5.2. It can be seen from this table that the stiffness of the pier is ineffectual to the impact forces unless k is very small (this case is shaded in the table). From static calculations, the elastic stiffness of barge bows is approximately 70 MN/m corresponding to the pier to barge width ratio $\alpha = 0.1$.

Therefore, the influence of pier stiffness on the impact forces may be ignored if the pier is stiffer than the barge bow, namely $k_p \geq k_{cr}$, where k_p is the pier stiffness corresponding to the translational displacement of the collision point, and k_{cr} is given by:

$$k_{cr} = 46 + 6465\alpha - 2701\alpha^2 \quad \text{for rectangular piers} \tag{5.18}$$

$$k_{cr} = 473 + 453\alpha - 160\alpha^2 \quad \text{for circular piers} \tag{5.19}$$

where $\alpha = 0.05 \sim 1.0$ is the pier to barge width ratio; k_p is in MN.

Eqs. (5.18) and (5.19) originate from extensive FE simulations. If $k_p < k_{cr}$, the influence of the pier stiffness should be taken into account in the determination of the impact forces and the impact time duration. Otherwise, the pier can be assumed to be rigid.

Table 5.2. Summary of a fully loaded barge impacting a square body ($\alpha = 0.1$)

V_i (m/s)	k (MN/m)	Impact force (MN)		Duration t_d (s)	Pier max displacement $\Delta_{\max}$ (cm)	Damage depth a_B (cm)
		$P_{\max}$	$\frac{\bar{P}}{P_{\max}}$			
2	70.06	10.28	0.45	0.61	9.8	7.92
	350.26	10.28	0.36	0.61	8.7	11.81
	1571.28	10.30	0.37	0.60	8.4	11.96
	2802.04	10.31	0.37	0.60	2.4	11.98
4	70.06	13.80	0.23	1.43	2.3	72.44
	350.26	13.80	0.22	1.43	2.3	75.13
	1571.28	13.80	0.22	1.40	0.6	75.52
	2802.04	13.80	0.22	1.40	0.6	75.80
6	70.06	15.30	0.32	1.28	0.6	146.76
	350.26	15.30	0.31	1.29	0.4	145.26
	1571.28	15.30	0.32	1.28	0.4	145.49
	2802.04	15.30	0.32	1.28	0.4	144.63

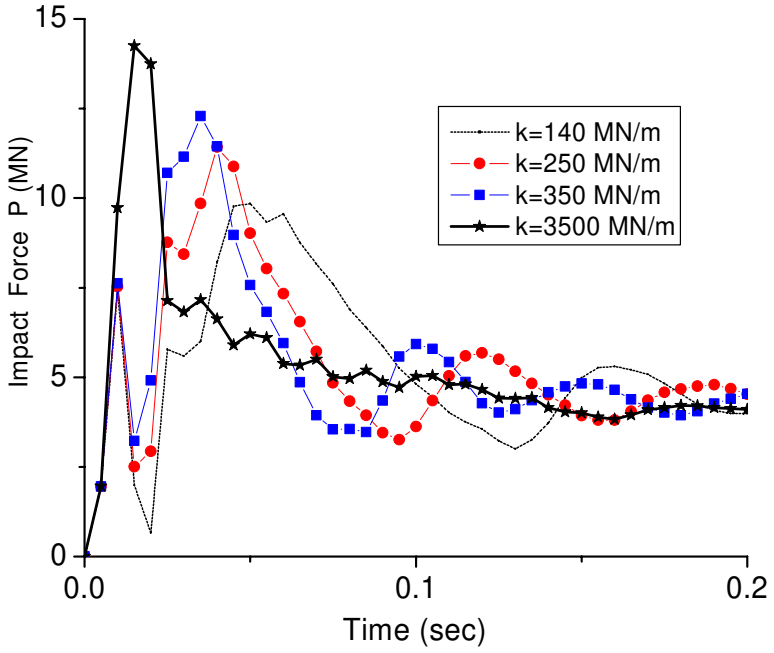

Figure 5.7 Impact force time-histories generated by a fully loaded barge impacting piers with different stiffness

Figure 5.7 shows the impact force time-histories of piers with various stiffness, which is generated by a fully loaded barge ($V_i = 2.06$ m/s) impacting a pier ($\alpha = 0.1$). From this figure, it can be seen that the variations of the pier stiffness affect the maximum impact forces in a short period (< 0.25 seconds). The impact force curves approach the same value as time increases due to the greatly decreased resistance of the barge as the pier entry deepens.

5.3 Summary

In general, the structural response to impact can be divided into two stages: a very brief contact stage followed by a global structural deformation stage. The first stage begins with a severe velocity discontinuity in the contact region, and is characterized by a local velocity change together with local contact dissipation. In the second stage, a

restoring instant exists at which the behavior of the stiffer structure transforms from an energy dissipation state to a non-dissipation state, and the total energy dissipated by this structure is termed the restoring energy. The remaining kinetic energy after this restoring instant will be completely dissipated by the weaker structure, if the weaker structure exhibits no deformation-hardening. For a structure with constant load-carrying capacity during its large plastic deformation, the initial velocity will not affect the energy partitioning. However, an increase of the relative mass of the impinging structure will cause the energy-partitioning pattern to approach an elementary static condition, that is, the structure with lower strength will dissipate all the input energy.

The analytical and numerical results show that the influence of pier flexibility on impact forces is not significant when the translational stiffness coefficient at the collision point of the pier is large enough. In addition, most of the kinetic impact energy is dissipated by the barge (weaker structure) as long as the pier is more than five times stiffer than the barge. Unless a pier is very flexible, it consumes a small portion of impact energy and may be assumed to be infinitely rigid as well as infinitely massive. Moreover, the initial impact velocity does not affect the energy partitioning.

For most practical cases, the impact forces are not sensitive to pier stiffness variations as long as the stiffness is within the normal range. Generally, the impact energy dissipation is dominated by the deformation of the barge structure instead of the pier. The effect of pier flexibility may be conservatively neglected for design purposes [10]. Whenever possible, it is preferable to use rigid piers for dynamic simulations because such elements are invariably more efficient in terms of CPU calculation time. Therefore, all of the piers in this study are assumed to be rigid unless otherwise specified.

Chapter 6 Multi-Barge Flotilla Impact Simulations

In Chapter 4, FE simulations of single barges impacting bridge piers are discussed. In reality, the organized inland-water cargo movement is by means of flotillas, in which a number of barges are tied together and moved as one unit. For that reason, the study of impact forces generated by multi-barge flotillas is more significant than the study of impact forces generated from single-barge collisions. According to Whitney [10], the AASHTO method [9] is not adequate for barge flotillas. Until now few technical publications have discussed the flotilla-bridge collision problems.

To investigate the impact forces generated by multi-barge flotillas, this chapter describes a series of crash simulations that were conducted using the program LS-DYNA [14]. Due to the large computation time needed to simulate multi-barge collisions with piers, only a string (column) of barges is considered herein. This chapter focuses on some fundamental features of barge flotilla to pier impacts. An analytical model for multi-barge flotillas is addressed in Chapter 9.

6.1 Flotilla Configurations

A rake barge, built with one end sloped or raked at a sharp angle to form a bow, is shown in Figure 3.1. The slanted bow of this type of barge allows easier movement through water as compared to square-ended, box hopper barges. Rake barges are used primarily as lead barges in a flotilla and are also placed in the back of flotillas to permit towboat pilots to slow and turn the tow more quickly. As shown in Figure 6.1, box barges, 61 m (200 ft) long and 10.7 m (35 ft) wide, are more difficult to push. As opposed to filling the role of lead barges, box barges, are often used to connect rake

barges in a flotilla. Barge tows (flotillas) often include a mixture of both kinds of barges. This configuration takes advantage of both the storage capacity of box hopper barges and the fuel efficiency of raked hopper barges.

(a) (b)

Figure 6.1 Box barge: (a) an actual box barge; (b) the FE model of box barges

Figure 6.2 shows a 12-barge tow traveling on the Ohio River in the United States. A typical 15-barge flotilla is built with three rakes abreast facing forward and leading each column, and three rakes abreast facing rearward at the stern of each string when loaded. If one column contains only two barges, two loaded rakes are placed back to back (box ends together) to form a unit; otherwise box barges are often put between the rake barges, creating a multi-piece unit. Although barge flotillas are not entirely composed of one barge size or type, the vast majority of barges in a given flotilla generally consist of mostly the same barge size and type. The standardized JH, 10.7 m (35 ft) wide and 61 m (200ft) long, is the most widely used barge type in the U.S. for inland waterway barge operations [10]. Figure 6.3 is a sketch of a typical 15-barge tow.

The barge number in a flotilla is restricted due to narrow channels and limited due to lengths and widths allowed inside of lock chambers. The U.S. Army Corps of Engineers operates 275 lock chambers, which are generally 33.5 m (110 ft) wide, and either 182.9 m (600 ft) or 365.8 m (1200 ft) long [4]. The most typical tow size through

these locks is three barges wide and five long. The smaller tributaries, such as the Alabama River, contain locks that are 25.6 m (84 ft) wide and 182.9 m (600 ft) long, which can support tows of two-barge width and length. A tow of fifteen JHs that are lashed together, three wide and five long, is the maximum configuration that is presented in this study.

Figure 6.2 A 12-barge flotilla traveling on the Ohio River

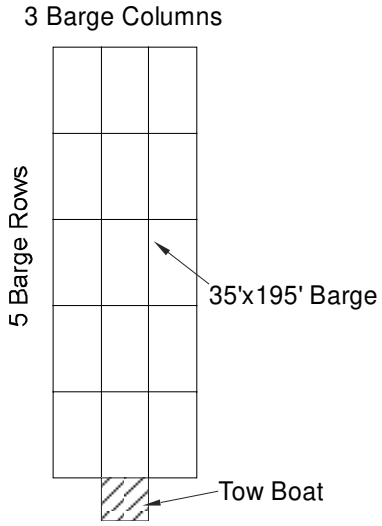

Figure 6.3 A typical 15-barge flotilla layout

The connection between barges is conventionally comprised of steel wire ropes as shown in Figures 6.4 and 6.5. The mechanical properties of the wire ropes are available

in most steel handbooks. Some common wire ropes used for lashing barges are presented in Table 6.1 [38]. The FE models of flotillas, an extension of the JH model, are comprised of single-barge models that are tied together using the cable elements described in Chapter 3.

Figure 6.4 Wire ropes connecting barges in a multi-barge flotilla

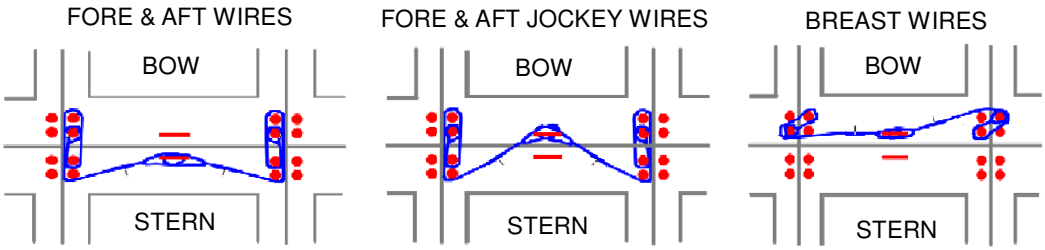

Figure 6.5 **Barge connection methods**

Table 6.1. Stainless steel wire ropes used for lashing barges

Cable diameter	Minimum breaking strength (kips)
1/2" (0.013 m)	20.5 (91.2 KN)
3/4" (0.019 m)	49.6 (220.6 KN)
1" (0.025 m)	89.8 (339.5 KN)

As previously mentioned, FE simulations of multi-barge flotillas impacting bridges are prohibitively expensive with respect to both model generation and computation time. For example, one simulation of a 4-barge flotilla impact requires more

than one-hundred hours. Hence, this chapter only pertains to a single-column flotilla, and multi-column flotillas are discussed in Chapter 9.

For convenience of discussion, an n-barge column flotilla will be designated as FLn. For example, FL3 denotes a 3-barge column.

6.2 Simulation of a 2-Barge Column

As shown in Figure 6.6, the FL2 model consists of two raked barges, oriented back to back. Crash simulations of a FL2 impinging perpendicularly upon a series of square and circular piers with different sizes ($\alpha = 0.1 - 1.1$) were conducted using the program LS-DYNA970. Both the mass and velocity of FL2 vary within the respective practical ranges: $V_i = 0.51$ to 3.09 m/s (1 to 6 knots), and $m_B = 861.8$ to 3447.3 metric tons.

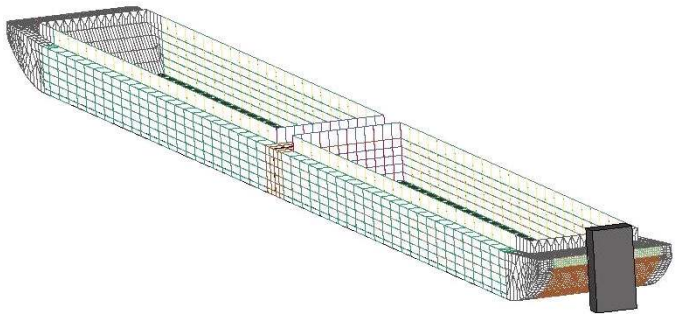

Figure 6.6 FE model of a 2-barge column (FL2)

Figure 6.7 shows the time–histories for a fully loaded FL2 (3447.3 metric tons) impacting a square pier ($\alpha = 0.1$) under several different velocities. From this figure, it can be seen that the maximum impact forces sharply decrease within 0.1 seconds regardless of their initial magnitudes. Then, the impact forces range between 3 MN and 6 MN for most of the remaining event. The impact time duration t_d is dependent on, but

not simply proportional to, the initial impact velocity. A larger velocity prolongs the whole impact process. Moreover, the impact time t_d increases at an accelerating rate as V_i approaches 1.54 m/s (3.0 knots), and t_d increases at a decelerating rate as V_i becomes greater and greater, relative to 1.54 m/s. This phenomenon signifies that the average impact forces vary with the impact velocities. Similar to single barge impacts, large plastic deformations occur as the impact velocity $V_i \geq 1.54$ m/s due to the accompanying high impact energy. Under these circumstances, the plastic deformation of the barge bow dominates the impact process.

According to the impulse-momentum law, the impulse of the system is:

$$\int_0^{t_d} P(t)dt = I(t_d) - I(0) \tag{6.1}$$

or

$$\bar{P}t_d = m_B \sum_{j=1}^{2} \left(V_j(t_d) - V_i \right) \tag{6.2}$$

where $\bar{P}$ is the average impact force, m_B is the mass of a single barge, t_d is the impact duration, V_i is the initial velocity of the flotilla, and $V_j(t_d)$ is the velocity of *the j*th barge after impact.

From Eq (6.2) and Figure 6.7, it is apparent that the barges within the FL2 have different velocities after impact. Consequently, the two barges experience certain interactions between one another during the impact. The coefficient of restitution, used as an indicator of single-barge impacts in Chapter 4, is not appropriate for describing multi-barge flotilla impacts.

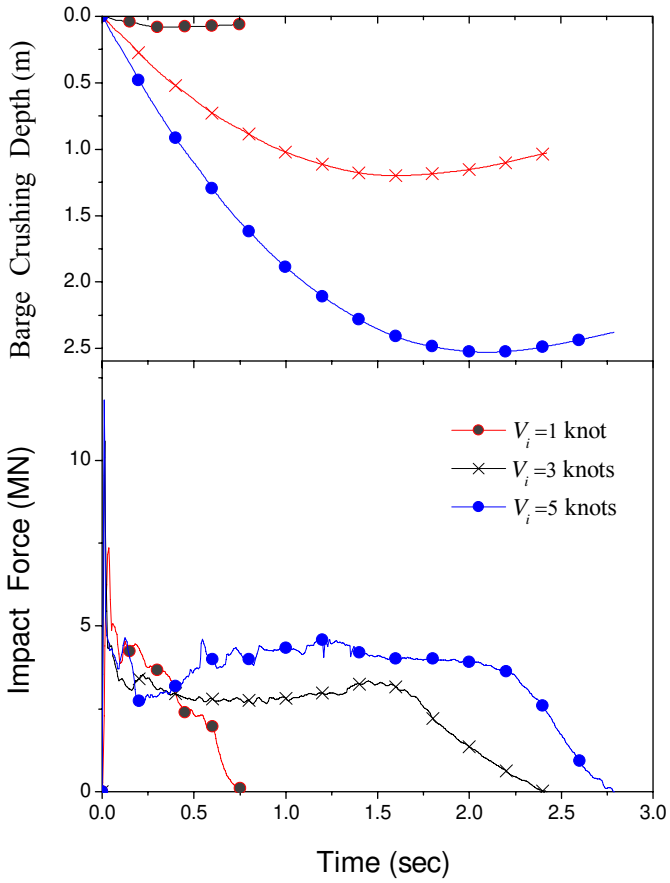

Figure 6.7 Time histories of the impact force and barge damage depth caused by a fully loaded FL2 impacting a square pier ($\alpha = 0.1$) with different initial velocities

Table 6.2. Summary of the simulations of a fully loaded FL2 impacting a square rigid pier ($\alpha = 0.1$)

Velocity V_i (knot)	Momentum I_i (MNs)	Impact force (MN)			Impact Duration t_d (s)	Damage depth a_B (m)
		$P_{\max}$	$\frac{\overline{P}_{1/2}}{P_{\max}}$	$\frac{\overline{P}}{P_{\max}}$		
1.0	1.77	7.36	0.56	0.39	0.77	0.06
2.0	3.55	8.91	0.37	0.29	1.58	0.42
3.0	5.32	10.58	0.29	0.24	2.43	1.03
4.0	7.09	11.52	0.31	0.26	2.69	1.68
5.0	8.87	11.83	0.34	0.30	2.79	2.38

Note: (a) 1 knot = 0.514 m/s.

(b) $\overline{P}_{1/2}$ = the average impact force during the first $0.5t_d$.

(c) $\overline{P}$ = the average impact force during t_d .

Table 6.2 compares some important results of the simulations. The impact force plateaus in Figure 6.7 are approximately equal to the corresponding mean force $\overline{P}_{1/2}\,(=0.3\sim0.4P_{\max})$ in Table 6.1. The upper bound of the plateaus is 6 MN, which is the same with the constant in the AASHTO formulas [9]. Additionally, the average force values, $\overline{P}_{1/2}$ and $\overline{P}$, are very close except for the case with a very small velocity ($V_i = 1.0$ knot).

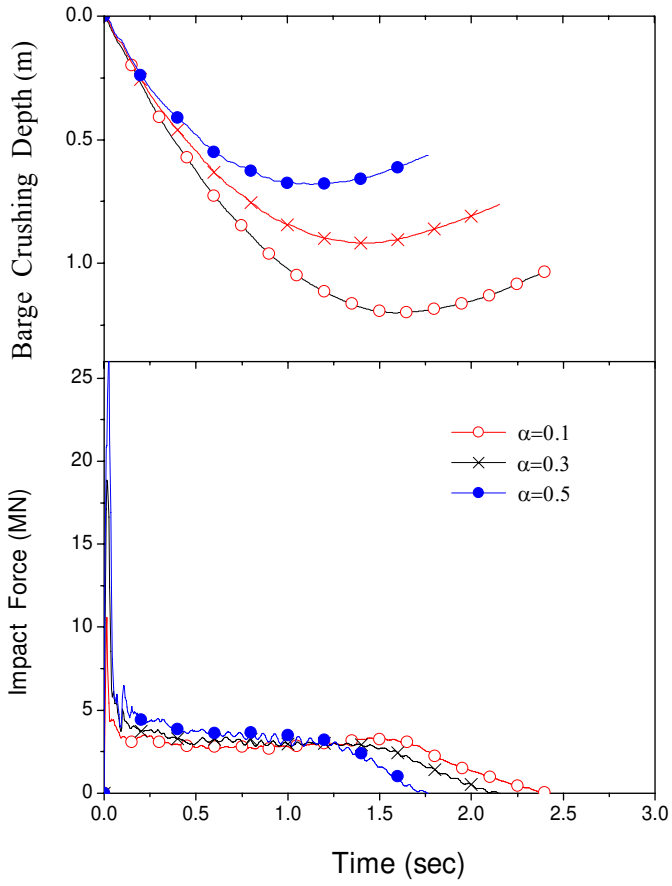

Figure 6.8 Time histories of the impact force and barge crushing depth generated by a fully loaded FL2 impacting a set of square piers with an initial velocity V_i=3.5 knots

Similar to single-barges, the impact force of multi-barge flotillas is also dependent on the pier shape and size. Figure 6.8 presents the time histories of a fully loaded FL2

impacting different square piers ($\alpha = 0.1$ to 0.5) with an initial velocity of $V_i = 1.8$ m/s (3.5 knots). As indicated by Figure 6.8, an increase in α is conducive to an increase in the maximum impact force $P_{\max}$. Since the resistance of a barge becomes stable after the plastic deformation develops, the width of the impacted pier does not significantly affect the resulting force plateaus as long as the initial impact energy is large enough.

Using the data obtained from 200 FE simulations of a FL2 impacting square and circular piers, the following regression formulas were derived. These formulas, applicable to FL2s, calculate the maximum impact force, average impact force, and impact time duration, respectively.

For square piers:

$$P_{\max} = -7.274 + 45.233\alpha - 21.029\alpha^2 + 0.798I_i + 7.052V_i \tag{6.3}$$

$$\overline{P} = 2.480 + 6.003\alpha - 0.147\alpha^2 - 0.209I_i + 0.088V_i \tag{6.4}$$

$$t_d = 0.650 - 1.468\alpha + 0.491\alpha^2 + 0.236I_i + 0.060V_i \tag{6.5}$$

and for circular piers:

$$P_{\max} = 2.074 + 4.343\alpha - 2.798\alpha^2 + 0.234I_i + 0.511V_i \tag{6.6}$$

$$\overline{P} = 1.529 + 1.204\alpha - 0.582\alpha^2 + 0.165I_i + 0.148V_i \tag{6.7}$$

$$t_d = 0.602 - 0.711\alpha + 0.372\alpha^2 + 0.290I_i - 0.006V_i \tag{6.8}$$

where the initial momentum I_i and velocity V_i of a FL2 are in MN and m/s, respectively; and the barge to pier width ratio α is in the range from 0.1 to 1.0.

The correlations between the regression formulas and the FE simulations are good when the initial velocity V_i is between 0.77 m/s (1.5 knots) and 3.09 m/s (6.0 knots).

6.3 Simulation of a 3-Barge Column

A FL3, shown in Figure 6.9, consists of two raked barges and one box barge. The total length of a FL3 is 182.9 m (600 ft). The global response of the FL3 in a collision would be delayed to some extent due to the great length of the flotilla structure as well as the gaps between barges in the column. As an important characteristic of flotilla-pier impacts in general, the global-response delay, results in a decrease of the maximum impact forces that usually occur in the very beginning of collisions.

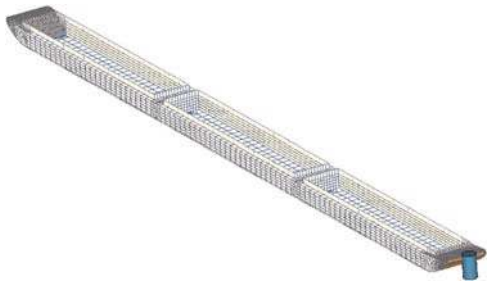

Figure 6.9 FE model of a 3-barge column (FL3)

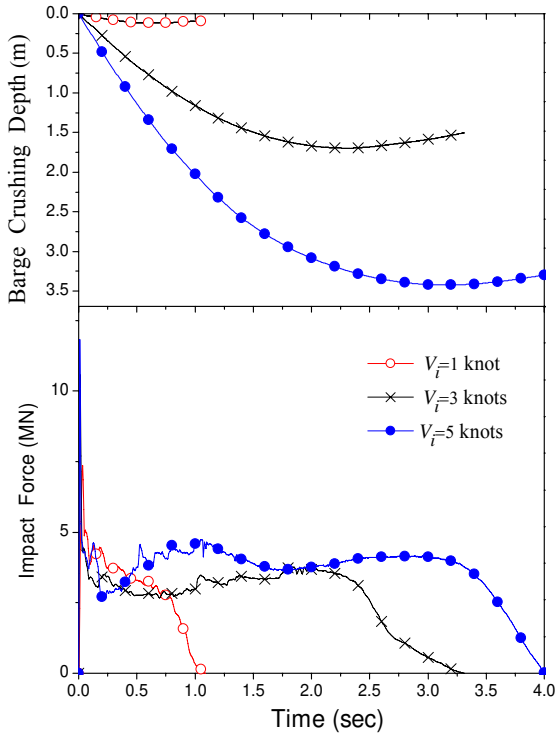

Figure 6.10 Time histories of the impact force and barge crushing depth generated by a fully loaded FL3 impacting a square pier ($\alpha = 0.1$) with different initial velocities

Figure 6.10 shows the time-histories of the barge crushing depth and impact force generated by a fully loaded FL3 (5171 metric tons) impacting a square pier ($\alpha = 0.1$) under different velocities. A comparison of Figures 6.7 and 6.10 shows that the impact forces do not increase proportionally to the number of barges in a given flotilla. The average impact forces for both FL2 and FL3 are close to 5 MN. However, the impact duration increases as the impact energy increases.

A long flotilla, such as a FL3 with distributed mass, acts as a "capacitor" that stores energy through elastic deformation, and as an energy dissipater that absorbs impact energy through plastic deformation. Figure 6.11 shows the deformation time histories of the lead barge and the whole FL3, which impacts a rigid square pier ($\alpha = 0.2$) with an initial velocity of $V_i = 2.06$ m/s (4 knots). As shown in Figure 6.11, the difference between the overall deformation x_2 and the barge crushing distance x_1 becomes larger as time increases. At the end of the impact, the relative difference, $(x_2 - x_1)/x_1$, is as large as 19.8%. The energy dissipated through the deformation of the barge bow can be roughly calculated as:

$$E_1 = \int_0^{x_1(t_d)} P(t)dx = 9.04 \text{ MJ} \tag{6.9}$$

and the total energy loss is

$$E_2 = \int_0^{x_2(t_d)} P(t)dx = 10.84 \text{ MJ} \tag{6.10}$$

so that,

$$\frac{E_1}{E_2} = 83.4\% \tag{6.11}$$

Therefore, the barge bow that contacts the pier and the other components of the

flotilla dissipate the kinetic impact energy together. However, the bow consumes a large part of the total impact energy.

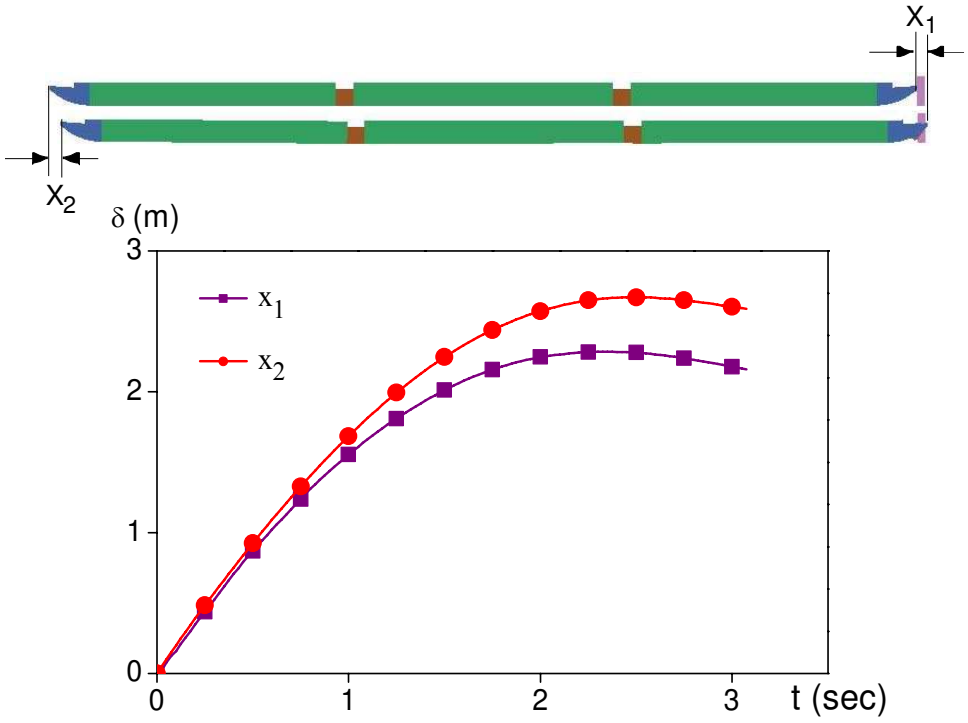

Figure 6.11 Barge deformation time histories of a fully loaded FL3 impacting a square pier ($\alpha = 0.2$) with an initial velocity $V_i = 2.06$ m/s (4 knots)

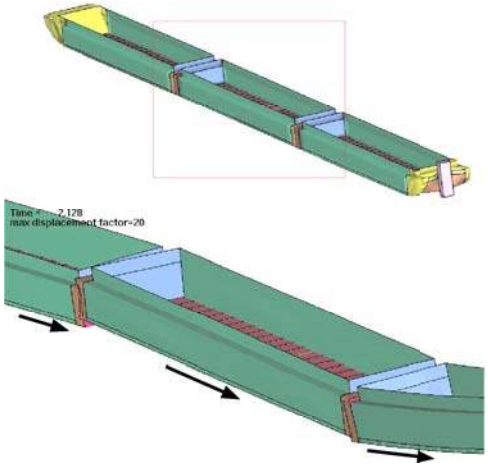

Figure 6.12 Relative vertical motion of barges during impact (magnification factor = 20)

Another interesting finding from the simulations of the FL3-pier collisions is that a relative vertical motion between barges, as shown in Figure 6.12, occurs in addition to longitudinal motions during impact. Note that the displacement magnification factor in Figure 6.12 has a magnitude of twenty. Since the impact process of a multi-barge flotilla lasts several seconds, the vertical displacements of barges would affect impact forces notably as water translates barges up and down in a real collision event. This phenomenon is another important feature of the multi-barge flotilla impacts. In general, this behavior of flotillas acts to decrease the impact intensity on piers.

Using the data from 200 FE simulations of a FL3 impacting square and circular piers, the following regression formulas are derived to calculate the maximum impact force, average impact force, and impact time duration for FL3s, respectively.

For square piers:

$$P_{\max} = -6.952 + 43.934\alpha - 20.393\alpha^2 + 0.951I_i + 5.019V_i \tag{6.12}$$

$$\overline{P} = 2.560 + 5.075\alpha - 0.270\alpha^2 + 0.0344I_i - 0.386V_i \tag{6.13}$$

$$t_d = 0.993 - 2.106\alpha + 0.819\alpha^2 + 0.211I_i + 0.0465V_i \tag{6.14}$$

and for circular piers:

$$P_{\max} = 1.734 + 4.371\alpha - 2.543\alpha^2 + 0.268I_i + 0.351V_i \tag{6.15}$$

$$\overline{P} = 1.276 + 1.479\alpha - 0.698\alpha^2 + 0.197I_i + 0.082V_i \tag{6.16}$$

$$t_d = 1.045 - 1.158\alpha + 0.606\alpha^2 + 0.249I_i - 0.116V_i \tag{6.17}$$

where the initial momentum I_i and velocity V_i of a FL3 are in MN and m/s, respectively; the barge to pier width ratio α is in the range from 0.1 to 1.0.

The correlations between the regression formulas and the FE simulations are good if the initial velocity V_i is in the range between 0.77 m/s (1.5 knots) and 3.09 m/s (6.0 knots).

6.4 Simulation of 4-Barge and 5-Barge Columns

The regression formulas for FL4s and FL5s, and a comparison of the impact characteristics between different flotillas, are presented in this section.

Figure 6.13 FE models for FL4s and FL5s

Figure 6.13 shows the FE models for FL4s and FL5s. Using the data from 200 FE simulations, the following regression formulas are developed for FL4s:

For square piers:

$$P_{\max} = -6.951 + 43.933\alpha - 20.394\alpha^2 + 0.713I_i + 5.02V_i \tag{6.18}$$

$$\overline{P} = 2.073 + 4.284\alpha + 0.159\alpha^2 + 0.095I_i - 0.201V_i \tag{6.19}$$

$$t_d = 1.358 - 2.577\alpha + 0.999\alpha^2 + 0.184I_i + 0.0436V_i \tag{6.20}$$

and for circular piers:

$$P_{\max} = 1.194 + 4.2401\alpha - 1.934\alpha^2 + 0.274I_i + 0.473V_i \tag{6.21}$$

$$\overline{P} = 0.970 + 1.659\alpha - 0.627\alpha^2 + 0.180I_i + 0.221V_i \tag{6.22}$$

$$t_d = 1.478 - 1.515\alpha + 0.721\alpha^2 + 0.195I_i - 0.050V_i . \tag{6.23}$$

From the results of 200 FE simulations, the following regression formulas are developed for FL5s.

For square piers:

$$P_{\max} = -5.215 + 43.514\alpha - 17.301\alpha^2 + 0.404I_i + 4.791V_i \tag{6.24}$$

$$\overline{P} = 1.233 + 5.022\alpha - 0.675\alpha^2 + 0.118I_i + 0.0753V_i \tag{6.25}$$

$$t_d = 2.041 - 3.126\alpha + 1.061\alpha^2 + 0.171I_i - 0.136V_i \tag{6.26}$$

and for circular piers:

$$P_{\max} = 0.718 + 3.875\alpha - 1.25\alpha^2 + 0.290I_i + 0.559V_i \tag{6.27}$$

$$\overline{P} = 0.644 + 1.967\alpha - 0.764\alpha^2 + 0.171I_i + 0.345V_i \tag{6.28}$$

$$t_d = 1.913 - 1.935\alpha + 0.963\alpha^2 + 0.171I_i - 0.106V_i \tag{6.29}$$

where the initial momentum I_i and velocity V_i are in MN and m/s, respectively; the barge to pier width ratio α is in the range from 0.1 to 1.0.

The correlations between the regression formulas and the FE simulations are good if the initial velocity V_i is within the range of 0.77 m/s (1.5 knots) to 3.09 m/s (6.0 knots).

The configuration of a given flotilla affects the dynamic behavior of the system during impact. The main difference between different barge columns impacting the same pier with the same velocity resides in the maximum impact force and, to an even greater

event, the impact time duration. Figure 6.14 compares the time histories of the impact forces generated by different barge columns with the same pier and the same initial velocity. From Figure 6.14, it can be seen that impact force curves of the barge flotillas are similar excepting the maximum impact force and the impact time duration. The lead barge in a column provides the resistance to pier crushing directly; however, other barges provide boundary conditions that constrain the motion of the first barge. Therefore, impact forces on piers are mostly dependent on the strength of the barge bow structure. This is the primary reason that impact forces do not increase proportionally with an increasing number of barges in a flotilla. Similar to a non-hardening plastic spring, the bow absorbs impact energy through deformation while its resisting force remains at a relatively constant level.

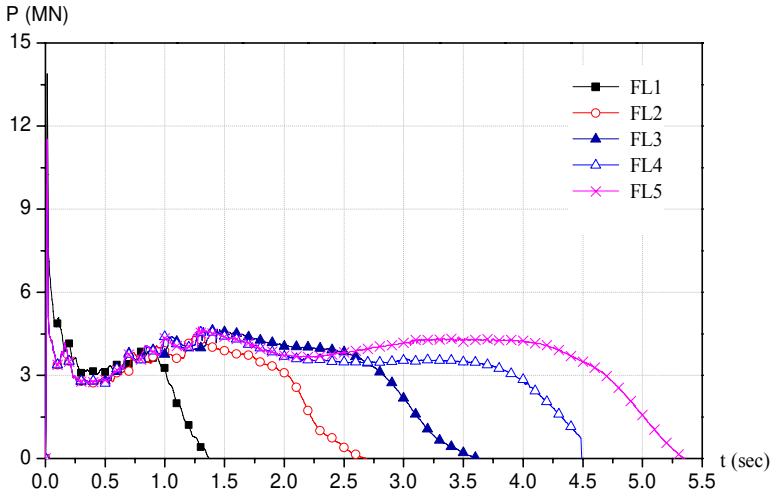

Figure 6.14 Comparison of the impact force time-histories generated by different barge columns impacting a rigid square pier ($\alpha = 0.1$) with a velocity of $V_i = 2.06$ m/s (4 knots)

In order to verify the influence of barge interactions, Table 6.3 compares the results from FL2 and FL1 impacts, where the initial kinetic impact energy is the same.

Obviously, the FL2 produces greater impact duration and crushing depth, but simultaneously, a smaller maximum impact force and average force.

The average impact forces of the barge columns versus the impact kinetic energy are plotted in Figure 6.15, which shows that the pier to barge width ratio α is important in the determination of flotilla impact forces. As α increases, the impact forces increase. When α is large enough, for example $\alpha \geq 0.3$, the average impact force curves of the flotillas tend to converge. The behavior of FL1s (single barges) is different from other configurations (multi-barge flotillas), as indicated by the gaps between the curves in the figures. The crushing speed of the bow also affects the interaction of barges.

Table 6.3 Comparison between a fully loaded FL1 and a half loaded FL2 impacting a square pier ($\alpha = 0.1$)

Velocity V_i (knot)	Impact force (MN)			Duration t_d (s)	Damage depth a_B (m)
	$P_{\max}$	$\frac{\overline{P}_{1/2}}{P_{\max}}$	$\frac{\overline{P}}{P_{\max}}$		
1	6.93	0.61	0.36	0.46	0.02
1	8.48	0.63	0.40	0.35	0.03
2	8.81	0.40	0.29	0.85	0.18
2	10.59	0.50	0.36	0.59	0.12
3	10.54	0.31	0.25	1.27	0.48
3	12.39	0.31	0.23	1.17	0.39
4	11.50	0.26	0.21	1.81	0.92
4	13.88	0.28	0.22	1.38	0.75
5	11.83	0.30	0.25	1.77	1.36
5	14.04	0.34	0.29	1.30	1.05

Note: (a) 1 knot = 0.514 m/s.
(b) $\overline{P}_{1/2}$ = the average impact force during the first $0.5t_d$.
(c) $\overline{P}$ = the average impact force in t_d.
(d) The shaded lines are for the single barge.

For wider piers, the AASHTO method may underestimate the impact forces of multi-barge flotillas within the low impact energy range, and overestimate the impact

forces within the higher impact energy range. For narrow piers, the AASHTO method overestimates the impact forces regardless of the kinetic energy.

Because the impact force curves in Figure 6.15 are similar, envelopes may be used to conservatively estimate the corresponding impact forces. It is interesting to note that the average impact force curves for circular piers are similar to the curve of a

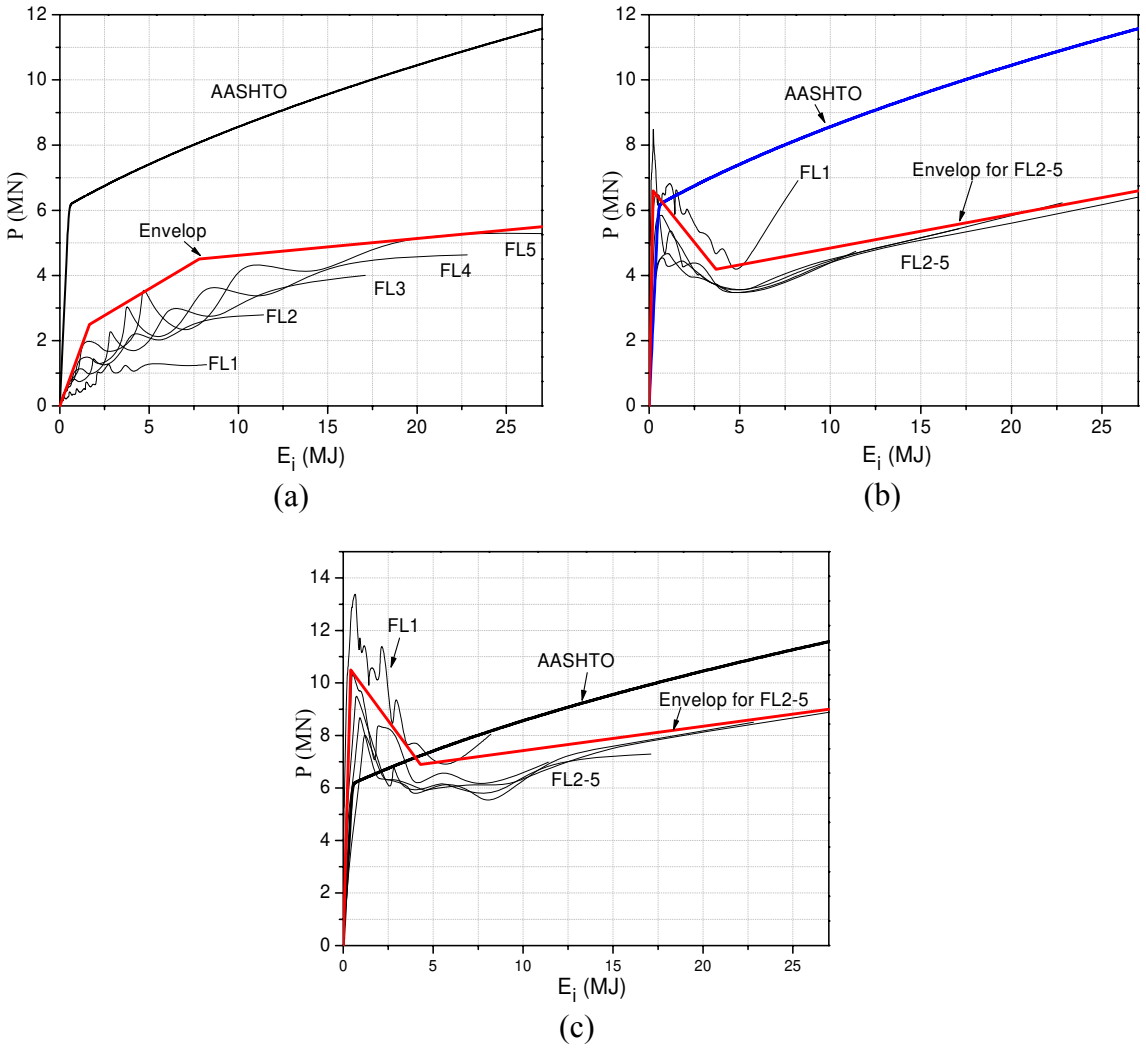

Figure 6.15 Average impact force P versus impact energy E_i for square pier: (a) $\alpha = 0.1$; (b) $\alpha = 0.5$; (c) $\alpha = 0.9$

rectangular pier with $\alpha = 0.1$. The following functions are used to describe the upper bounds of the average impact forces in the energy domain for square piers:

$$\tilde{P}_{\alpha=0.1} = \begin{cases} 1.515E_i & \text{for } E_i \le 1.65 \\ 1.963 + 0.325E_i & \text{for } 1.65 < E_i \le 7.8 \\ 4.094 + 0.52E_i & \text{for } 7.8 < E_i \le 27 \end{cases} \tag{6.30}$$

$$\tilde{P}_{\alpha=0.5} = \begin{cases} 30E_i & \text{for } E_i \le 0.22 \\ 6.752 - 0.693E_i & \text{for } 0.22 < E_i \le 3.7 \\ 3.807 + 0.103E_i & \text{for } 3.7 < E_i \le 27 \end{cases} \tag{6.31}$$

$$\tilde{P}_{\alpha=0.9} = \begin{cases} 25E_i & \text{for } E_i \le 0.42 \\ 10.89 - 0.928E_i & \text{for } 0.42 < E_i \le 4.3 \\ 6.502 + 0.093E_i & \text{for } 4.3 < E_i \le 27 \end{cases} \tag{6.32}$$

where the upper bound of the average impact forces for square piers , $\tilde{P}_\alpha$, is in MN, and the initial kinetic energy of barge columns (2 - 5 barges), E_i ,is in MJ.

6.5 Summary

The most important features of multi-barge flotilla impacts have been discussed in this chapter. The interactions between barges in a multi-barge flotilla influence the impact process and the dynamic loadings on piers. Approximately 10% of the kinetic impact energy is dissipated through the interactions among the barges. More important, the impact forces are not proportional to the number of barges in a flotilla. The structural strength of the barge bow that contacts the pier is the key factor in determining the resulting impact forces. Moreover, the impact duration apparently increases as the number of barges increases, partly due to barge interactions.

Based on the FE simulations, the regression formulas to calculate the maximum impact force, average impact force, and impact duration have been developed for the

barge columns impacting a rigid pier. In addition, the upper bounds of the average impact forces in the impact energy domain are provided, which can be used to estimate the impact intensity of a barge column.

Finally, the results from the FE simulations were compared with those from the AASHTO formulas. Since many important factors are ignored by the AASHTO method, it overestimates the impact forces when the impact energy is not very small. Likewise, at times, the AASHTO method underestimates the impact forces when the impact energy is small.

Chapter 7 Upper Bounds of Barge Impact Forces

In the previous chapters, extensive finite element (FE) simulations were conducted. FE simulations are very costly with respect to both model generation and computational time. It is not currently practical to run a supercomputer analysis to check a bridge pier design. The objective of this chapter is to find methods that are both rational in mechanics and simple in mathematics to predict impact loads of barges and dynamic response of piers in an acceptable, conservative manner.

This chapter presents a numerical study and an analytical derivation of empirical formulas to determinate the barge impact loads on bridge piers. The new impact loading functions account for pier shape and size. In addition, an impact spectrum procedure to determine the dynamic response of piers is proposed. The analytical techniques presented herein transform the complex dynamics of barge-pier impacts into simple problems that can be solved through hand calculations or design charts. The proposed methods are illustrated through the analysis of an actual pier.

7.1 Barge Bow Resistance to Crushing

Since barge-bridge collisions are very complex phenomena, many factors influence the exact calculation of the impact forces. However, quasi upper bounds of the impact forces may be ascertained by excluding some factors that do not significantly contribute to bridge capacity or only lessen impact intensity on piers. The determination of the upper bounds of impact forces is very helpful for establishing permissible load limits or evaluating the extreme capacity of bridges.

Extensive FE simulations conducted in both Chapter 4 and Chapter 6 verify that barge impact forces are mostly dependent on the structural strength of the barge bow. This section details the force-deformation relationship of the barge bow structure for impacts. As shown in Figure 7.1, the bow (of a JH) under examination is fixed on a rigid wall, which is to be crushed by rigid columns with different velocities. For each crash simulation, both the pier geometry and the crushing speed are invariable. The motion of the columns is controlled by increasing the crushing distance at a constant rate and is only allowed along the symmetrical axis of the bow. There are only three variables in the specified simulations, the pier size, shape, and velocity. The difference between the force-displacement curves obtained in this way is due only to these three factors. Apparently, the simulation results are similar to those from static analyses when the columns move very slowly.

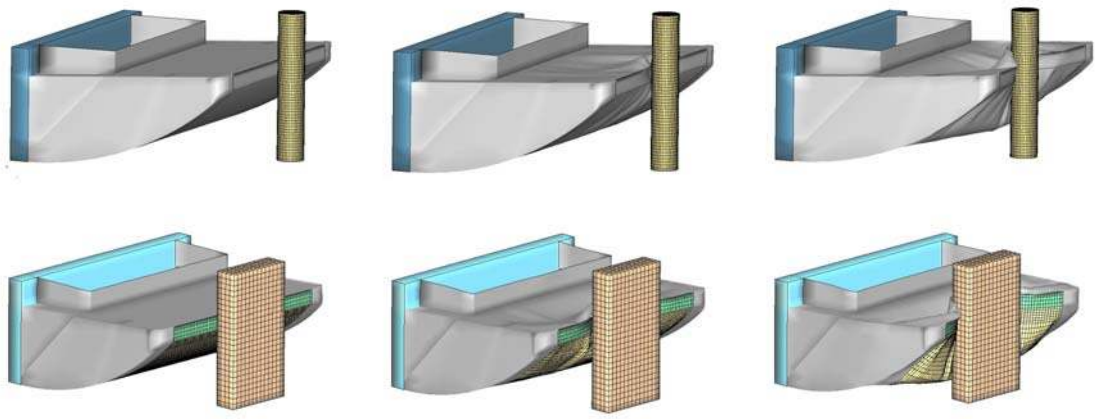

Figure 7.1 Barge bows crushed by circular and rectangular piers at a constant rate

According to Whitney et al. [10], the average traveling velocity of inland barges is 2.06 m/s (4 knots) and the maximum is 3.09 m/s (6 knots). Therefore, barge-bridge collisions are not high-speed impact events. As indicated in Chapter 5, a bow structural

response to an impact can be divided into two stages: a very brief collision stage, followed by a global structural deformation stage. However, the time duration of the maximum contact force (0.05 - 0.1 seconds) is too brief to significantly damage most bridge structures except for those that are very slender. This is true even though the peak force is much larger than the average force in most cases [9]. During barge-bridge collision events, a major part of the kinetic impact energy is dissipated through the deformation and damage of the barge bow. The above dynamic features lead to two assertions: 1. the contact forces at the initial stage are not significantly detrimental to bridge structural stability and therefore can be ignored; 2. the static force-deformation curve of the barge bow is the "skeleton" of various impact force-deformation curves.

Since the barge bow in Figure 7.1 can neither rebound nor avoid the continuous crushing, both the barge body and pier are rigid, only the bow dissipates the impact energy, and the crushing velocity is a non-decreasing constant value. The obtained force-displacement curve should be the upper bound of the bow resistance under the given conditions. In reality, the striking barge moves in a 3-D space and the structural configuration of the bow varies between given JHs. Therefore, real impact forces may locally fluctuate around one upper bound curve. The upper bounds may be more accurately described as envelopes of the average impact forces in the displacement domain.

As shown in Figures 7.2 and 7.3, four sets of force-deformation curves for square and circular piers have been developed, where the crushing velocities are 1.27 m/s (2.5 knots) and 3.09 m/s (6 knots), and the pier to barge width ratio α vary in the range between 0.1 and 1.1.

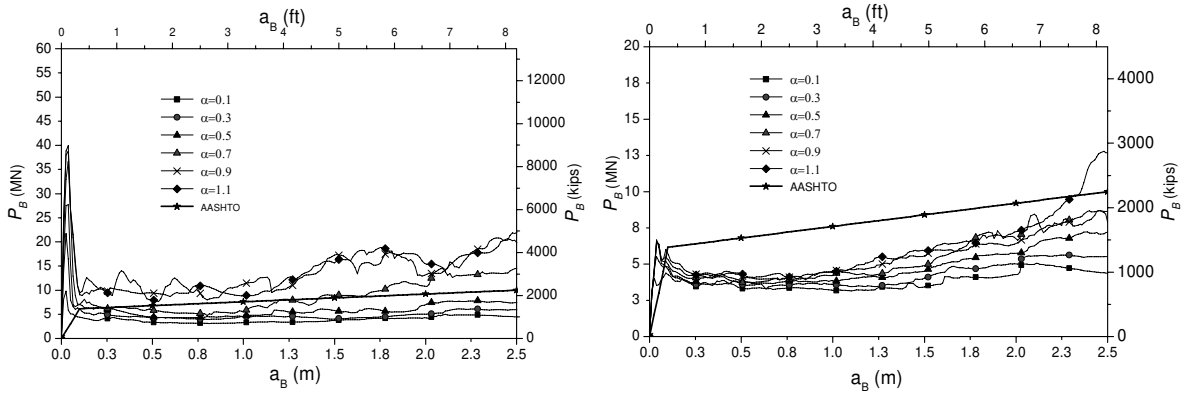

(a) (b)

Figure 7.2 Impact force P_B versus damage depth a_B for a JH bow crushed at a velocity of 1.27 m/s (2.5 knots): (a) square piers (b) circular piers

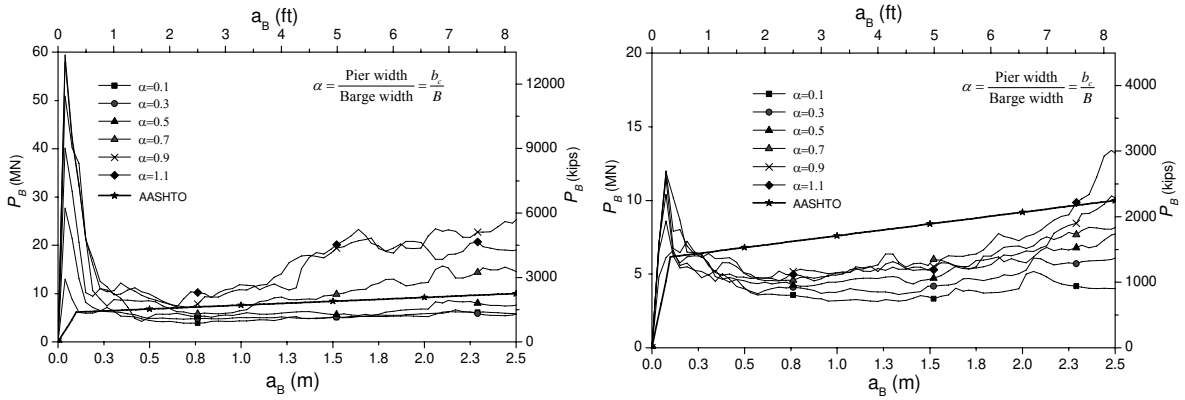

(a) (b)

Figure 7.3 Impact force P_B versus damage depth a_B for a JH bow crushed at a velocity of 3.06 m/s (6 knots): (a) square piers (b) circular piers

The following conclusions may be made from the FE simulations. First, the crushing speed does not significantly affect the resistance of the bow except for the contact forces at the very beginning of impact. Second, dynamic effects do not play a significant role as the plastic deformation develops. These conclusions comply with Meir-Dornberg's observations [11]. However, before plastic deformation develops, the resistance of the bow is much larger than his predictions. Both pier shape and size, which is ignored by Meir-Dornberg, have great influence on the bow resistance.

Based on the discussion above, the respective curves in Figure 7.3 may be treated as the upper bounds of the impact forces for a single barge and a multi-barge flotilla when the pier geometry is given.

7.2 Average Impact Force

Current AASHTO design specifications use average impact forces to describe vessel impact loadings. Although this approach is not accurate, it eases bridge design.

The average impact forces $\overline{P}$ against the crushing path for the curves in Figure 7.3 are given by

$$\overline{P}(a_B,\alpha)=\frac{\int_0^{a_B} P_B(\delta,\alpha)d\delta}{a_B} \tag{7.1}$$

where a_B is the damage depth of the barge bow (referring to Figure 7.4).

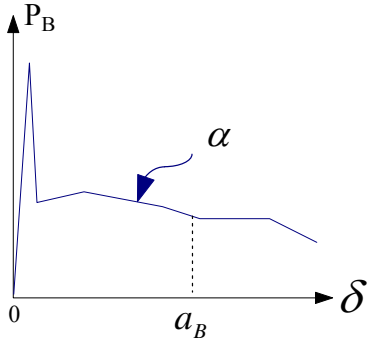

Figure 7.4 Schematic diagram of the impact force-deformation relationship

From Eq. (7.1), the mean force $\overline{P}$ versus the damage depth a_B is presented in Figure 7.5. A set of regression equations for $\alpha \geq 0.05$ to fit the curves in Figure 7.5 are derived as follows.

For square piers:

$$\bar{P}(\alpha, a_B) = \left(4.53 + 646.06\alpha - 270.53\alpha^2\right) a_B \text{ for } 0 \le a_B \le 0.1 \tag{7.2}$$

$$\bar{P}(\alpha, a_B) = 4.53 - 1.78\alpha - 6.27\alpha^2 - \left(1.08 - 16.66\alpha - 3.61\alpha^2\right) a_B + \left(1.72 - 28.11\alpha + 9.18\alpha^2\right) \ln(a_B) - \left(0.05 + \alpha + 1.02\alpha^2\right) a_B^2 \text{ for } a_B > 0.1 \tag{7.3}$$

For circular piers:

$$\bar{P}(\alpha, a_B) = \left(47.99 + 45.43\alpha - 16.28\alpha^2\right) a_B \text{ for } 0 \le a_B \le 0.1 \tag{7.4}$$

$$\bar{P}(\alpha, a_B) = 4.85 - 2.84\alpha + 4.62\alpha^2 - \left(1.23 - 6.46\alpha + 6.90\alpha^2\right) a_B - \left(0.03 + 2.93\alpha - 2.42\alpha^2\right) \ln(a_B) + \left(0.27 - 0.98\alpha + 1.45\alpha^2\right) a_B^2 \text{ for } 1.0 \ge a_B > 0.1 \tag{7.5}$$

where the average impact force $\bar{P}$ is in MN, and the bow damage depth a_B is in meters.

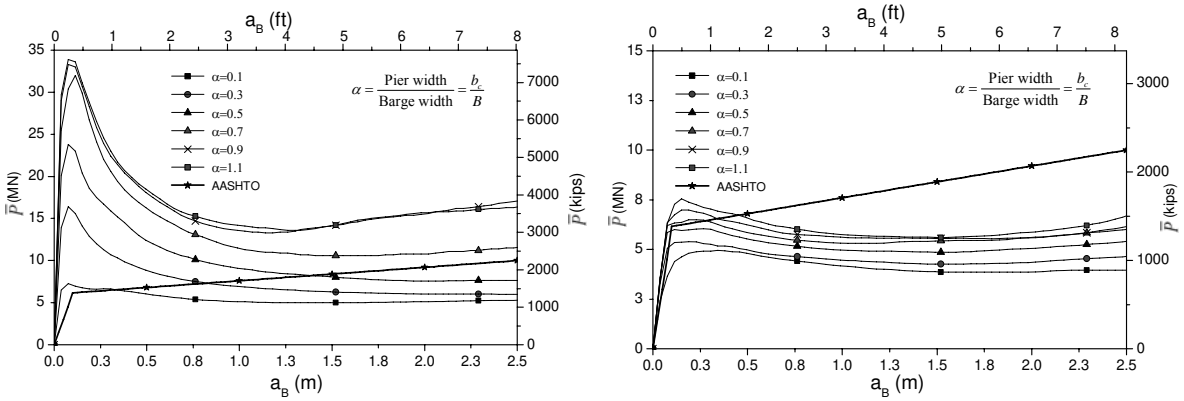

Figure 7.5 Average impact force $\bar{P}$ versus barge damage depth a_B : (a) square piers; (b) circular piers

Note the following relationship exists for rectangular piers

$$\bar{P}(\alpha > 1.0, a_B) = \bar{P}(\alpha = 1.0, a_B)\,. \tag{7.6}$$

Figure 7.5 also indicates that the AASHTO method overestimates the average impact forces for circular piers and underestimates the average impact forces for rectangular piers with $\alpha \ge 0.3$. However, these comparisons may not be applicable when

extended to pier dynamic responses due to the time-varying nature of the impact loads and occurrence of inertia forces.

7.3 Barge Damage Depth and Impact Duration

Except for barge impact on very slender bridge piers, which are rare, most of the impact energy is absorbed by the barge, and the pier flexibility does not significantly affect the average impact forces. As shown in Chapter 5, the rigid-pier assumption results in a conservative estimation of the barge impact forces.

For head-on impacts on rigid piers, the coefficient of restitution (COR) is defined as

$$e = \frac{V_{t_d}}{V_i} \tag{7.7}$$

where V_i is the barge initial velocity, and V_{t_d} is the barge velocity following the impact and at the moment the impact force reduces to zero.

From Chapter 4, the following equations can be used to calculate the COR for single barges.

For square piers with $0.05 \le \alpha \le 1.0$:

$$e = 0.28 + 0.04\alpha - (0.08 + 0.04\alpha)\ln E_k \tag{7.8}$$

For circular piers with $0.05 \le \alpha \le 1.0$:

$$e = 0.06 + 0.06\alpha - (0.16 - 0.01\alpha)\ln E_k \text{ for } 0 < E_k \le 0.114 \tag{7.9}$$

$$e = 0.27 + 0.01\alpha - 0.05\ln E_k \text{ for } E_k > 0.114 \tag{7.10}$$

where the kinetic impact energy E_k is in MJ.

The losses of the kinetic impact energy during a collision event can be determined From Eq. (7.7) as

$$\Delta E_k = (1-e^2)E_i \tag{7.11}$$

or $$\Delta E_k = \frac{1}{2}(1-e^2)m_B V_i^2 \tag{7.12}$$

where m_B is the total mass of the barge.

The work done by the pier during impact is given by

$$W = \int_0^{a_B} P(\alpha, x)dx = \overline{P}(\alpha, a_B)\cdot a_B \tag{7.13}$$

Based on the discussion in section 4.4, comparing Eq. (7.12) with Eq. (7.13) yields

$$\frac{1}{2}(1-e^2)m_B V_i^2 = \overline{P}(\alpha, a_B)\cdot a_B \tag{7.14}$$

Eq. (7.14) is a nonlinear equation of variable a_B when the pier shape and size, and the barge mass m_B and velocity V_i are assigned. This expression contributes to the determination of the barge damage depth a_B. Thus, the average impact force $\overline{P}$ can be determined by substituting the solution of Eq. (7.14) into Eqs. (7.12) through (7.15). For convenience, the relationships between E_k, a_B, and $\overline{P}$ are presented in Figure 7.6.

According to the impulse-momentum law [40], the time duration of impact is given by

$$t_d = \frac{1+e}{\overline{P}(\alpha, a_B)} I_i \tag{7.15}$$

where $I_i = m_B V_i$ is the initial momentum of the barge.

Since $0 \le e \le 1$, the impact duration t_d is satisfied with the following relationship:

$$\frac{I_i}{\overline{P}} \le t_d \le \frac{2I_i}{\overline{P}}. \tag{7.16}$$

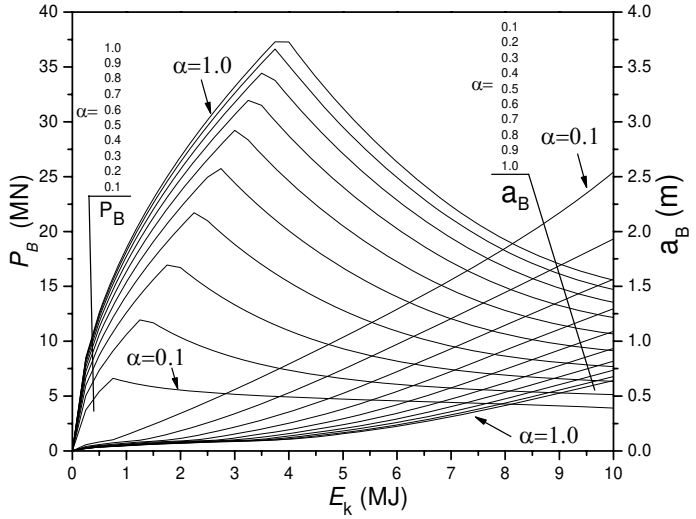

(a)

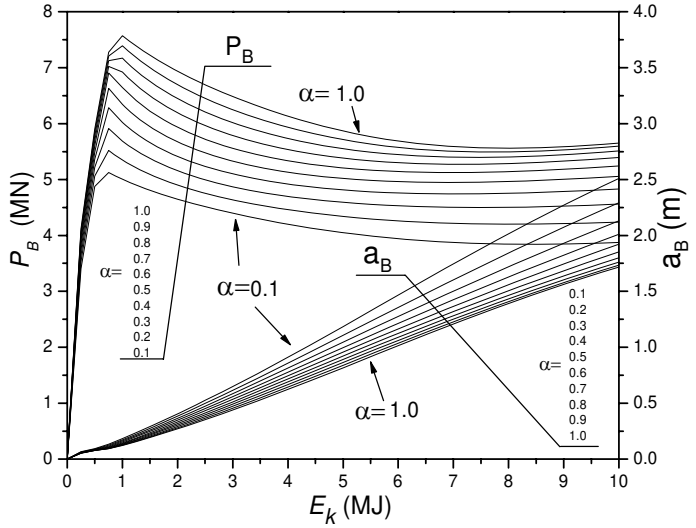

(b)

Figure 7.6 Impact force P_B and barge damage length a_B in relation to the kinetic impact energy E_k : (a) square piers; (b) circular piers

In addition to the general discussion of barge impact loads with respect to magnitude, impact intensity is briefly discussed below. The intensity of a collision is

given by the impulse $\int_0^{t_d} P(t)dt$, which is the combination of the collision force $P(t)$ and the impact duration t_d. Since the average impact force $\overline{P}$ is based on the upper bound of barge resistance, the impact force prediction is conservative. Consequently, the impact duration t_d is shorter than that found in the actual event due to the conservation of momentum. Finally, an equivalent rectangular load can be constructed when the force $\overline{P}$ and duration t_d are known.

7.4 Comparison to the Frieze Method

Frieze [44], with the assistance of Woisin, gathered previous research and test results concerning vessel bow damage from impacts with bridge piers. He proposed the following equation to calculate the absorbed energy by the damaged bow:

$$W = (60.5\Omega)\frac{\sigma_d}{\sigma_y} + 3.0t^2 l \tag{7.17}$$

$$\frac{\sigma_d}{\sigma_y} = \begin{cases} 1 & \text{for } \varepsilon' < 0.001\text{s}^{-1} \\ 1.393 + 0.131\log\varepsilon' & \text{for } 0.001 \le \varepsilon' < 1\text{s}^{-1} \\ 1.393 + 0.393\log\varepsilon' & \text{for } \varepsilon' \ge 1\text{s}^{-1} \end{cases} \tag{7.18}$$

where the absorbed energy W is in MJ; the damaged (not torn) volume of steel Ω is in m^3; t is the thickness of plating in meters; and l is the length of the tear in meters.

In Eq. (7.17), the term 60.5Ω represents the work done statically in bending, stretching, compressing, scraping (friction), buckling, crushing, and folding; the term $3.0t^2 l$ represents tearing effects (6.0 for double-sided tearing); and the term σ_d / σ_y represents the dynamic effects. For a slow barge impacting with a pier, Eq. (7.17) may be simplified as:

$$W = 60.5\Omega \tag{7.19}$$

The incremental procedure to apply the Frieze method is presented in Figure 7.7, and the corresponding program in MathCAD [45] can be found in Appendix A.

Figure 7.8 compares Eqs (7.2) and (7.3) with the Frieze equations for barges impacting rigid square piers. The impact forces obtained from both the proposed method and the Frieze method are the average impact force over the barge crushing distance. Considering the complexity of barge-pier impact problems, the two methods agree well. In contrast to the AASHTO load equations, both the proposed equations and the Frieze equations correlate the absorbed energy with the damaged material volume. Nonetheless, the proposed equations account for not only the damaged material volume but also the coordinated resistance of the material, while the Frieze method simply proportions the absorbed energy to the damaged material. That is the reason why the gap between the two Frieze curves in Figure 7.8 is larger than the gap between the proposed curves. Specifically, the proposed loading equations accounts for the pier shape in addition to its size. As a result, the proposed loading equations may be considered more accurate for predicting barge impact loads. However, the Frieze equations were derived from over 50 model tests and are suitable for many kinds of vessels and a wide range of impacting velocities. Hence, the impact force calculated by the Frieze method can be considered as an approximation to the one calculated by the proposed method. In particular, the Frieze method is very useful when the actual collision situation is different from the scenario used in the deduction of the proposed equations, for example, if the vessel is not a JH or the velocity is very large.

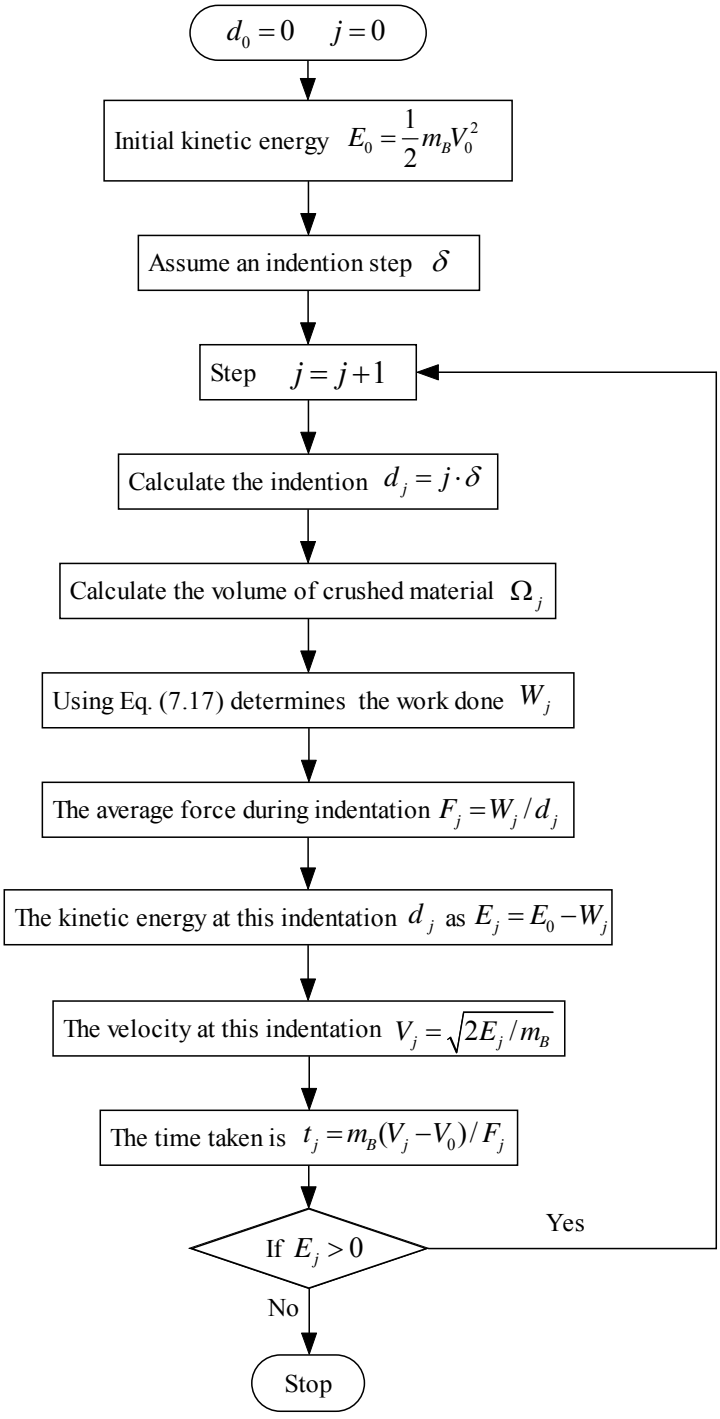

Figure 7.7 Flow chart of the Frieze algorithm

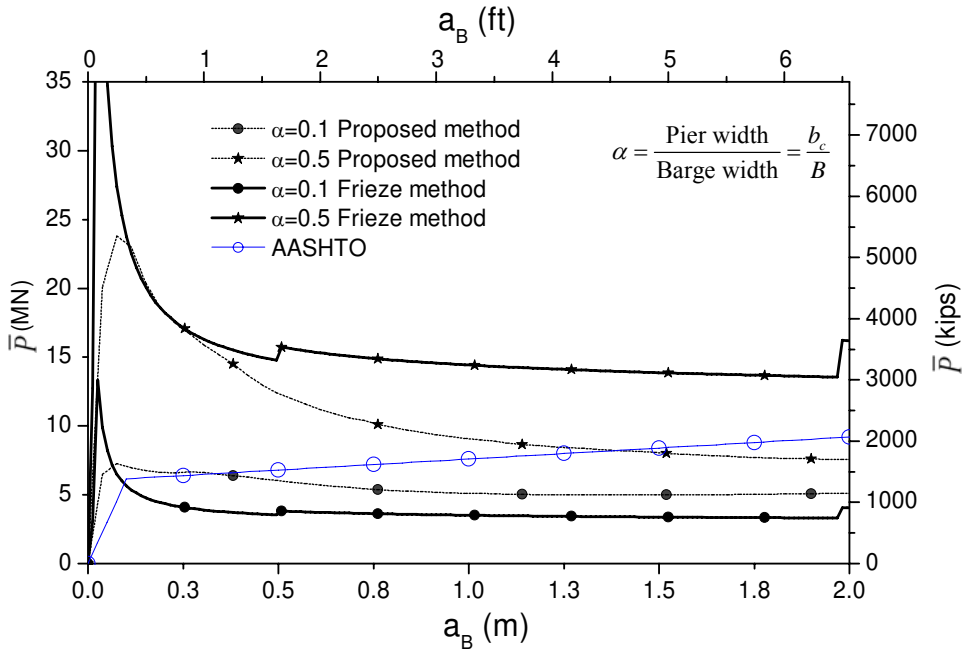

Figure 7.8 Comparison between the Frieze method, the proposed method, and the AASHTO method for square piers

7.5 Response of Bridge Piers Subjected to Barge Impact

One of the attractive aspects of the AASHTO equivalent static design methodology [9] is its simplicity of integration into the design process. In order for a new revised design methodology to be of practical benefit, simple hand solutions of typical impact problems must be feasible.

7.5.1 Response Spectrum Analysis

The impact response of a pier may be determined using a modal response spectrum analysis similar to the analysis procedures used in earthquake designs. The response spectrum is a convenient means of encapsulating the maximum response of a system to a specified excitation force over a wide range of natural frequencies or periods. In many practical situations, the design engineer is primarily interested in the maximum

response of the system to a specified input. In such circumstances, a response spectrum analysis is quite useful.

The maximum modal response for the *r*th mode of a MDOF system to a specified input, expressed in physical coordinates, is given by:

$$\{x\}_r^{\max} = \left|\{\Phi\}_r \Gamma_r DMF_r\right| \tag{7.20}$$

$$\Gamma_r = \frac{\{\Phi\}_r^T \{P\}}{\omega_r^2 \{\Phi\}_r^T [m] \{\Phi\}_r} \tag{7.21}$$

where the subscript *r* identifies the mode of vibration, $\{x\}_r^{\max}$ is the maximum response, $\{\Phi\}_r$ is the modal vector, Γ_r is the modal participation factor, DMF_r is the dynamic magnification factor determined from the appropriate response spectrum, [*m*] is the mass matrix of the system, and $\{P\}$ is the force vector.

The dynamic magnification factor for a rectangular pulse is given by

$$DMF = \begin{cases} 2\sin\left(\dfrac{\pi t_d}{T}\right), & 0 \le \dfrac{t_d}{T} < 0.5 \\ 2.0, & \dfrac{t_d}{T} \ge 0.5 \end{cases} \tag{7.22}$$

where T is the natural period of the undamped oscillator representing the bridge pier, and t_d is the time duration of the force. Using Eq. (7.22), a plot of *DMF* versus the dimensionless frequency parameter t_d / T can be generated as an impact spectrum for the rectangular pulse force.

A popular method for combining modal maxima, known as the square root of the sum of the squares (SRSS), is expressed as

$$\{x\}^{\max} = \sum_{r=1}^{n} \left[\left(\{\Phi\}_r \Gamma_r DMF_r \right)^2 \right]^{1/2} \tag{7.23}$$

where $\{x\}^{\max}$ is the maximum displacement vector.

7.5.2 Dynamic Response of Piers

In lieu of exact methods, common bridge piers may be idealized as a 4-DOF column carrying two lumped masses, M_1 and M_2, as shown in Figure7.9. The lumped masses are written as

$$M_1 = 0.5(L_1 + L_2) = 0.5L\bar{m} \tag{7.24}$$

$$M_2 = m_s + 0.5L_2\bar{m} \tag{7.25}$$

where $\bar{m}$ is the mass per unit length of the pier, m_s is the sum of other masses supported by the simplified pier, L_1 identifies the location of the collision point, L_2 is the distance from the collision point to the pier top, and L is the total length of the pier.

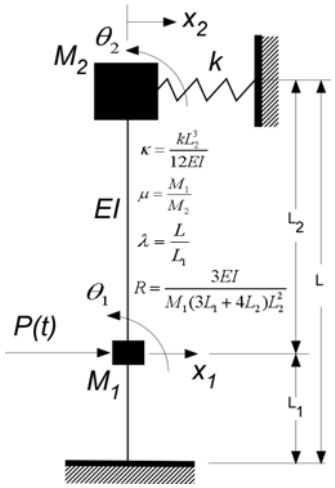

Figure 7.9 Idealized pier model for dynamic analysis

Application of the static condensation technique to the stiffness matrix eliminates the 2-DOF associated with rotation. The two translational natural frequencies corresponding to translational vibrations of the pier are

$$\omega_{1,2}^2 = R\left[2\lambda^3 + 2\mu\left(1+4\kappa+\frac{3\kappa}{\lambda-1}\right) \mp \sqrt{\left[2\lambda^3 - 2\mu\left(1+4\kappa+\frac{3\kappa}{\lambda-1}\right)\right]^2 + 4\mu(-3\lambda+1)^2}\right] \tag{7.26}$$

in which

$$\lambda = \frac{L}{L_1},\ \mu = \frac{M_1}{M_2},\ \kappa = \frac{L_2{}^3 k}{12EI},\ R = \frac{3EI}{M_1(3L_1+4L_2)L_2^2}.$$

Since $T_{1,2} = 2\pi/\omega_{1,2}$, the dynamic magnification factors $DMF_{1,2}$ can be determined from Eq. (7.22). To obtain the dynamic response, the modal matrix is constructed in terms of the modal vectors as

$$\{\Phi\} = [\{\Phi_1\},\{\Phi_2\}] = \begin{bmatrix} 1 & 1 \\ \phi_1 & \phi_2 \end{bmatrix} \tag{7.27}$$

$$\phi_{1,2} = \frac{\omega_{1,2}^2 - 4R\cdot\lambda^3}{2R\cdot(1-3\lambda)} \tag{7.28}$$

Expressed in terms of ϕ_1 and ϕ_2 directly, Eq. (7.20) becomes

$$x_1^{\max} = \frac{\mu\bar{P}}{M_1}\sqrt{\left[\frac{DMF_1}{\omega_1^2\left(\mu+\phi_1^2\right)}\right]^2 + \left[\frac{DMF_2}{\omega_2^2\left(\mu+\phi_2^2\right)}\right]^2} \tag{7.29}$$

$$x_2^{\max} = \frac{\mu\bar{P}}{M_1}\sqrt{\left[\frac{\phi_1\cdot DMF_1}{\omega_1^2\left(\mu+\phi_1^2\right)}\right]^2 + \left[\frac{\phi_2\cdot DMF_2}{\omega_2^2\left(\mu+\phi_2^2\right)}\right]^2} \tag{7.30}$$

where $x_1^{\max}$ and $x_2^{\max}$ correspond to the maximum displacements of the collision point and pier top, respectively.

For ordinary applications, the variation of the mass ratio η ranging from 0.01 to 0.14 does not significantly affect the maximum displacements $x_1^{\max}$ and $x_2^{\max}$, and

DMF=2.0 because most impact durations t_d are larger than $0.5T$. The maximum displacement curves, plotted on a semi-log graph, are represented in Figure 7.10. These curves may be conveniently employed to evaluate the dynamic response of piers subjected to barge impacts for the majority of cases.

It should be noted that the shear force might contribute partially to the displacements of the pier with a height to depth ratio less than 10, which is ignored by the proposed method. In addition, the material plasticity and geometric non-linearity of bridge piers are not considered in the proposed method.

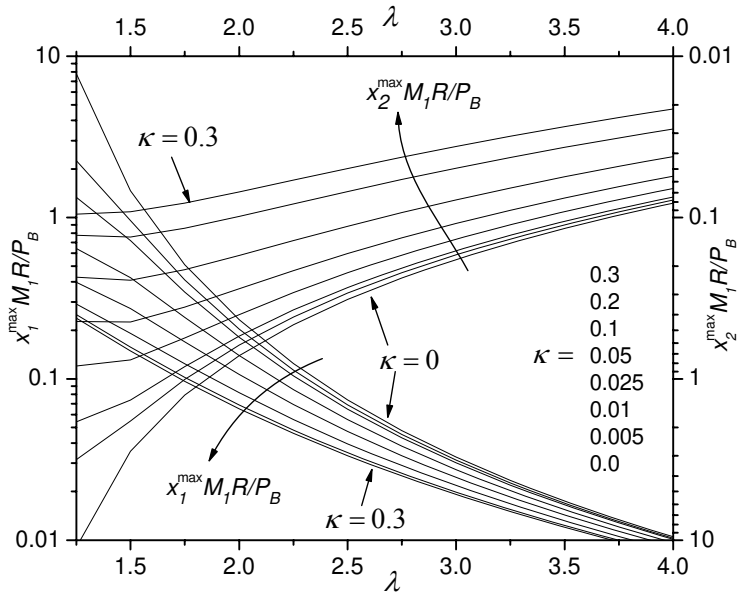

Figure 7.10 Design chart for maximum displacements $x_1^{\max}$ and $x_2^{\max}$ at the collision point and top of the idealized pier, respectively

Loss of spans due to insufficient seat width on the impacted bridge pier cap is probably the most common mode of bridge failure. For a multi-span bridge, it is at expansion joints where this failure mode is most likely. To avoid loss of span, sufficient seat width should be provided at the top of the pier. In the interest of focusing on the maximum displacement at the pier top when a barge tow collides with a pier, the pier

may be modeled as a single-degree-of- freedom system as shown in Figure 7.11. It is conservative to ignore pier self-weight, and such ignorance does not hurt the accuracy of results much [50]. The equation of motion of the pier can be expressed as

$$m_s\ddot{x}_2 + k_{22}x_2 + k_{21}x_1 = 0 \tag{7.31}$$

$$k_{12}x_2 + k_{11}x_1 = P_B \tag{7.32}$$

where m_s is the topside mass of the pier; c is the viscous damping coefficient; k_{11}, k_{22}, and $k_{21}(=k_{12})$ are the stiffness coefficients of the pier; x_1 and x_2 are the displacements at the collision point and top of the pier, respectively.

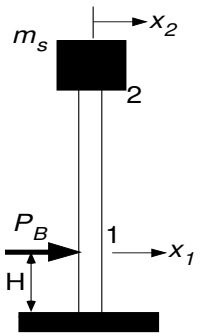

Figure 7.11 Simplified pier model

Substituting Eq. (7.32) into Eq. (7.31) and rearranging items results in

$$m_s\ddot{x}_2 + \frac{k_{22}k_{11} - k_{12}^2}{k_{22}}x_2 = -\frac{k_{12}}{k_{22}}P_B \tag{7.33}$$

The natural frequency of the pier system is expressed as

$$\omega_b = \sqrt{\frac{k_{22}k_{11} - k_{12}^2}{m_s k_{22}}} \tag{7.34}$$

Thus, the amplitude of the steady-state response, $x_2^{\max}$, is equal to the equivalent static deflection multiplied by the dynamic magnification factor *DMF* given by Eq. 7.22. That is, the maximum displacement of the pier top is

$$x_1^{\max} = \frac{\bar{P}k_{21}(DMF)}{k_{11}k_{22} - k_{21}^2} \tag{7.35}$$

Note that Eq. (7.35) is more general than Eq. (7.29) with respect to the variation of pier geometry because only the generalized stiffness coefficients are related to the given bridges. A comparison between these formulas is presented in Table 7.2.

7.6 Application

The following example illustrates the application of the previously developed methods. Then, a comparison between the different methods is conducted.

Example: A fully loaded JH with a mass $m_b = 1.724 \times 10^6$ kg (1900 short tons) and an initial velocity $V = 3.087$ m/s (6 knots) collides head-on with the pier shown in Figure 7.12. Determine (a) the equivalent rectangular load on the pier and (b) the maximum displacements at the collision point and top of the pier, respectively.

Solution: For brevity, the process to solve problems (a) and (b) is tabulated in Tables. 7.1. Alternatively, the same results can be obtained directly from the design charts, Figures 7.6(a) and 7.10.

Figure 7.13 shows the equivalent rectangular load developed in this example, which compares with the impact force time-history from the FE simulation using the program LS-DYNA970. A comparison between different methods is presented in Table 7.1. The proposed methods agree with the detailed FE analysis. Moreover, the pier top displacement generated by the AASHTO equivalent static load is $x_2 = 0.04$ m, which is the smallest displacement in comparison to its counterparts in Table 7.2. Hence, the AASHTO method underestimates the dynamic response of the pier in this case, although

the resulting impact force is much larger than the impact forces predicted by other methods.

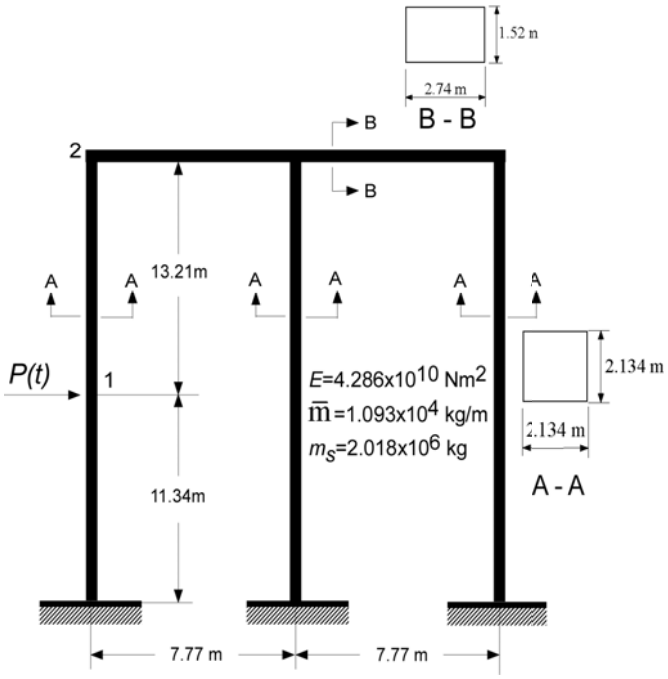

Figure 7.12 Pier frame of the example

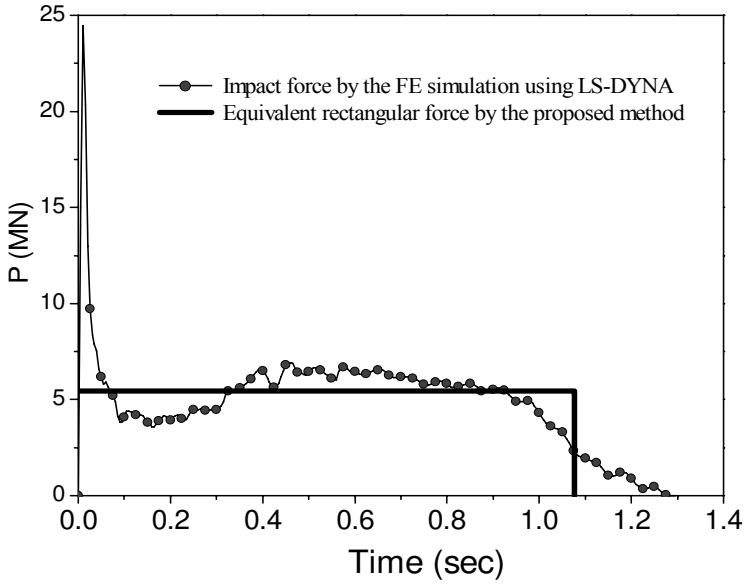

Figure 7.13 Comparison between the force time-history generated by the FE simulation and the equivalent rectangular load developed by the proposed method

Table 7.1 Solutions to problems (a) and (b) of the example

Problem	Step	Parameter	Value	Note
(a)	1	Width ratio α	0.2	$\alpha = b_c / B$
	2	Initial kinetic energy E_k	8.21 MJ	$E_k = 0.5 m_b V_i^2$
	3	Initial momentum I_i	5.32 $\text{MN}\cdot\text{sec}$	$I_i = m_b V_i$
	4	Coefficient of restitution e	0.10	Eq. (7.8)
	5	Average impact force $\overline{P}$	5.53 MN	Eq. (7.5) or Figure 7.6(a)
	6	Barge damage depth a_B	1.50 m	Eq. (7.14) or Figure 7.6(a)
	7	Impact time duration t_d	1.08 sec	Eq. (7.15)
(b)	1	Stiffness coefficient k	4.35×10^7 N/m	Since the equivalent spring constant for the simplified pier is between the cantilever and fixed-fixed cases, it is estimated by $k = 2\times\left(\frac{3+12}{2}\right)\frac{EI}{L^3}$.
	2	Lumped masses M_1, M_2	1.34×10^5kg 2.09×10^6kg	From Eqs. (22) and (23)
	3	λ, κ, μ	2.165, 0.195, 0.064	Constants
	4	R	63.23 sec^{-2}	Constant
	5	Natural frequencies ω_1, ω_2	4.98 Hz, 50.78 Hz	From Eq. (7.26)
	6	Dynamic Magnification Factors $DMF_{1,2}$	2.0, 2.0	$\frac{\omega_1 t_d}{2\pi} = 0.85 > 0.5$ From Eq. (7.22)
	7	Maximum displacements at the collision point and pier top, $x_1^{\max}$ and $x_2^{\max}$	0.03 m, 0.05 m	From Eqs. (7.29) and (7.30) or Figure 7.10

Table 7.2 Comparison between different methods

Item	Proposed method[a]	AASHTO method	LS-DYNA simulation[b]	Frieze Method[d]	SAP2000	Simple Method[e]
Average force $\overline{P}$ (MN)	5.43	8.17	4.83	8.08	NA	5.43
Impact duration t_d (sec)	1.08	NA	1.30	0.77	NA	1.08
Barge damage depth a_B (m)	1.50	1.36	1.29	1.19	NA	1.50
Max displacement $x_1^{\max}$ (m)	0.03	0.04[c]	0.03	NA	0.04	0.04
Max displacement $x_2^{\max}$ (m)	0.05	0.04[c]	0.06	NA	0.05	NA

Note: a. Hand computation time: 10 minutes.
b. PC computation time: 36 hours.
c. Static analysis using SAP2000.
d. Computation time (including data preparation): 8 hours.
e. Using Eq. (7.35).

7.7 Empirical Formulas

From the numerical evaluation of the lengthy formulas in section 7.2, it is possible, after approximating the coefficients, to propose empirical formulas to estimate the impact forces.

To uncouple the equations, the relationships between the average impact force and the barge damage depth may be altered to take the following forms.

For rectangular piers:

$$\psi_s = 4.5 + 646.1\alpha - 270.5\alpha^2 \tag{7.36}$$

$$\frac{\overline{P}}{\psi_s} = \begin{cases} a_B & \text{for } 0 \le a_B \le 0.1 \\ 0.022\sqrt{a_B} + 0.11e^{-1.68a_B} & \text{for } a_B > 0.1 \end{cases} \tag{7.37}$$

For circular piers:

$$\psi_r = 48.0 + 45.4\alpha - 16.3\alpha^2 \tag{7.38}$$

$$\frac{\overline{P}}{\psi_r} = \begin{cases} a_B & \text{for } 0 \le a_B \le 0.1 \\ 0.0287a_B + 0.1058e^{-0.851a_B} & \text{for } a_B > 0.1 \end{cases} \tag{7.39}$$

where the average impact force $\overline{P}$ is in MN, and the barge damage depth a_B is in meters.

The above simplified formulas are reasonably accurate for common cases, except Eq. (7.37) is about 25% less than Eq. (7.3) when the width ratio $\alpha < 0.15$. Assuming that the kinetic impact energy is completely absorbed by the barge bow, Eq. (7.12) can be rewritten as

$$E_i = \overline{P} \cdot a_B \tag{7.40}$$

By substituting Eqs (7.37) and (7.39) into Eq. (7.40), respectively, the relationships between the initial kinetic energy E_i and the barge damage depth a_B are

obtained for rectangular and circular piers, respectively, as shown in Figure 7.14. The dependence of the barge damage depth a_B on the kinetic energy E_i is analyzed by regression analysis. Comparisons between the numerical and analytical results are also presented in Figure 7.14.

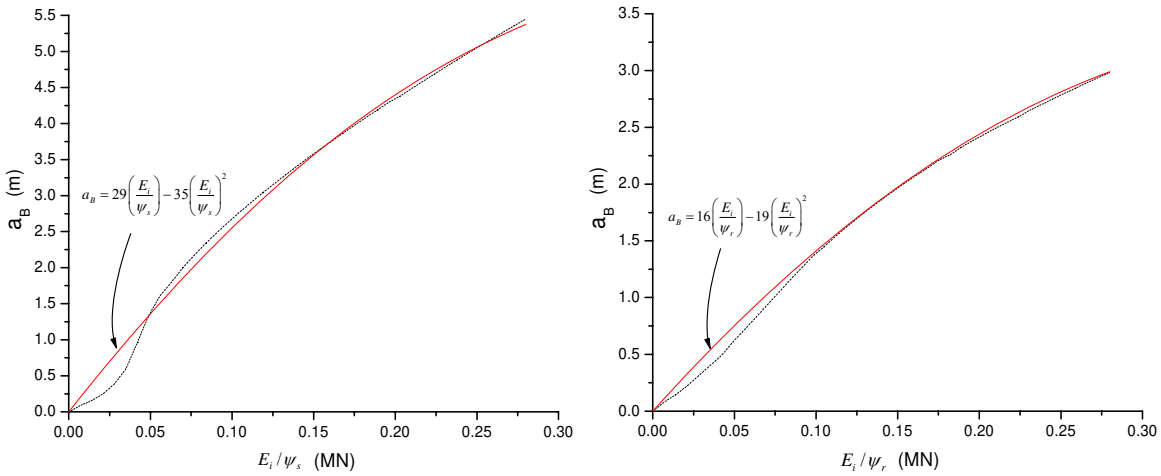

(a) (b)

Figure 7.14 Approximate formulation of the barge damage depth a_B as a function of the kinetic impact energy E_i : (a) for rectangular piers; (b) for circular piers

For rectangular piers, the barge damage depth is expressed as

$$a_B = 29\left(\frac{E_i}{\psi_s}\right) - 35\left(\frac{E_i}{\psi_s}\right)^2 \tag{7.41}$$

For circular piers, the barge damage depth is

$$a_B = 16\left(\frac{E_i}{\psi_r}\right) - 19\left(\frac{E_i}{\psi_r}\right)^2 \tag{7.42}$$

Where the kinetic impact energy E_i is in MJ, and the barge damaged depth a_B is in meters.

Although these formulas postulated herein are not highly accurate, especially when the kinetic energy is small, they can be used to estimate the impact force conveniently for common cases. More important, these decoupled formulas reveal the fundamental influence of the involved parameters. From Eqs. (7.37) and (7.39), it is known that the average impact force tend to be constant when the impact energy is great enough, for example, $E_i > 3\,\text{MJ}$ and $E_i > 8$ for rectangular and circular piers, respectively. For convenience, kinetic impact energy benchmarks are presented in Table 7.3.

Table 7.3 Kinetic impact energy benchmarks

Barge	Mass	Kinetic energy (MJ)		
		2 knots	4 knots	6 knots
Single JH	1900 tons	0.9	3.7	8.3

7.8 Summary

The methods described in this chapter are intended to improve the analysis of bridges susceptible to single-barge impacts. Both impact load generation of barges and the dynamic response of bridges are discussed. Analytical expressions are developed to predict the average impact forces. Comparisons of the results with finite element calculations are favorable. Since the maximum transient forces occur for a very short duration, during which the pier does not have time to respond, the equivalent dynamic force is computed as a simple measure of the design structural demand. A comparison between the forces and displacements generated from different methods indicate that the derived functions are dependable over a wide range of barge-pier collision problems. In addition, the proposed methods are very easy to employ in bridge design.

The AASHTO method contains limitations regarding the prediction of barge impact loads on bridges due to a lack of consideration of many important factors. From

Meir-Dornberg's perspective [11], the "equivalent static force" means that the barge impact forces obtained in his dynamic experiments are similar to those found in the static experiments. It does not mean that the barge impact forces from his formulas are the equivalent static load on bridges. The dynamic response of bridges is not only dependent on impact forces, but also the structural characteristics of bridges. However, the term "equivalent static load" of AASHTO is often misused in technical literature because AASHTO provides little information about the dynamic characteristics of barge impacts.

Chapter 8 Dynamic System Identification

It is known from the foregoing chapters that the progressive dynamic collapse of a barge bow consists of a series of elastic, elastoplastic hardening, and softening behaviors. In this chapter, the formulation of the dynamic system identification of a barge crushed by a pier is presented. This dynamic system identification establishes a simple mathematical representation that describes the crushing behavior of a barge under a collision-loading environment. A representation of the resisting force of a single-degree-of-freedom (SDOF) system is developed in the displacement domain using the elastoplastic-collapse concept. The crushed barge is simplified as a SDOF lumped-mass system that contains a set of resistance elements that become active or inactive at different displacement stages. The resistance versus crushing depth curve is interpreted as the elastoplastic-collapse or crushing behavior of the barge. In the proposed formulation, the resistant elements will be simply referred to as "elements".

8.1 Elatoplastic-Collapse Elements

Nonlinear springs can be used to describe complicated structural behaviors. A general equation between the force f and the relative displacement δ for nonlinear springs is

$$f = k_1 x + k_2 x^2 + k_3 x^3 + ... = \sum_{i=1}^{N} k_i x^i \tag{8.1}$$

where k_i is the spring stiffness, and N is the highest degree of the approximating polynomial.

Because of the magnitudes and signs of the constants k_i special cases emerge. For instance, a stiffening spring can be represented by the following equation:

$$f = k_1 x + k_3 x^3 \tag{8.2}$$

Because the associated mathematical description is usually complicated, nonlinear springs are often linearized for analysis purposes. Springs with stops, as shown in Figure 8.1, are represented by the following equation:

$$f = \begin{cases} kx & \text{for } x_1 < x < x_2 \\ kx + k_1\left(x - x_1\right) & \text{for } x < x_1 \\ kx + k_2\left(x - x_2\right) & \text{for } x_2 < x \end{cases} \tag{8.3}$$

Eq. (8.3) may be considered as the linearization of the non-linear spring described by Eq. (8.2). In the following, a mathematical representation with linear springs that describes the complicated crushing behavior of a barge during a collision event is developed.

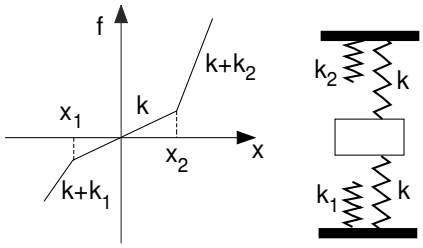

Figure 8.1 Springs with stops

When a barge collides with a bridge pier, the pier is subjected to impact loads produced by the moving barge. Concurrently, the pier exerts an equal but oppositely directed force on the barge. To generate the resisting forces of a barge, the moving barge may be modeled as a lumped mass with a set of parallel force elements that become active or inactive in a sequential order, as shown in Figure 8.2. Each element works only

in its displacement domain. The first element acts in the first displacement domain, and then it becomes inactive. The second element becomes active after the first displacement domain, and then the third element after the second displacement domain, and so on. Consequently, a series of such elements covers the entire crushing process. As such, the springs capture the dynamic plastic collapse behavior of the barge.

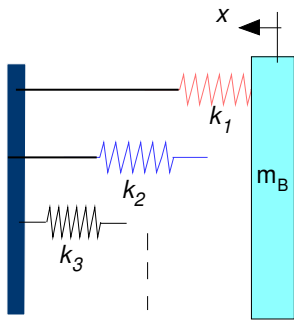

Figure 8.2 Schematic diagram of an undamped SDOF system

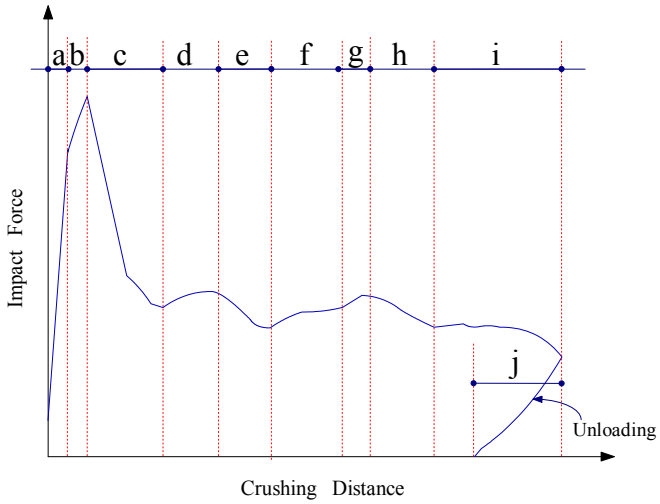

Figure 8.3 A typical force-deformation curve of a bow structure during impact

Figure 8.3 shows a typical force-displacement curve for a barge crushed by a pier. It can be seen that the barge bow initially undergoes elastic deformation, shown in range a, followed by plastic deformation, shown in range b. In range c, the barge bow experiences plastic collapse, as displacement increases with decreasing forces. The

unloading process (range j) begins when the barge bow reaches its maximum displacement. Because of the distinct behavior exhibited between each range, each of the failure modes may be modeled using one element to represent one range of the resistance curve.

Figure 8.4 shows a schematic diagram of the elastoplastic elements that form a piecewise linear function that expresses the crushing force in terms of the crushing distance. This representation makes it possible to obtain an analytical solution of the equation of motion that governs the simplified model for the barge. Each linear function can have a positive slope, negative slope or no slope. A constant slope defines the stiffness for the subdomain. If the function has a positive slope, then the behavior of the structure may be classified as elastic. Collapse behavior occurs when the function has a negative slope. If the function has a negative slope, then it represents the collapse behavior. When the function exhibits no slope, or "zero" slope, it is interpreted as perfect plastic behavior. However, any displacement subdomains presented in Fig 8.3 may contain several elements. If the functions defined in one subdomain have two different positive slopes, the phenomenon is interpreted as an elastoplastic behavior, i.e., a hardening or a softening behavior. The determination of a piecewise linear function for the resisting forces is formulated as an optimization problem for system identification.

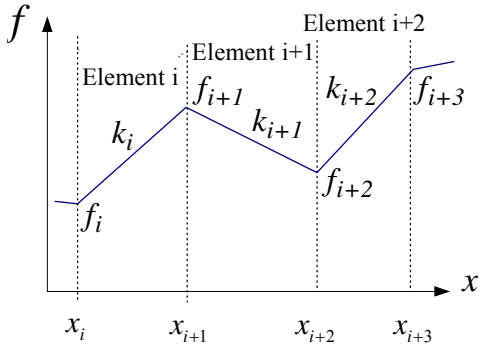

Figure 8.4 Schematic diagram of the elastoplastic elements

8.2 Equation of Motion

As shown in Figure 8.2, the simplified SDOF system for the barge is governed by the following equation of motion:

$$m_b\ddot{x}(t) + f[x(t)] = 0 \tag{8.4}$$

$$x(0) = 0 \text{ and } \dot{x}(0) = V_i \tag{8.5}$$

where m_B and V_i is the mass and initial velocity of the barge, respectively. The restoring force $f(\delta)$ is defined by a series of elements as

$$f(x) = k_i(x - x_i) + \sum_{j=1}^{i-1} k_j\left(x_{j+1} - x_j\right) \text{ for } x_{i+1} > x \geq x_i,\ i \geq 1, \text{ and } x_1 = 0 \tag{8.6}$$

$$k_i = \frac{f_{i+1} - f_i}{x_{i+1} - x_i} \tag{8.7}$$

where x and $f(x)$ are the crushing distance and resisting force, respectively, and (x_i, f_i) is the stating point of the *i*th element.

Alternatively, the restoring force in the *i*th subdomain can be written as

$$f(x) = k_i x - b_i \text{ for } x_{i-1} \leq x < x_{i+1} \tag{8.8}$$

$$b_i = k_i x_i - f_i \tag{8.9}$$

where both k_i and b_i are constants in the *i*th subdomain.

Substituting Eq. (8.8) into Eq. (8.4) yields

$$m\ddot{x} + k_i x = b_i,\ i = 1 \ldots N \tag{8.10}$$

where *N* is the total number of the elastoplastic elements of the system.

Once the values of x_i, f_i, x_{i+1}, and f_{i+1} are known, the equation of motion in Eq. (8.10) has a closed form solution. Denoting $\lambda_i = k_i / m$, the solution of the equation is given as follows.

$$x(t) = \begin{cases} c_1 e^{\sqrt{-\lambda_i}t} + c_2 e^{-\sqrt{-\lambda_i}t} + \dfrac{b_i}{k_i} & \text{for } \lambda_i < 0 \\ c_1 + c_2 t & \text{for } \lambda_i = 0 \\ \sin\sqrt{\lambda_i}t + c_2 \cos\sqrt{\lambda_i}t + \dfrac{b_i}{k_i} & \text{for } \lambda_i > 0 \end{cases} \tag{8.11}$$

where the arbitrary constants c_1 and c_2 are evaluated by the initial conditions or the boundary conditions.

Using the analytical solution in Eq. (8.11), an optimization problem may be defined for the dynamic system identification. The optimization problem minimizes the error function defined between the given system quantity from numerical simulations and the quantity computed from the analytical solution. Thus, the obtained mathematical representation for the force-displacement curve identifies the simplified model for the barge.

8.3 Optimization Formulation for System Identification

To formulate the identification problem, assume *N* elements, and let x_i, $i = 1$ to *N* denote all the displacement break points for the entire domain. Also, let f_i represent the corresponding force values. Then the unknowns of the identification problem can be collectively represented in the vector *q* as

$$q = [x_1, x_2, \cdots x_{N+1}, f_1, f_2, \cdots f_{N+1}]^T \tag{8.12}$$

The system identification problem is to reduce the error between the given data and its analytical representation. Using the L_2 norm, the error function is defined as

$$\text{Minimize } E(q) = \sum_{i=1}^{N} \int_{t_i}^{t_{i+1}} [f(x) - m\ddot{x}(q,t)]^2 \, dt \tag{8.13}$$

Subject to $x_{i+1} > x_i$

$x_1 = 0$, $f_1 = 0$, $x_{N+1} = x_{\max}$

$0 \le f_i \le \max[f(x)]$

where $f(x)$ is the given impact force data from the FE simulations, and $\ddot{x}(q,t)$ is available from Eq. (8.11).

The total number of optimization variables is $2N-1$ because x_1, f_1, and x_{N+1} are known. To solve the constrained nonlinear optimization problem, a program has been written using the Sequential Quadratic Programming (SQP) method in MATLAB 6.5 [40].

8.4 Numerical Example

The impact force time-history of a fully loaded barge impacting a square pier ($\alpha = 1.0$) with a velocity of 1.8 m/s (3.5 knots) has been simulated using the program LS-DYNA. The crushing resistance of the barge is identified with eight elements, as shown in Figure 8.5. Since the resisting force is obtained as a piecewise linear function of the displacement, the slope of the force curve in a displacement subdomain indicates transient stiffness for that domain. The stiffness of each element is presented in Table 8.1.

From Table 8.1, it can be seen that most of the elements are collapse elements with negative stiffness coefficients. The first element is the stiffest and the second

element deflects at the greatest rate due to the damage of the structural members during the activity of element 2. After these processes, even though the collapse process continues, the impact force remains relatively stable. Elements 7 and 8 have positive stiffness coefficients because the bow structure is strong enough to resist the impact forces while these elements are active.

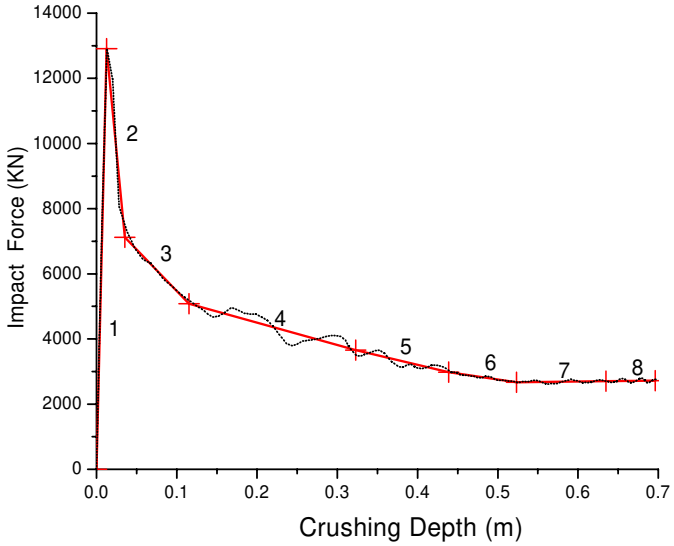

Figure 8.5 Impact force vs. crushing depth from a fully loaded barge impacting a square pier at a velocity of 1.8 m/s

Table 8.1. Identified stiffness coefficients for a barge impacting a square pier (α=0.1) with a velocity of 1.8 m/s

Element i	Stiffness k_i (MN/m)
1	1034.47
2	-254.49
3	-25.43
4	-6.88
5	-5.83
6	-3.60
7	0.29
8	0.27

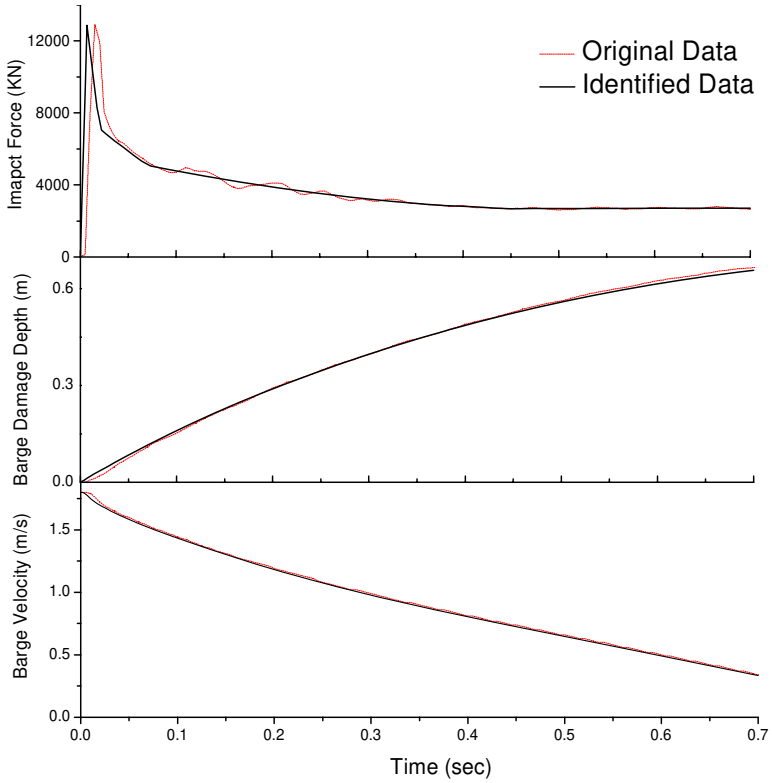

Figure 8.6 Impact time histories reproduced using the identified parameters for a fully loaded barge impacting a square pier at a velocity of 1.8 m/s

Various structural configurations that are used in practice cause the FE results to fluctuate. Since this study pertains to general collision cases, the individual barge configuration may be ignored. Although a greater number of force elements increase the accuracy of the approximation, eight elements efficiently represent the dynamic strength of the bow structure.

Once a barge-pier collision problem is identified, the time variation of the impact force, crushing distance, and so on, can be easily reproduced using Eq. (8.11). As for the example presented in this section, the corresponding relationships are shown in Figure 8.6. The results from the simple SDOF system correlate well with those from the FE simulation. Containing several elements, this particular representation of the nonlinear force-deformation relationship greatly simplifies the subsequent analyses. The

significance of the system identification is far more than a mere simplification of the force-deformation representation, but that topic is beyond the scope of this dissertation.

8.5 Identification of a Damped System

As demonstrated in Chapters 4 and 7, the impact velocity affects the impact process. In order to account for the influence of velocity, the forgoing formulation for the undamped SDOF system should be extended to a damped SDOF system shown in Figure 8.7. With damping added, the system's free vibration is described by the differential equation of motion:

$$m_B\ddot{x}(t) + c_i\dot{x} + k_i x(t) = b_i \tag{8.14}$$

where c_i is the damping coefficient of the *i*th element.

Assume that the damping is coupled with the displacement, and takes the form:

$$c_i = C_{i,1} + C_{i,2}x \tag{8.15}$$

where $C_{i,1}$ and $C_{i,2}$ are the constants to be determined.

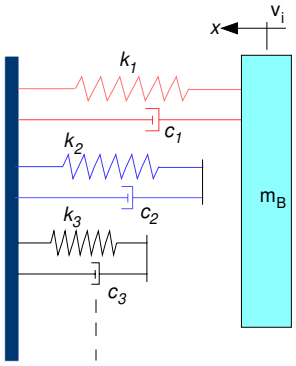

Figure 8.7 Schematic diagram of a damped SDOF system

In order to solve the second order non-homogeneous Eq. (8.15), a series of approximation or numerical solutions is necessary. The vector q is also altered to include the damping parameters:

$$q = [x_1, x_2, \cdots x_{N+1}, f_1, f_2, \cdots f_{N+1}, C_{1,1}, C_{1,2}, \cdots C_{N+1,1}, C_{N+1,2}]^T \tag{8.16}$$

The cost function remains the same as Eq. (8.13) except for the addition of one more constraint $C_{1,1} = 0$. The optimization algorithm was implemented in MATLAB6.5. Eight elements were used to identify the same impact problem as in the previous section. The identified parameters are presented in Table 8.2.

The element parameters in Table 8.2 can be used to predict a different impact scenario than the original. As a second example, consider a case where the initial velocity is $V_i = 1.29$ m/s (2.5 knots) instead of $V_i = 1.8$ m/s (3.5 knots), and the barge mass m_B remains the same as in the first example. Using the identified parameters in Table 8.2, Eq. (8.11) gives the time histories of the impact force, barge damage depth, and barge velocity, which are shown in Figure 8.8. The difference between the analytical solution and results from the FE simulation is minor.

Table 8.2. Damped-SDOF-System elements identified for a barge impacting a square pier (α=0.1) with a velocity of 1.8 m/s

Element i	X_i (m)	Y_i (KN)	$C_{i,1}$ (KN×s/m)	$C_{i,2}$ (KN×s/m^2)
1	0.000	0.000	0.000	491.563
	0.007	7161.978		
2			2748.088	758.287
	0.034	4319.111		
3			1445.618	102.556
	0.132	3216.159		
4			939.499	967.296
	0.282	2577.714		
5			820.015	230.319
	0.428	2206.101		
6			727.262	259.994
	0.516	2143.522		
7			786.610	429.005
	0.619	1971.833		
8			906.312	808.525
	0.696	2466.894		

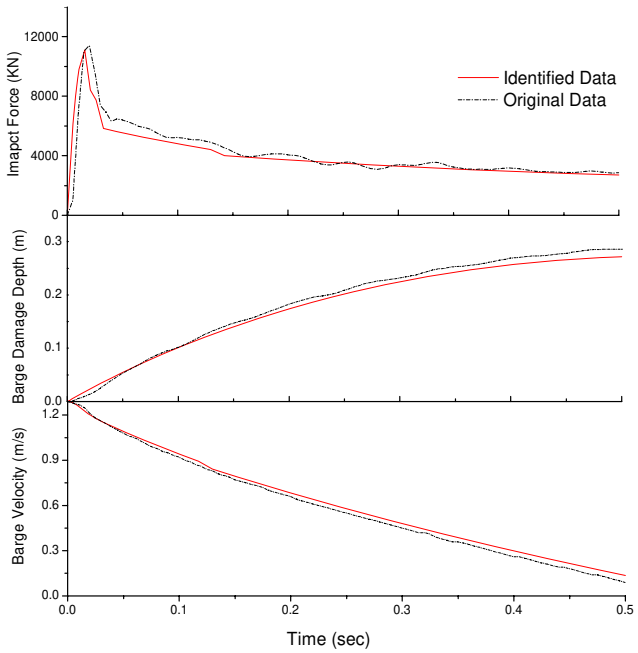

Figure 8.8 Impact time histories predicted using the identified parameters for a fully loaded barge impacting a square pier ($\alpha = 0.1$) at a velocity of 1.8 m/s

8.6 Summary

In this chapter, a representation for the crushing force of barges is developed in the displacement domain with the elastoplastic-collapse elements. The elastoplastic-collapse concept introduced here allows physical interpretation of the force-deformation or force-time curves. Moreover, using the developed formulations, the transformation from the force-deformation history to the force-time history can be performed, and vice versa. When the force-time or force-deformation histories are specified, they can be used to construct a SDOF oscillation system, which provides the fundamental features of barge impact loadings. In addition, the formulation makes it possible to describe the progressive dynamic collapse of a barge during impact with a piecewise linear function. Application of the procedures to model the dynamic stiffness of barge bows is presented in Chapter 9.

Chapter 9 Spring-Mass Model for Barge Flotillas Impacting Bridge Piers

This chapter introduces an elastoplastic spring-mass model to analyze multi-barge flotillas colliding with bridge piers. The model accounts for the essential factors pertaining to barge-flotilla impacts, such as the pier geometry, stiffness, and dynamic interactions between barges. Nonlinear spring elements are used in this model. Although a one-dimensional (1-D) multi-degree of freedom (MDOF) model is presented in this chapter, it can be converted into a two-dimensional (2-D) MDOF model if required. The proposed model generates impact force time-histories for numerous simulation cases in a matter of minutes, which is especially valuable in probabilistic analysis which requires many collision simulations. Furthermore, the results from the proposed model are compatible with the respective impact time-histories produced by exhaustive finite element simulation. Analysis of a bridge pier subjected to a 15-barge flotilla impact is included as an example.

9.1 Stiffness of Barge Body

In Chapter 7, the barge bow stiffness was discussed in detail. However, it is also important to know the barge body stiffness in investigating the interactions between barges in a multi-barge flotilla during an impact event. Prior to developing a flotilla model, the stiffness of the barge body must to be identified. Similar to the method used in Chapter 7, the stiffness of individual barge bodies contained in a flotilla is obtained through FE simulations. Figure 9.1 shows the FE model of JH bodies. The barge body is fixed on one end and pressed by a rigid wall from the other end.

The force-deformation relationship of the barge body is presented in Figure 9.2. Since barge bodies are very stiff and remain elastic for most cases, a bilinear model based on the envelope of the dynamic stiffness is used to describe the barge-body resistance to compression, which is given by:

$$f_B(\delta_B) = \begin{cases} 1.2 \times 10^3 \delta_B & \text{for } \delta_B \le 0.125 \\ 147.8 + 17.6\delta_B & \text{for } \delta_B > 0.125 \end{cases} \tag{9.1}$$

where the barge resisting force $f_B(\delta_B)$ and barge body deformation δ_B are in MN and m, respectively.

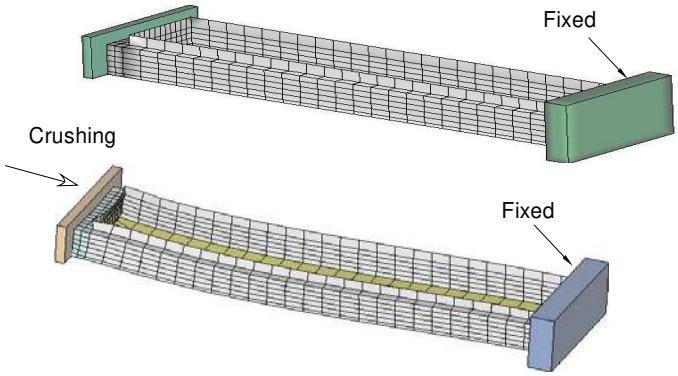

Figure 9.1 FE simulation of JH body stiffness by compressing the body structure with a rigid wall

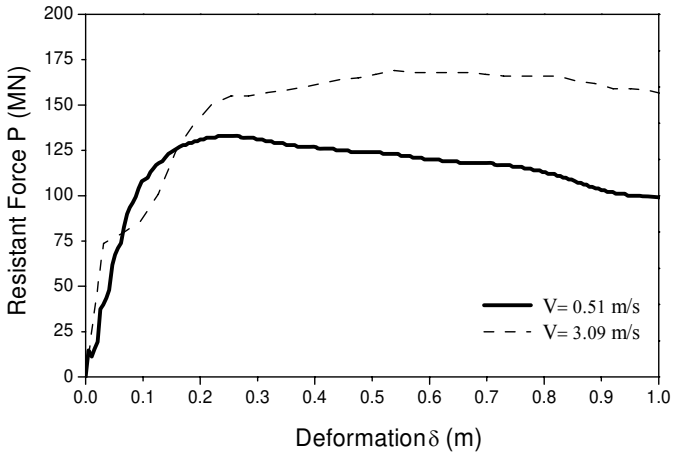

Figure 9.2 Force-Deformation relationships for JH bodies under different deformation rates

Note that Eq. (9.1) is only valid for longitudinally symmetric compression. It is consistent with this study that discriminating between impact angles is not important for predicting the maximum impact forces on bridge piers.

9.2 Stiffness of Barge Bows and Lashing Cables

As demonstrated in Chapter 8, the complex nonlinear behavior of the crushed barge bow during impact can be represented with the piecewise linear spring elements. The resisting force of the i*th* element is expressed as

$$f_b(\delta_b) = k_{b,i}(\delta_b - \delta_{b,i}) + \sum_{j=1}^{i-1} k_{b,j}\left(\delta_{b,j+1} - \delta_{b,j}\right) \text{ for } \delta_{b,i+1} > \delta_b \geq \delta_{b,i},\ i \geq 1, \text{ and } \delta_{b,1} = 0 \quad (9.2)$$

$$k_{b,i} = \frac{f_{b,i+1} - f_{b,i}}{\delta_{b,i+1} - \delta_{b,i}} \quad (9.3)$$

where δ_b and $f_b(\delta_b)$ are the crushing distance and resisting force of the barge bow, respectively, and ($\delta_{b,i}$, $f_{b,i}$) is the stating point of the *i*th element.

The connection method between barges is described in Chapter 6. For brevity only, the following material model for the steel cables is adopted.

$$f_B(\delta_B) = \begin{cases} 1.2 \times 10^3 \delta_B & \text{for } \delta_B \leq 0.125 \\ 147.8 + 17.6\delta_B & \text{for } \delta_B > 0.125 \end{cases} \quad (9.4)$$

where the barge resisting force $f_B(\delta_B)$ and body deformation δ_B are in MN and m, respectively.

9.3 Resistance-Displacement Relationships of the Connections

For a MDOF system exhibiting elastoplastic behavior, expressions for the restoring forces can be written and incorporated into the time integration algorithms.

These expressions depend on the magnitude of the restoring force as well as on whether the relative displacements between masses in the system are increasing or decreasing. In the multi-barge flotilla model, three types of nonlinear springs are used to represent the force-displacement relationships for a barge flotilla.

The force-displacement relationship for the barge bow in contact with the pier is schematically shown in Figure 9.3(a). The resisting forces *F* at time t for each stage are given by

$$\text{Loading: } F(t) = f_b[\delta(t)] \tag{9.5}$$

$$\text{Unloading: } F(t) = \begin{cases} \dfrac{f_b(\delta_\beta)[\delta(t) - \delta_\alpha]}{\delta_\beta - \delta_\alpha} & \text{for } \delta(t) > \delta_\alpha \\ 0 & \text{for } \delta(t) \le \delta_\alpha \end{cases} \tag{9.6}$$

$$\text{Reloading: } F(t) = \begin{cases} f_b[\delta(t)] & \text{for } \delta(t) > \delta_\beta \\ \dfrac{f_b(\delta_\beta)[\delta(t) - \delta_\alpha]}{\delta_\beta - \delta_\alpha} & \text{for } \delta(t) \le \delta_\beta \\ 0 & \text{for } \delta(t) < \delta_\alpha \end{cases} \tag{9.7}$$

where δ_α and δ_β, determined by the relative displacement $\delta(t) = x_i(t) - x_{M1}(t)$, identify the beginning of separation and unloading processes, respectively; $x_i(t)$ is the displacement of the barge contacting with the pier.

The adjacent barges in the same column have two interaction modes: push and pull. A mixed spring element is used to describe this type of interaction. In addition, gaps between the barges and the relaxation of lashing cables should be considered. Referring to Figure 9.3(b), the resisting forces *F* at time t for each stage are given by

$$\text{Loading: } F(t)=\begin{cases} 0 & \text{for } d_b \ge \delta(t) \ge d_c \\ f_d[\delta(t)] & \text{for } \delta(t) \ge d_b \\ f_c[\delta(t)] & \text{for } \delta(t) \le d_c \end{cases} \tag{9.8}$$

$$\text{Unloading: } F(t)=\begin{cases} \dfrac{f_d(\delta_{\beta 1})[\delta(t)-\delta_{\alpha 1}]}{\delta_{\beta 1}-\delta_{\alpha 1}} & \text{for } \delta(t) \ge \delta_{\alpha 1} \\ 0 & \text{for } \delta_{\alpha 2} \le \delta(t) \le \delta_{\alpha 1} \\ \dfrac{f_c(\delta_{\beta 2})[\delta(t)-\delta_{\alpha 2}]}{\delta_{\beta 2}-\delta_{\alpha 2}} & \text{for } \delta(t) < \delta_{\alpha 2} \end{cases} \tag{9.10}$$

$$\text{Reloading: } F(t)=\begin{cases} 0 & \text{for } \delta_{\alpha 2} \le \delta(t) \le \delta_{\alpha 1} \\ \dfrac{f_d(\delta_{\beta 1})[\delta(t)-\delta_{\alpha 1}]}{\delta_{\beta 1}-\delta_{\alpha 1}} & \text{for } \delta_{\beta 1} \ge \delta(t) > \delta_{\alpha 1} \\ \dfrac{f_c(\delta_{\beta 2})[\delta(t)-\delta_{\alpha 2}]}{\delta_{\beta 2}-\delta_{\alpha 2}} & \text{for } \delta_{\beta 2} \le \delta(t) < \delta_{\alpha 2} \\ f_d[\delta(t)] & \text{for } \delta(t) > \delta_{\beta 1} \\ f_c[\delta(t)] & \text{for } \delta(t) < \delta_{\beta 2} \end{cases} \tag{9.11}$$

where $\delta_{\alpha 1}, \delta_{\beta 1}, \delta_{\alpha 2}$, and $\delta_{\beta 2}$ are breakpoints determined by the relative displacements $\delta(t) = x_i(t) - x_j(t)$; $x_i(t)$ and $x_j(t)$ are the displacements of the two adjacent barges in the same column, respectively; d_b and d_c are the gaps between the barges for compression and tension, respectively.

A tension-only spring element, as shown in Figure 9.3(c), is used to describe the connections between barge columns. The resisting forces *F* at time t for each stage are given by

$$\text{Loading : } F(t)=\begin{cases} 0 & \text{for } |\delta(t)| \le d_c \\ f_c[\delta(t)] & \text{for } |\delta(t)| > d_c \end{cases} \tag{9.12}$$

$$\text{Unloading: } F(t)=\begin{cases} \dfrac{f_c(\delta_{\beta})[\delta(t)-\delta_{\alpha}]}{\delta_{\beta}-\delta_{\alpha}} & \text{for } |\delta(t)| \ge \delta_{\alpha} \\ 0 & \text{for } |\delta(t)| < \delta_{\alpha} \end{cases} \tag{9.13}$$

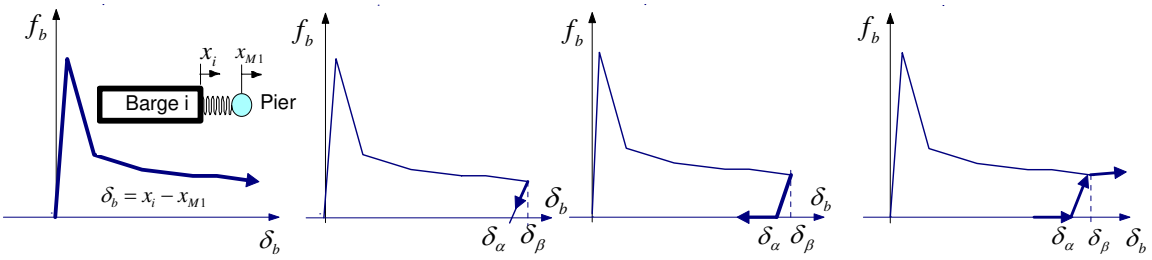

(i) Loading (ii) Unloading (iii) Reloading

(a)

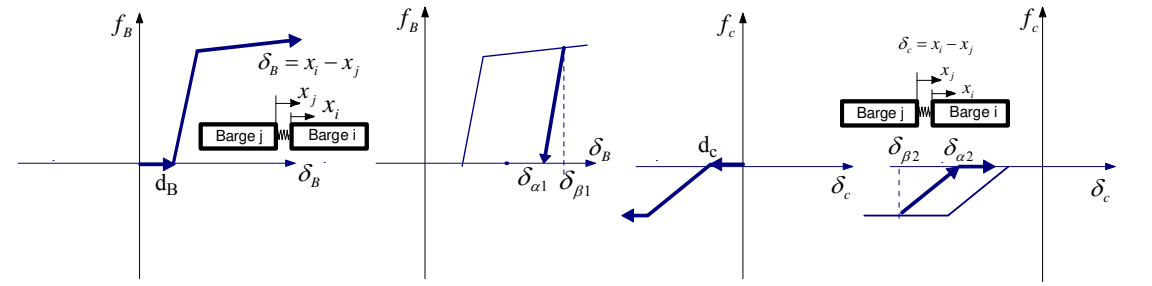

(i) Barge compression loading (ii) Barge compression unloading (iii) Cable tension loading (iv) Cable tension unloading

(b)

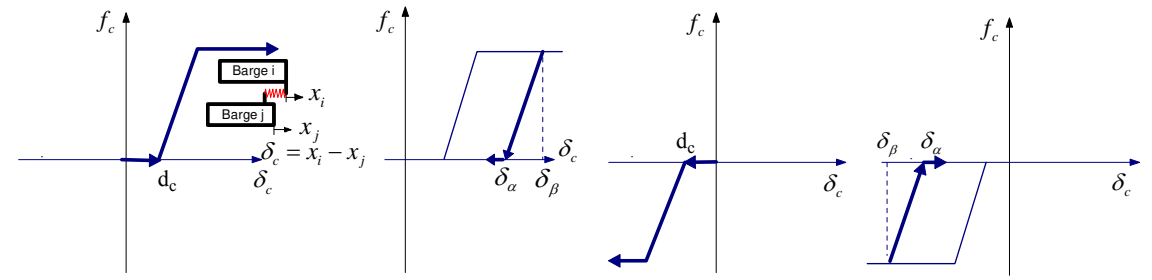

(i) Positive tension loading (ii) Positive tension unloading (iii) Negative tension loading (iv) Negative tension unloading

(c)

Figure 9.3 Force vs. relative displacement model formulation: (a) barge-pier interaction; (b) barge-barge interaction in the same column; (c) barge-barge interaction between adjacent columns

$$\text{Reloading: } F(t) = \begin{cases} 0 & \text{for } |\delta(t)| \le \delta_\alpha \\ \dfrac{f_c(\delta_\beta)[\delta(t) - \delta_\alpha]}{\delta_\beta - \delta_\alpha} & \text{for } \delta_\beta > |\delta(t)| > \delta_\alpha \\ f_c[\delta(t)] & \text{for } |\delta(t)| \ge \delta_\beta \end{cases} \tag{9.14}$$

where δ_α and δ_β are breakpoints determined by the relative displacement $\delta(t) = x_i(t) - x_j(t)$; $x_i(t)$ and $x_j(t)$ are the displacements of the two adjacent barges in the same row, respectively; d_c is the gap for cable tension.

9.4 Dynamic Response of the Pier

As shown in Figure 9.4, a common bridge pier may be idealized as a cantilever column with four degrees of freedom (DOF): two translational, x_{M1} and x_{M2}, and two rotational, θ_{M1} and θ_{M2}. Two lumped masses, M_1 and M_2, are associated with the pier displacements at the top and collision point, respectively, and are written as

$$M_1 = 0.5(L_1 + L_2)\bar{m} \tag{9.15}$$

$$M_2 = m_s + 0.5L_2\bar{m} \tag{9.16}$$

where L_1 is the collision position on the pier; L_2 is the distance between the collision point and the pier top; $\bar{m}$ is the mass per unit length of the column; m_s is the sum of the other masses attributed to the pier.

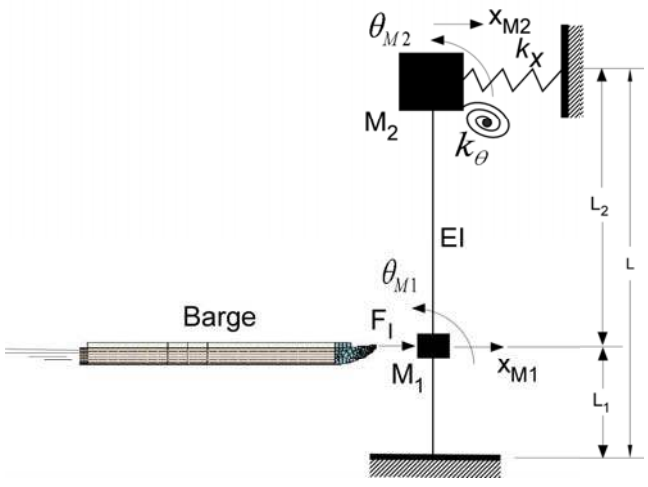

Figure 9.4 Idealized pier model for the dynamic analysis

The static force-displacement relationship for this structure, as expressed through the stiffness matrix, can be written as

$$EI\begin{bmatrix} \frac{12}{L_1^3}+\frac{12}{L_2^3} & -\frac{12}{L_2^3} & \frac{6}{L_1^2}-\frac{6}{L_2^2} & -\frac{6}{L_2^2} \\ -\frac{12}{L_2^3} & \frac{12}{L_2^3}+\frac{k_x}{EI} & \frac{6}{L_2^2} & \frac{6}{L_2^2} \\ \frac{6}{L_1^2}-\frac{6}{L_2^2} & \frac{6}{L_2^2} & \frac{4}{L_1}+\frac{4}{L_2} & \frac{2}{L_2} \\ -\frac{6}{L_2^2} & \frac{6}{L_2^2} & \frac{2}{L_2} & \frac{4}{L_2}+\frac{k_\theta}{EI} \end{bmatrix}\begin{Bmatrix} x_{M1} \\ x_{M2} \\ \theta_{M1} \\ \theta_{M2} \end{Bmatrix}=\begin{Bmatrix} F_I(t) \\ 0 \\ 0 \\ 0 \end{Bmatrix} \tag{9.17}$$

where EI, k_x and k_θ are the flexural rigidity of the pier, translational and rotational stiffness coefficients of mass M_1, respectively; $F_I(t)$ is the flotilla impact force on the pier.

Since the kinetic energy component associated with rotational DOF is negligible in comparison to that corresponding to the translational DOF, static condensation can be used on the stiffness matrix (4×4) to eliminate the two rotational DOF (θ_{M1} and θ_{M2}). The expression for the condensed stiffness matrix is thus given by:

$$[k]=\frac{3}{L_2^2\left[3L_1+4L_2+\frac{k_\theta L_2(L_1+L_2)}{EI}\right]}\begin{bmatrix} k_{11} & k_{12} \\ k_{21} & k_{22} \end{bmatrix} \tag{9.18}$$

in which

$$k_{11}=\left(1+\frac{L_2}{L_1}\right)^3\left[4EI+\left(L_1+L_2\right)k_\theta\right],$$

$$k_{22}=4EI+\left(L_1+4L_2\right)k_\theta+L_2^2\left(3L_1+4L_2\right)\frac{k_x}{3}+L_2^3\frac{(L_1+L_2)k_xk_\theta}{3EI},$$

$$k_{12} = k_{21} = -2\left(2 + \frac{3L_2}{L_1}\right)EI - \left(1 + \frac{3L_2}{L_1}\right)\left(L_1 + L_2\right)k_\theta .$$

Subsequently, the equation of motion can be written in matrix form as

$$[m]\{\ddot{x}\} + [c]\{\dot{x}\} + [k]\{x\} = \{f(t)\} \tag{9.19}$$

where

$$[m] = \begin{bmatrix} M_1 & 0 \\ 0 & M_2 \end{bmatrix},\ [c] = \begin{bmatrix} c_1 & 0 \\ 0 & c_2 \end{bmatrix},\ \{f(t)\} = \begin{Bmatrix} F_I(t) \\ 0 \end{Bmatrix},$$

and c_1 and c_2 are the viscous damping coefficients.

9.5 Modeling of a Multi-Barge Flotilla Impacting a Bridge Pier

The general matrix formulation of the equations of motion for an MDOF elastoplastic system is given by:

$$[m]\{\ddot{x}\} + [c]\{\dot{x}\} + \{f(x)\} = 0 \tag{9.20}$$

where $[m]$ and $[c]$ are the $n \times n$ mass and damping matrices, respectively; $\{\dot{x}\}$ and $\{\ddot{x}\}$ are the $n \times 1$ velocity and acceleration vectors (in physical coordinates), respectively; $\{f(x)\}$ is the $n \times 1$ restoring force vector.

In a uniform way, Eq. (9.20) can be determined using Lagrangian equations given by

$$\frac{d}{dt}\left[\frac{\partial L}{\partial \dot{x}_z}\right] - \frac{\partial L}{\partial x_z} = Q_z^* \tag{9.21}$$

where L is the Lagrangian, x_z ($z = 1 \ldots n$) are the generalized coordinates, and Q_z^* are the generalized forces.

However, the direct stiffness method is more convenient to assemble the equations of motion for the barge-pier system. To clarify the discussion, consider a 6-barge flotilla impacting on a pier with the initial velocity V_0, as schematically shown in Figure 9.5. The system has eight DOF (including x_{M1} and x_{M2}) and eight spring elements. The barge mass and damping matrices are written in a standard way and are not provided herein. The restoring force vector at time *t* is given by

$$\{f[x(t)]\} = \begin{Bmatrix} F_{11,12} - F_{11,21} \\ F_{11,21} + F_{21,22} \\ F_I - F_{11,12} + F_{12,13} - F_{12,22} \\ F_{12,22} + F_{22,23} - F_{21,22} \\ -F_{12,13} - F_{13,23} \\ -F_{22,23} + F_{13,23} \\ F_{M1} \\ F_{M2} \end{Bmatrix} \tag{9.22}$$

$$\begin{Bmatrix} F_{M1} \\ F_{M2} \end{Bmatrix} = [k] \begin{Bmatrix} x_{M1} \\ x_{M2} \end{Bmatrix} - \begin{Bmatrix} F_I \\ 0 \end{Bmatrix} \tag{9.23}$$

where the interaction force of the barge at the *i*th row and *j*th column and the barge at the *r*th row and *s*th column, $F_{ij,rs}$, is dependent on the relative displacement $\delta_{ij,rs}(t) = x_{ij}(t) - x_{rs}(t)$; F_{M1} and F_{M2} are the restoring forces corresponding to the lumped masses M_1 and M_2, respectively.

Finally, the total kinetic energy of a flotilla with N_r rows and N_c columns at time *t* can be expressed as

$$E_k(t) = \frac{1}{2} \sum_{i=1}^{N_r} \sum_{j=1}^{N_c} m_{ij} \dot{x}_{ij}^2 \tag{9.24}$$

where m_{ij} and $\dot{x}_{ij}(t)$ are the mass and velocity of the barge at the *i*th row and *j*th column, respectively.

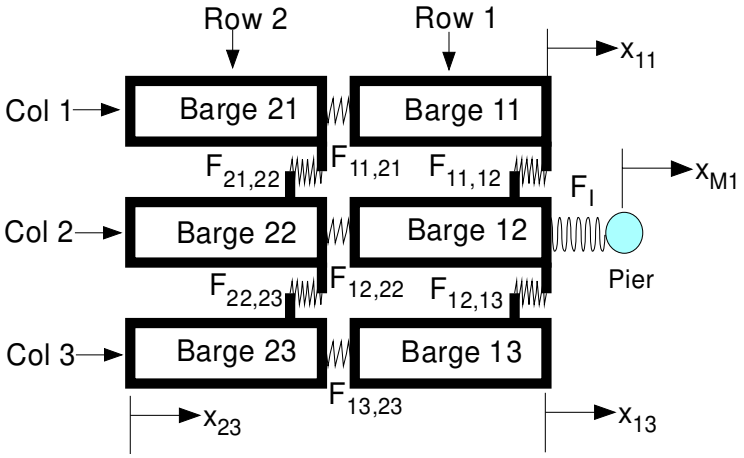

Figure 9.5 Layout of a 6-barge flotilla impacting a rigid pier

9.6 Numerical Evaluation

Since the equilibrium relation in Eq. (9.20) is a set of simultaneous ordinary differential equations with constant coefficients, any finite difference expressions to approximate the accelerations and velocities in terms of displacement can be used. The central difference method is utilized herein. A stable solution can be obtained only by selecting a time step $\Delta t \le \Delta t_{cr}$ [41], given by

$$\Delta t_{cr} = \frac{T_n}{\pi} \tag{9.25}$$

where T_n is the smallest natural period of the MDOF system.

The step-by-step central difference algorithm for the MDOF system is as follows.

(1) Initial calculations

$$\{\ddot{x}\}_0 = -[m]^{-1}[\{f\}_0 + [c]\{\dot{x}\}_0] \tag{9.26}$$

$$a_0 = \frac{1}{(\Delta t)^2},\ a_1 = \frac{1}{2\Delta t},\ a_2 = 2a_0,\ a_3 = \frac{1}{a_2} \tag{9.27}$$

$$\{x\}_{-\Delta t} = \{x\}_0 - \Delta t\{\dot{x}\}_0 + a_3\{\ddot{x}\}_0 \tag{9.28}$$

$$[\hat{m}] = a_0[m] + a_1[c] \tag{9.29}$$

(2) For each time step

$$\{\hat{F}\}_t = -\{f\}_t + a_2[m]\{x\}_t + \hat{m}\{x\}_{t-\Delta t} \tag{9.30}$$

$$\{x\}_{t+\Delta t} = [\hat{m}]^{-1}\{\hat{F}\}_t \tag{9.31}$$

The force vectors $\{f\}$ in Eqs. (9.26) and (9.30) are determined from Eqs. (9.22) and (9.23), depending on the resistance stage.

9.7 Model Validation

Figure 9.6 shows the 3-barge column FE model developed in Chapter 6, which consists of six element types and approximately 76,810 elements. Given an initial velocity $V_0 = 2.06$ m/s (4 knots), the collision between the fully loaded 3-barge flotilla (5.17×10^6 kg) and a rigid pier (cross section: 2.134×2.134 m^2) was simulated using the programs ANSYS8.0 and LS-DYNA970. The impact force time history is presented in Figure 9.7, which is the raw data filtered through a Butterworth filter at 100 Hz [37].

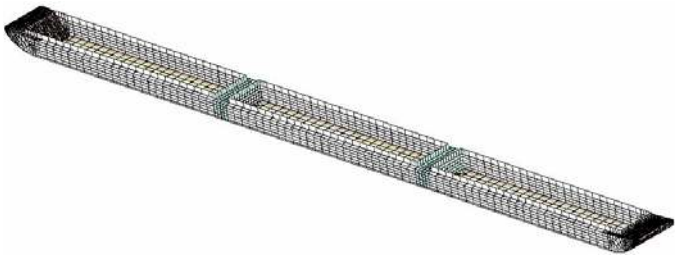

Figure 9.6 Detailed FE model of the 3-barge column developed using the program ANSYS8.0

The same problem was also solved by the proposed model. As indicated in Figure 9.7 and Table 9.1, a comparison of the two models shows excellent agreement. Both methods not only demonstrated correlation between the impact force and crushed distance but also reflect a similar dynamic response as well. By comparison, the AASHTO and Modjest & Masters design loads [42] considerably overestimate the impact force. However, the AASHTO method and the proposed model predict very similar values for the barge damage depth.

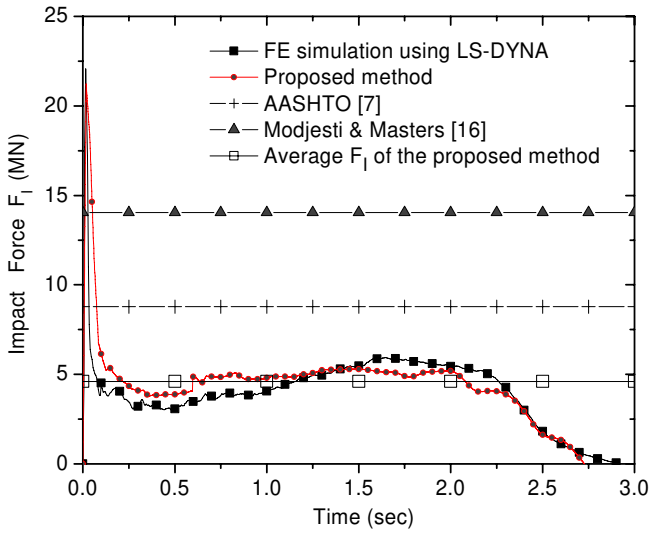

Figure 9.7 Comparison between the impact force time-histories for the 3-barge column impacting a rigid rectangular pier

Table 9.1. Comparison between the methods predicting barge impact forces

Method	Average impact force (MN)	Barge damage depth (m)	Impact duration (s)
Proposed method	4.6	1.8	2.7
LS-DYNA FE simulation	4.0	2.0	2.9
AASHTO method	8.8	1.7	NA
Modjest & Masters method	14.0	NA	NA

9.8 Example

A reinforced concrete bridge pier shown in Figure 9.8(a) is subject to the impact of a 15-barge flotilla (see Figure9.8 (b)), which has a total mass of $15 \times 1.72 \times 10^6$ kg and an initial velocity of 1.54 m/s (3.0 knots). The superstructure mass is $m_s = 8.5 \times 10^5$ kg, the damping coefficients of the pier are $c = 3.408 \times 10^5$ kg/s , the stiffness coefficients are $k_x = 1.430 \times 10^8$ N/m and $k_\theta = 1.533 \times 10^{10}$ N, and the flexural rigidity is $EI = 3.309 \times 10^{10}$ m^{2}N. The material plasticity of the pier is not considered.

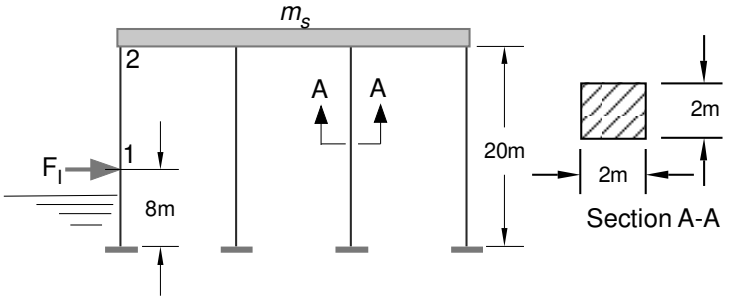

(a)

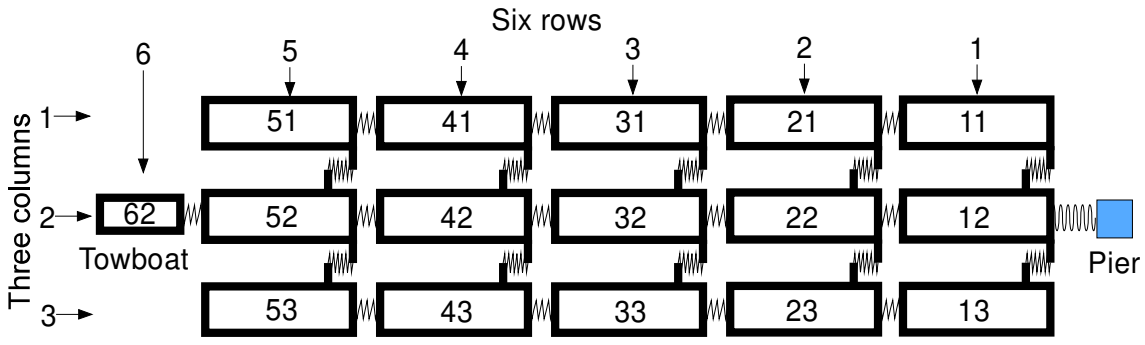

(b)

Figure 9.8 Example conditions: (a) layout of the pier frame; (b) layout of the 15-barge flotilla including a towboat

The pier was analyzed using the proposed model. The results are presented in Figure 9.9. From Figure 9.9(a), it is evident that the assumption of the AASHTO method

that the entire mass of the flotilla acts as a single rigid body produces very conservative results. From Figure 9.9(b), it can be seen that approximately 95% of the initial kinetic energy is dissipated during the collision. The kinetic energy decay is a non-monotonous function of time due to the interactions between barges. Aside from the flexibility of the connectivity of one barge to another, the delayed response of barges also plays an important role in the impact due to gaps. In addition, the barges loosen, or gain relative distance between one another at the end of the impact.

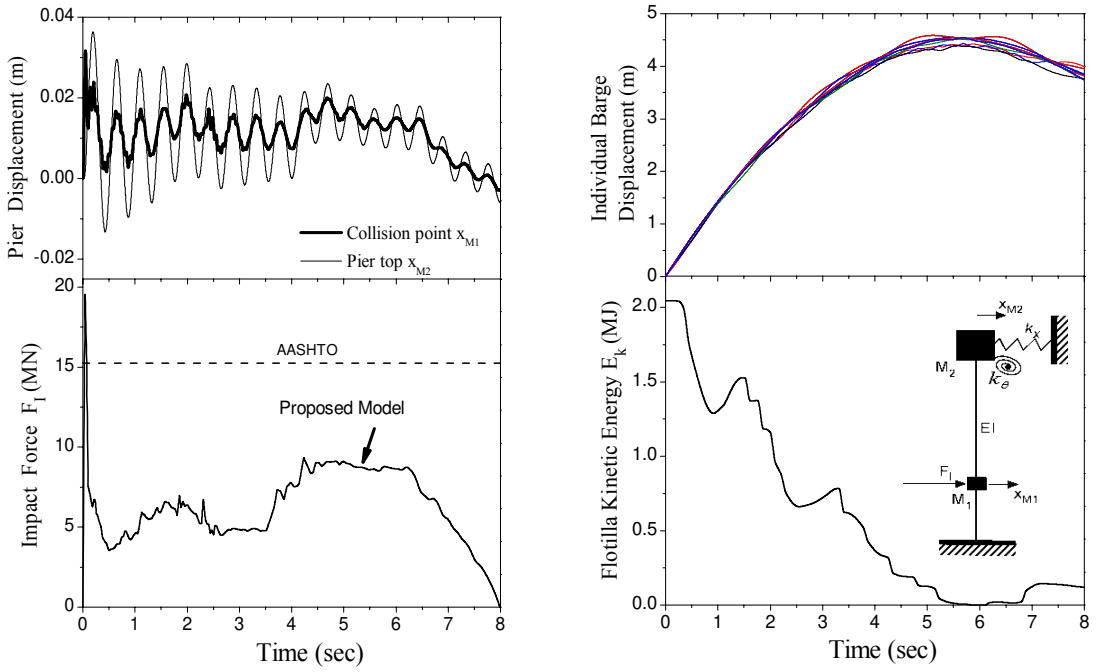

(a) (b)

Figure 9.9 Time histories of the example: (a) pier displacements and impact force; (b) individual barge displacements and flotilla kinetic energy

9.9 Summary

Rarely, if ever, is it possible to model all sources of nonlinearity and portray the actual behavior of practical structures in all of its detail. Normally, the problem is one of

selecting a method that falls short of the ideal in one way or another but that does provides adequate analytical simulation of the case at hand. To reveal the fundamental characteristics of structural impact/collisions with reduced complexity, a simple mass-spring system has been utilized, in which the complicated geometric analysis is no longer required while the two most essential factors for the structural dynamics – inertia and stiffness – are incorporated. The simplified mass-spring colliding system is found to be equivalent to the solution of flotilla-pier collisions, and therefore the system bears clear physical meaning.

It has been shown that the simplified flotilla model derived in this chapter is applicable to the analysis of bridges subjected to barge flotilla impact. All the results generated by the proposed model correlate well with the results from FE simulations.

FE simulations are considered more realistic than the simplified model, but the prohibitive numerical cost inhibits the feasibility of FE simulations in a non-research setting. A full FE model for the collision simulation of a 15-barge flotilla may require 500,000 elements in addition to a computer processing time of several weeks on a powerful computer. In contrast, the proposed simple model for the same flotilla requires mere seventeen elements and a couple of minutes on a common personal computer. Despite the short running time, the simplified approach can answer most of the questions encountered in bridge design. Besides, this method is capable of analyzing the nonlinear response of a pier as long as an appropriate material model is defined.

Since the proposed 1-D MDOF model is constructed to aid bridge designs, it is only suitable for analyzing symmetric impact scenarios. To account for non-symmetrical loading cases, modifications should be made to transform the 1-D MDOF model into a 2-

D MDOF model by adding springs in the transverse direction. With the 2-D capacity, the method could be easily incorporated into a probability-based framework to assess structural performance for a variety of collision scenarios.

Chapter 10 Applications

The foregoing chapters focused on the determination of barge impact forces on piers. Through three examples, this chapter investigates the dynamic response of real bridge structures subjected to barge impact loadings.

The first example, which uses the LS-DYNA970 code, simulates a single-barge impacting a reinforced concrete frame to determine the impact force and dynamic response of the frame. The frame is relatively slender and is assumed to rest on a flexible foundation. This example further reveals the dynamic nature of the barge-pier collision problem. The second example employs the impact force time-histories, developed previously, to analyze the dynamic response of a steel truss-bridge, which is modeled in the program SAP2000. The third example utilizes the program ANSYS8.0 and the previously developed impact force time-history to analyze a modern cable–stayed bridge impacted by a 15-barge flotilla.

Today, vessel impact is one of the most significant design considerations for bridges that span navigable waterways. Until twenty-five years ago, vessel impact loading was not even a consideration when designing bridges. The immediate objectives of the latter two examples are: characterize the global dynamic response of real bridges during barge impacts, evaluate the influence of barge loads on the stability of a whole bridge, and compare the differences between the static analysis and dynamic analysis.

10.1 Simulation of a Barge Impacting a Slender Pier

The reinforced concrete bridge pier in Figure 10.1 is to be analyzed for impact by a JH traveling at a velocity of $V_i = 2.06$ m/s (4 knots). The barge is fully loaded with a mass of $m_B = 1723.65$ metric tons. The example pier consists of four concrete pile columns that are rigidly connected to the concrete cap. A detailed description of the structural member properties and dimensions is given in Figure 10.2. The soil is comprised of five layers of clayey sands which are modeled using 3-D solid elements. The soil properties are presented in Table 10.1. The pier cap, including the superstructure mass supported by it, has a combined mass of 350 metric tons.

Table 10.1. Soil properties of the first example

Layer	Thickness (m)	Modulus of elasticity (MPa)	Density ($\times 10^3 kg/m^3$)
1	2.3	48.3	1.80
2	1.8	82.7	1.84
3	2.8	124.1	1.91
4	5.1	44.8	1.88
5	6.6	124.1	1.95

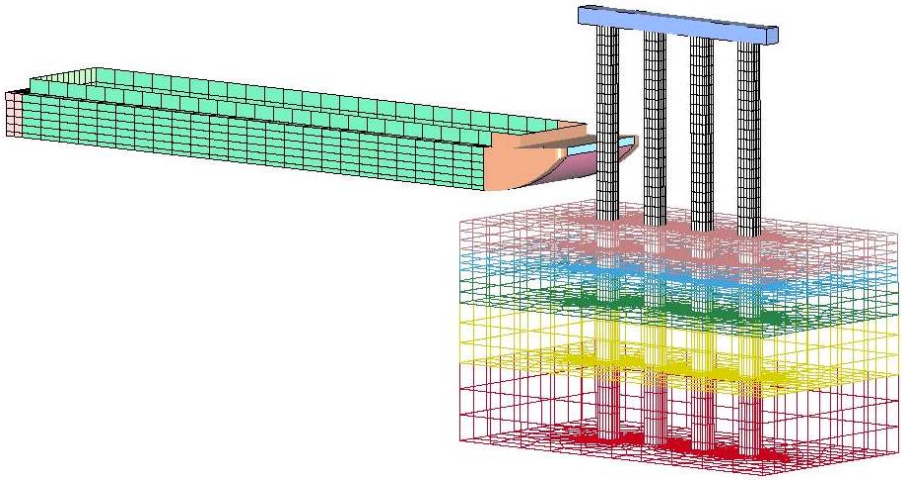

Figure 10.1 3-D view of a barge impacting a concrete pier at a velocity of 2.06 m/s (4 knots)

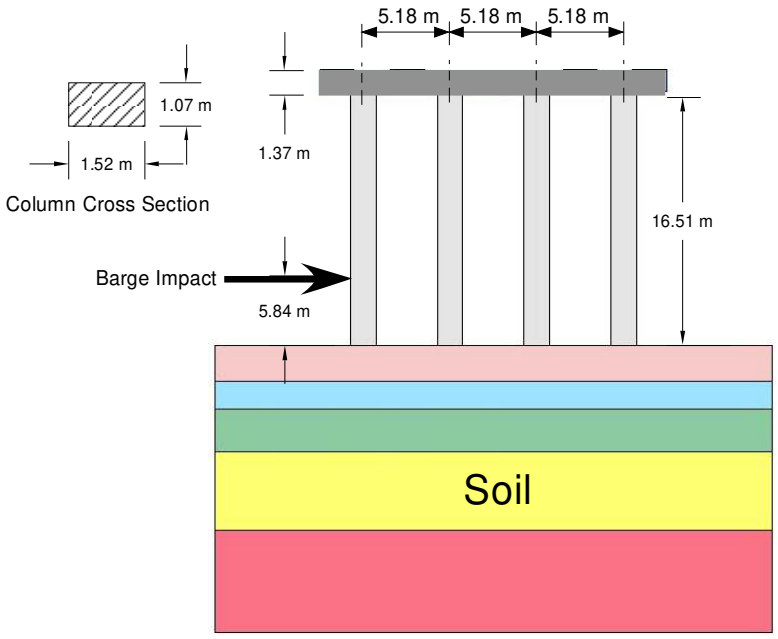

Figure 10.2 Cross-section of the reinforced concrete pier

The simulation of the barge impacting the pier is implemented in the program LS-DYNA970. The time histories of the pier deformation shape, the impact force, and the displacements at the collision point and pier top are presented in Figures 10.3, 10.4, and 10.5, respectively. Figure 10.3 clearly indicates that the static analysis of the pier is not appropriate in this case due to the time-varying nature of the excitation (impact loads) and the dynamic response of the pier. The patterns of the impact force time-histories shown in Figure 10.4 vary, especially at the beginning of impact. The maximum impact force for this flexible pier is much smaller than that for the rigid pier. As proven in Chapter 5, slender piers cannot be assumed to be rigid for the generation of barge impact loadings. Consequently, the interaction between the impacting barge and pier cannot be ignored in the determination of the impact load and dynamic response of the pier. For such cases, computationally intensive FE simulations may be the only current, feasible

method to determine the maximum impact forces. Fortunately, modern highway bridges that cross inland waterways rarely contain slender piers.

It is also found that the foundation of the pier experiences large deformation. Thus, bridge foundations subjected to barge impacts must withstand large lateral dynamic forces, which may largely control the components of bridge design. Moreover, a larger cross-section is required for the pier to resist the shear forces and local damage caused by barge impact.

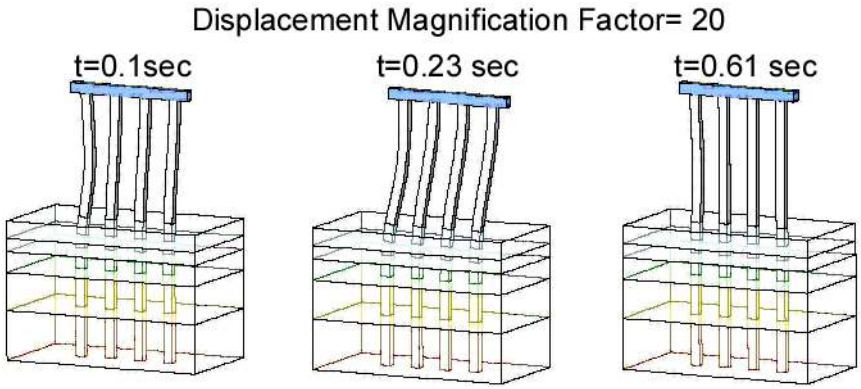

Figure 10.3 Deformation shape of the pier during impact

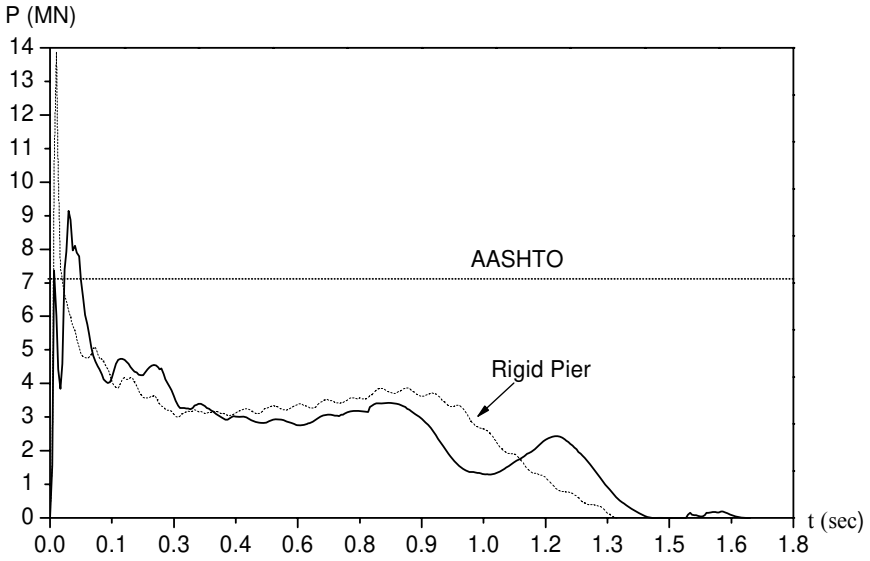

Figure 10.4 Impact force time-history of the pier impacted by a fully loaded JH at a velocity of 4 knots

From Figure 10.5, it can be seen that the pier structure vibrates at a frequency of 3Hz. Both the pier top and the collision point have a very large displacement. Concrete piers cannot endure such a large deformation without serious damage. Therefore, a slender pier is not suitable for resisting barge impacts despite a corresponding reduction in impact forces due to the interaction between the slender pier and the barge.

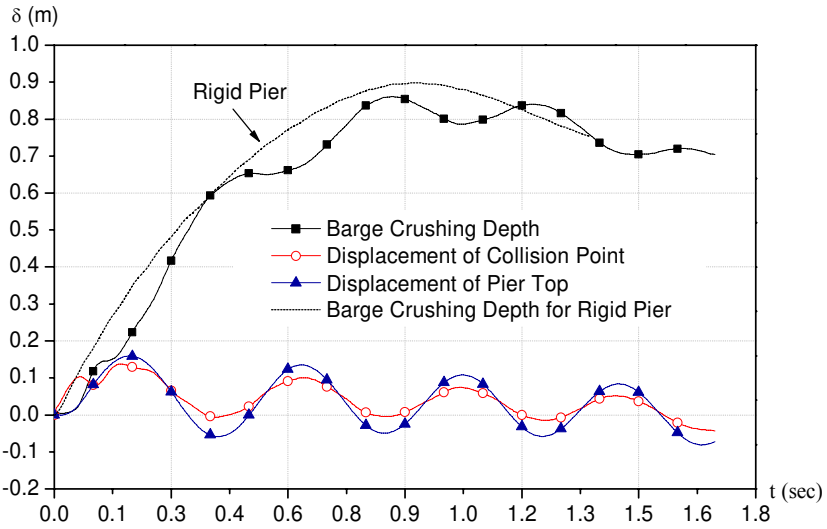

Figure 10.5 Time-histories of the pier displacements and barge crushing distance

Table 10.2. Comparison between the FE simulation, simple model, and AASHTO static analysis for the pier-top displacement

Displacement of the pier top	FE simulation (mm)	Simple model (mm)	AASHTO (mm)
Max(Δ_x)	171	193	140

The AASHTO method does not approximate this type of collision with sufficient accuracy because the analysis method prescribed by AASHTO neglects the pier stiffness. The AASHTO method overestimates the impact force but underestimates the dynamic response of the pier. The results from the AASHTO method and the simple model in Chapter 9 are compared with those from the FE simulation in Table 10.2, which shows

that the AASHTO method and the simplified flotilla model predict a smaller and a larger pier displacement, respectively. This example also indicates that the simplified model is not accurate for analyzing very slender piers.

10.2 Analysis of a Steel Truss Bridge Subjected to Barge Impact

Steel truss bridges are a traditional form of bridge superstructures. A large portion of these bridges contain no provisions that were specifically constructed to resist the forces generated by barge impacts. This example presents the barge flotilla impact evaluation of the US 41 Southbound Bridge over the Ohio River, as shown in Figure 10.6, which connects Evansville, Indiana and Henderson, Kentucky.

Figure 10.6 Side view of the US41 Bridge over the Ohio River

10.2.1 FE Model of the Bridge

The main bridge is a four-span cantilever through-truss type, a bridge type commonly employed for spans of 183 m (600 ft) to 457 m (1,500 ft) in the mid 1970s. The length of the four-span main bridge is 669 m (2,293 ft). The superstructure truss members are made of structural steel, and the substructure piers are made of reinforced concrete.

As shown in Figure 10.7, a 3-D FE model of the main bridge has been developed in the program SAP2000 for impact response analyses. All truss members of the superstructure and piers are modeled using two-node frame elements with three translational DOF and three rotational DOF at each node. The superstructure bearings are represented by a set of spring elements that simulate the behavior of real bearings. The soil reaction is taken into account as springs at the joints in the bridge piers located below the ground line.

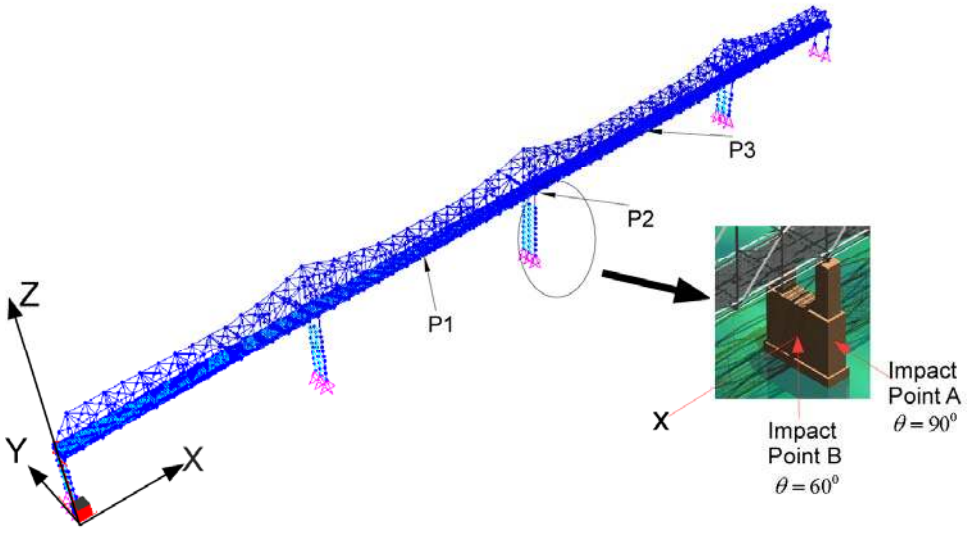

Figure 10.7 3-D view of the FE model of the US41 Southbound Bridge

10.2.2 Impact Load Time History

The impact force time-histories for the 3-, 9-, and 15-barge flotillas, as shown in Figure 10.8, are obtained using the methods described in Chapter 9. The impact loads are applied to the center pier of the main bridge at angles 60 and 90 degrees with the *x*-axis, respectively. The impact force components for the case with the 60-degree impact angle are computed from the 90-degree impact load, using the following relationship:

$$f_x(t) = \mu f_y(t) \tag{10.1}$$

$$f_y(t) = F(t)\sin(60^0) \tag{10.2}$$

where $F(t)$ is the impact force time-history for the head-on collision; $\mu = 0.35$ is the friction coefficient; $f_x(t)$ and $f_y(t)$ are the impact force components in the global *x*- and *y*-direction, respectively.

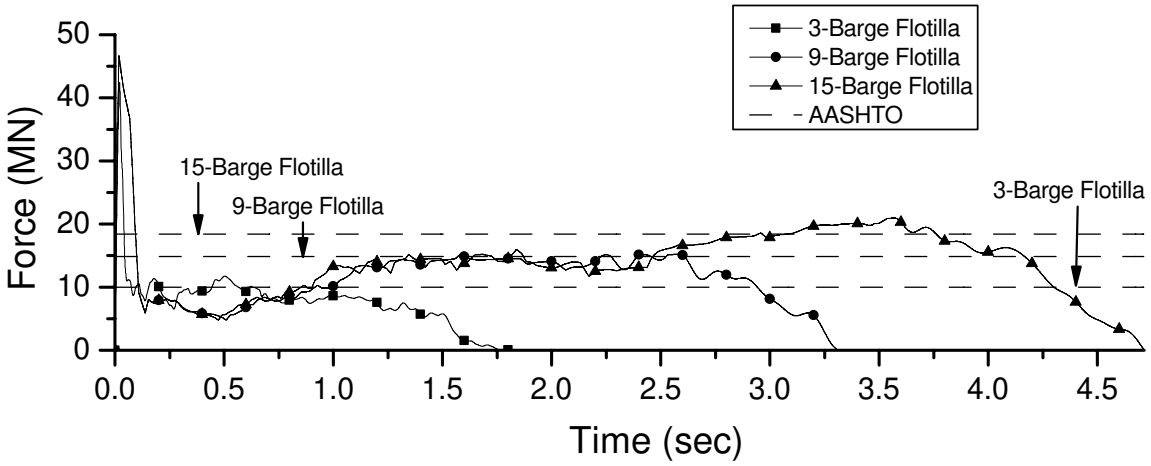

Figure 10.8 Impact loads for the US41 Southbound Bridge (head-on collision, $\theta = 90^0$)

Apparently, the impact force time-histories generated from Eqs. (10.1) and (10.2) are only an approximation of the real impact forces.

10.2.3 Dynamic Response of the Bridge

Regarding the head-on impact case ($\theta = 90^0$), the displacements of the points P1, P2, and P3 in both the global *x*- and *z*-direction are too small to be considered in the analysis. Therefore, only the displacement components in the *y*-direction are presented in Figure 10.9. The displacements of P1, P2, and P3 in the three directions for the oblique impact case ($\theta = 60^0$) are presented in Figure 10.10.

From the comparison between the two cases with different impact angles, two observations are made:

1) Although head-on collisions generally produce a larger impact force as compared to other forms of collision, head-on collisions may not be the worst loading case with respect to the dynamic response of the pier. The dynamic response of piers depends on the associated structural characteristics in addition to the loading. It is important to consider impact angles in bridge design.

2) Static analyses using AASHTO's impact loads may underestimate or overestimate the maximum response of the pier.

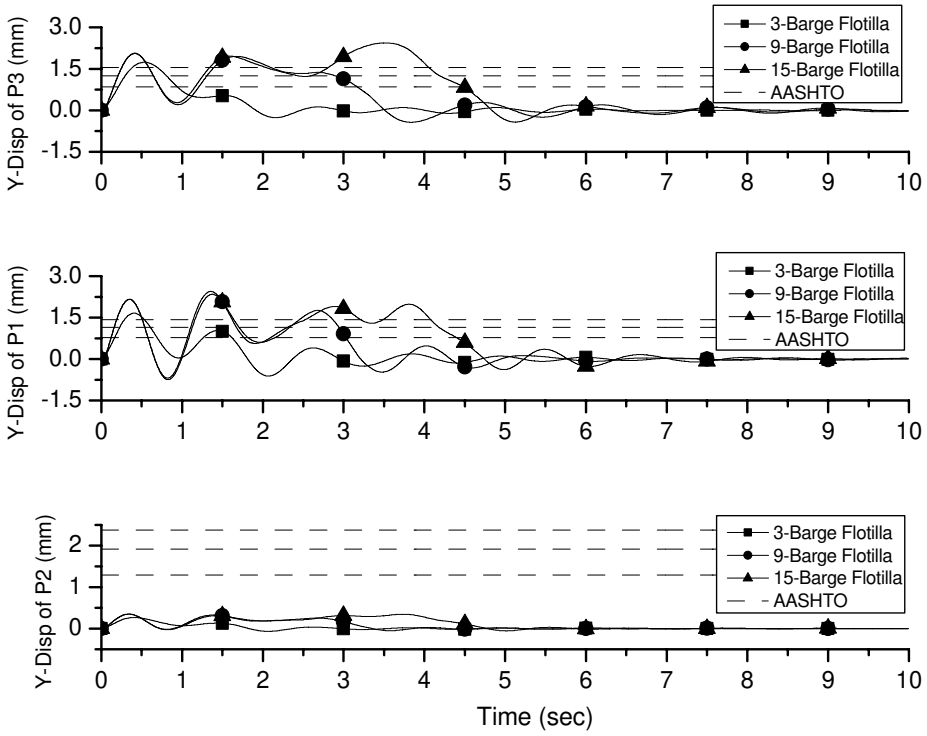

Figure 10.9 Displacements of P1, P2, and P3 in the global *y*-direction produced by the impact loads ($\theta = 90^0$)

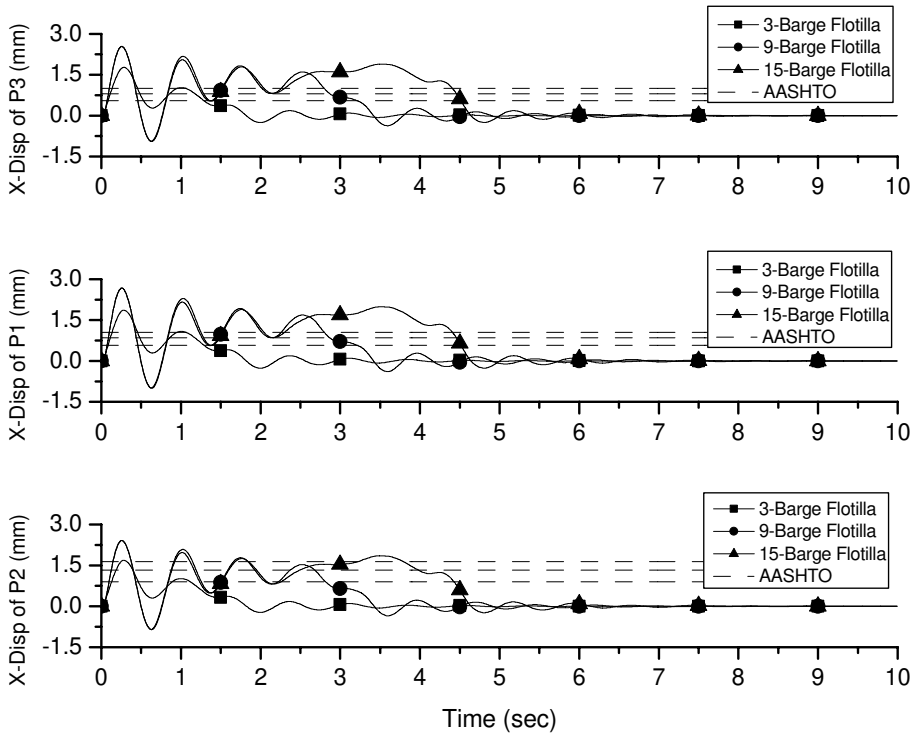

Figure 10.10 (a)

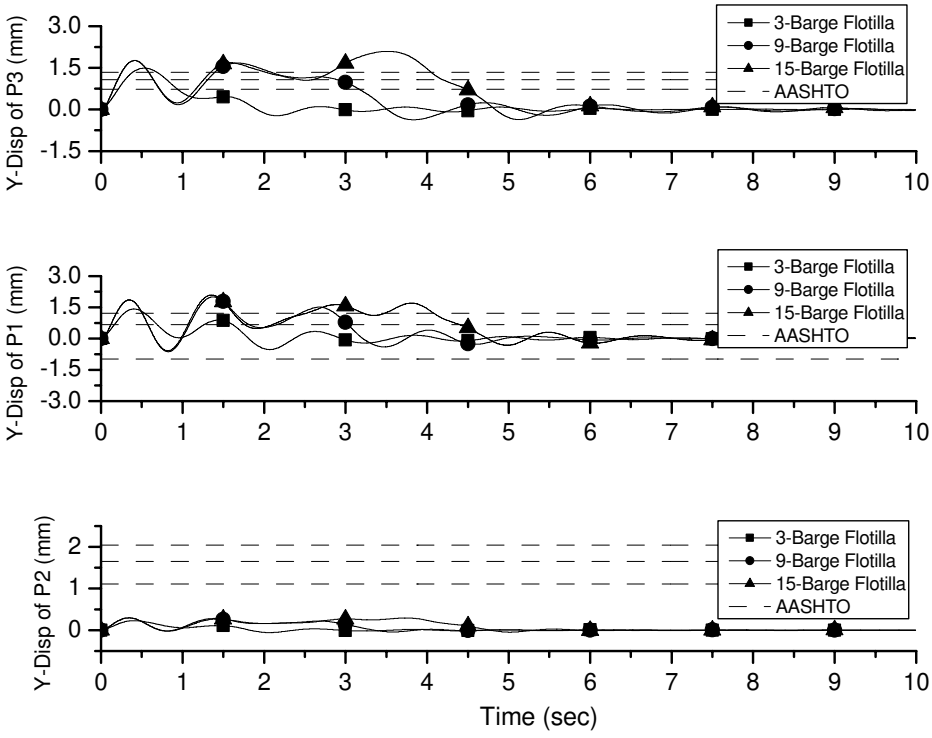

Figure 10.10 (b)

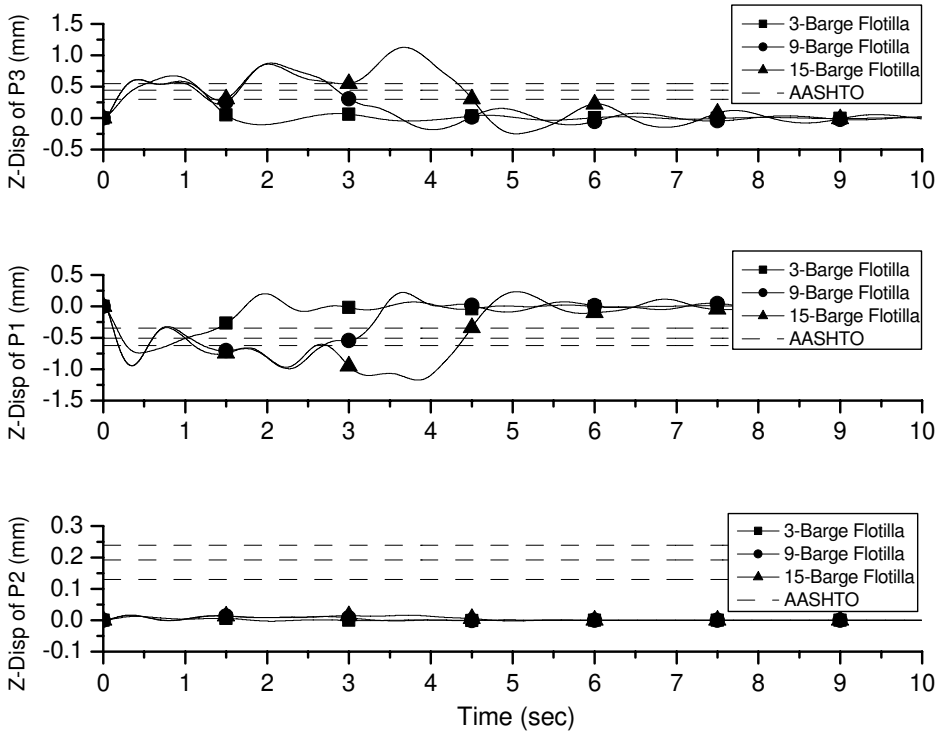

Figure 10.10 (c)

Figure 10.10 Displacements of P1, P2, and P3 produced by the impact loads ($\theta = 60^0$): (a) in x-direction; (b) in y-direction; (c) in z-direction

As shown in Figures 10.9 and 10.10, all the displacements are in the magnitude of millimeters, which should not be regarded as entirely accurate despite the two digit accuracy implied in the figures. However, the results indicate that the US41 Southbound Bridge can withstand a barge flotilla impact without experiencing major structural damage or loss-of-span. This example suggests that barge impact loadings are not a significant threat to large bridges due to the required strength of the piers and foundations in anticipation of other loads, such as earthquake and wind. Nevertheless, foundations should be securely placed in the surrounding soil as mentioned in the previous example.

10.3 Analysis of a Cable-Stayed Bridge Subjected to Barge Impact

Cable-stayed bridges are gaining popularity throughout the world because of their aesthetic appeal. The objective of this example is to investigate the dynamic response of a cable-stayed bridge using the impact force time-history developed in this study.

Figure 10.11 Aerial view of the Maysville Cable-Stayed Bridge

10.3.1 Bridge description

The Maysville Bridge is a cable-stayed bridge linking Maysville, Kentucky, and Aberdeen, Ohio. Figure 10.11 is an aerial view of the bridge. It was officially opened to traffic on January 12, 2001. The bridge is 640.1 m (2100 ft) long and 17.7 m (58 ft) wide, and has two 101.2 m (332 ft) high towers that are supported on drilled concrete shafts. The cable-stayed superstructure consists of a concrete deck supported by two 1.5 to 2.1 m (5 to 7 ft) deep steel plate girders, with floor beams spaced at 0.2 to 0.4 m (0.66 ft to 1.33 ft). The steel stay cables consist of a two-plane semi harped system with stays spaced at 15.2 m (50 ft) intervals along each edge of the deck.

10.3.2 Bridge Modeling

The FE model of the Maysville Cable-Stayed Bridge has been developed using the programs ANSYS8.1. The cable-stayed bridge model shown in Figure 10.12 consists of 1,319 finite elements with 5,160 active degrees of freedom. The initial strain is an important attribute of the cables, and it is accounted for in the analysis. The bases of the towers of the bridge are treated as fixed for all degrees-of-freedom. The north and south ends of the deck are connected to the piers by a tension-link mechanism that permits the end of the deck to rotate freely about the vertical (y) and transverse (z) axes. Rotation about the longitudinal axis (x) and all three translational degrees of freedom are modeled as fixed at each end of the deck. To connect the deck to the piers, the girder linkages are modeled using two rigid vertical links.

10.3.3 Transient Dynamic Analysis

The impact load has been obtained by means of the multi-barge flotilla model of Chapter 9 for a fully loaded 15-barge flotilla at a velocity of 2.57 m/s (5 knots). The multi-barge flotilla impacts the pier head-on, as shown in Figure 10.12. The time history of the impact force is shown in Figure 10.13. The impact load is applied in the z-direction.

The transient dynamic equilibrium equation of the bridge is expressed as follows.

$$[M]\{\ddot{u}\} + [C]\{\dot{u}\} + [K]\{u\} = \{F\} \tag{10.3}$$

where [M] is the structural mass matrix; [C] is the structural damping matrix; $\{\ddot{u}\}$ is the nodal acceleration vector; [K] is the structural stiffness matrix; $\{\dot{u}\}$ is the nodal velocity vector; $\{u\}$ is the nodal displacement vector; and $\{F\}$ is the applied load vector.

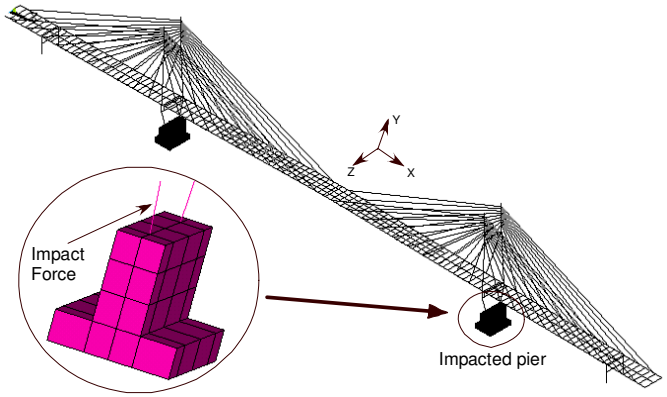

Figure 10.12 FE model of the Maysville Cable-Stayed Bridge

In the transient analysis, the Newton-Raphson method is employed along with the Newmark assumptions. Static load steps are performed prior to the transient time integration. A time step of 1/1000 seconds is the largest interval used in the temporal integration.

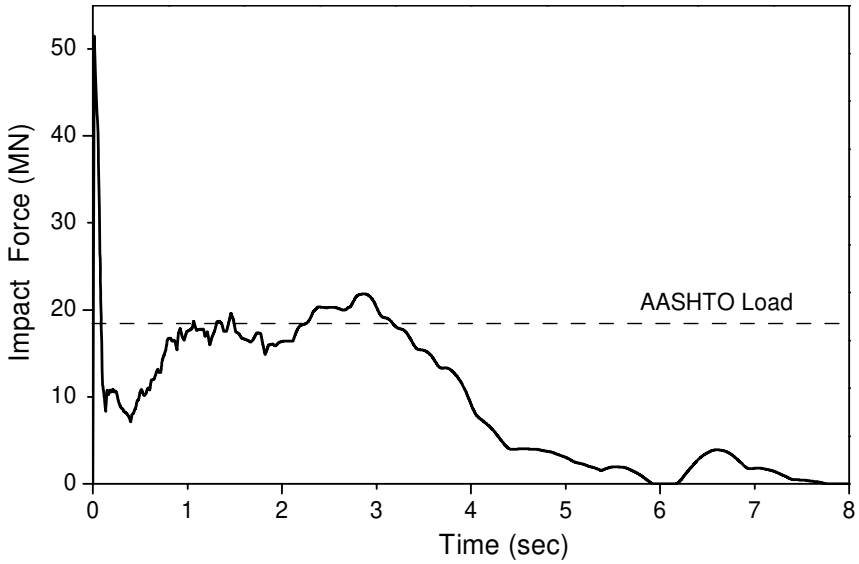

Figure 10.13 Impact force time-history generated by a fully loaded 15-barge flotilla at a velocity of 2.57 m/s

The displacements of the impacted-pier top are recorded, and their time histories are shown in Figure 10.14. It is observed that a unidirectional impact can excite the vibration of the entire bridge due to the coupled modes.

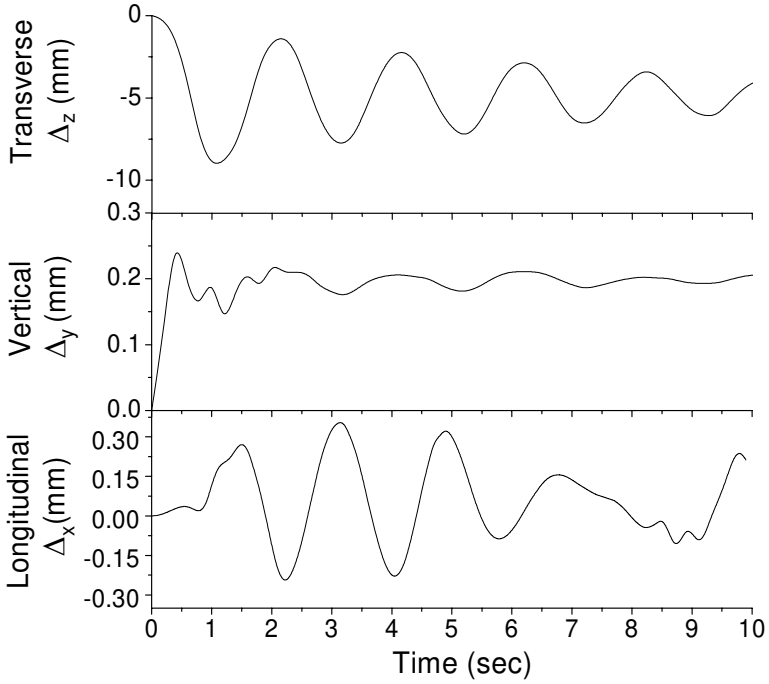

Figure 10.14 Time histories of the pier-top displacements resulting from the impact of a fully loaded 15-barge flotilla

Table 10.3 compares the displacements resulting from the dynamic analysis using the time history of the impact force with the static analysis using the AASHTO equivalent static load. The results clearly show that AASHTO underestimates the magnitude of the maximum displacements, especially in the directions normal to that of the impact force. The results show that there is a large difference in the displacements predicted by the dynamic analysis and the ASSHTO static analysis.

Regardless, the absolute values of the displacements calculated by this analysis are too small to cause any significant problems to the bridge. In fact, the bridge was designed to meet the criteria of impact from a fully loaded flotilla (3 barges wide by 5

barges long). Diamond-shape towers increase the superstructure's stiffness and add stability against dynamic loads.

Table 10.3. Comparison between the FE dynamic analysis and the AASHTO static analysis for the Maysville Cable-Stayed Bridge

Displacement	FE analysis (mm)	AASHTO (mm)	FE /AASHTO
Max(Δ_x)	0.36	0.08	4.5
Max(Δ_y)	0.24	0.11	2.2
Max(Δ_z)	9.14	5.71	1.8

10.4 Summary

The three examples presented in this chapter are intended to improve the analysis of bridges susceptible to barge flotilla impact. It has been shown that there is a considerable difference between the responses calculated using the current AASHTO equivalent static method and the time-history analysis given in this study

Although time-history analysis in earthquake design is not new by any means, time history analysis of bridges susceptible to barge impact is rare. Such analyses are made possible by utilizing the impact force time-histories developed in this study. Generally, an impact time-history analysis of a bridge would be required only for extremely important bridges. However, a time-history analysis of small bridges that have a high probability of barge impact may, in some cases, be warranted. It is not advisable for designers to rely solely on the equivalent static loads for barge protection design.

Chapter 11 Conclusions and Future Study

The objective of this study has been to determine the dynamic forces on bridge piers resulting from multi-barge flotilla impact. All the tasks listed in Chapter 1 have been successfully completed.

11.1 Contributions

Current specifications for highway bridge design provide empirical relationships for computing lateral impact loads generated during barge collisions. However, these relationships are based on limited experimental data. To better understand and characterize such loads, especially multi-barge flotilla loads, dynamic finite element analysis techniques have been employed in this study to simulate barge-pier collisions. Impact simulation results, including time histories of impact loads and barge deformations, are presented and compared to the data generated using current bridge design specifications. In addition to the extensive FE simulations, many analytical methods have been developed. Analysis and design procedures using the proposed methods are described in detail, and these procedures are suitable for adoption in practice.

The primary contributions of this dissertation are divided into two categories, scientific contributions and engineering contributions. The scientific contributions are the fundamental theoretical results and findings of this research while the engineering contributions are the applications or implementations of these results. Scientific contributions include:

1) revealing the fundamental characteristics of barge-pier collisions;
2) indicating the limitations of the AASHTO design specifications;

3) establishing the upper bound of barge-pier impact forces;
4) determining the influence of the pier geometry and stiffness on impact forces; and
5) developing the multi-barge flotilla impact model.

Engineering contributions include:

1) developing a hand-calculation method to predict the impact forces and impact duration for single barges;
2) developing a hand-calculation method to predict the dynamic response of piers;
3) deriving a set of regression formulas to predict barge impact loads;
4) developing a series of numerical barge-flotilla models, which can be used to study barge-bridge collisions for various purposes; and
5) generating more than 2,000 impact force time-histories for multi-barge flotilla impacting piers.

In summary, the tools developed, along with the results and insights obtained by the present study should be useful for more rational design of bridges against barge collisions and for more accurate evaluation of existing bridges menaced by barge impacts.

11.2 Conclusions

Through this study the following conclusions are made:

1) Barge-pier impact forces are mostly dependent on the barge crushing resistance, i.e., the impact forces are approximately limited to the plastic load-carrying capacity of the barge bow. This conclusion has been verified by the barge impact experiments [51]. Therefore, the static force-deformation relationship of the barge bow is the baseline of the impact forces generated by

barges unless the pier is very slender. Most of the impact energy is dissipated through the deformation of the bow structure. Meir-Dornberg's equations [11] reflect these facts to some extent.

2) The stiffness of ordinary piers has little effect on the mean impact force. However, the maximum impact forces (contact forces at the initial stage of impact) are very sensitive to the stiffness variation of weaker piers. Also, pier stiffness affects the impact time duration. For most cases, it is conservative to determine the impact forces by assuming that the pier is rigid.
3) The greatest challenge for bridge design that accounts for barge impact is the huge lateral impact forces exerted on the pier and foundation. Pier failures are likely to be of the shear type causing excessive damage. In addition, the pier top may displace excessively in the event of an impact due to its less stiffness. This may cause loss of a span because of insufficient seat width on bridge pier cap. For a multi-span bridge, the expansion joint is where this loss of span is probable. Thus, increasing pier stiffness improves collision performance of piers. The use of stiffer piers to resist barge impact is advantageous because stiffer piers inherently possess other benefits, such as the ability to resist dynamic earthquake and wind loads.
4) Two types of barge response to impact are distinguished by a threshold value of the kinetic impact energy. This conclusion is in agreement with AASHTO's current methodology. For the first type of response, a large part of the barge deformation is elastic, while a large part of the barge deformation is plastic for

the second type. In reality, most cases can be classified as the second type of response.

5) After onset of barge bow collapse, the impact force remains relatively constant. Therefore, increasing the number of barges in a flotilla does not proportionally increase the average impact force, but an increased number of barges in a flotilla may increase the impact duration. The notion that the impact forces increase proportionally to the number of barges in a flotilla may be common, but it is generally incorrect.
6) Pier geometry has a strong influence on the impact process, which is ignored by the current design code. Increasing the pier width results in an increase of impact forces. Under the same conditions, square piers usually produce a larger impact force than circular piers. Moreover, the size influence of square piers is more apparent than that of circular piers.
7) Application of the AASHTO method may either underestimate or overestimate the barge impact forces. In general, the AASHTO method overestimates the impact forces generated by multi-barge flotillas and underestimates the impact forces of single barges on wider square piers. More important, the equivalent static loads of ASSHTO may underestimate the dynamic response of bridges. It is not advisable for barge-pier impact force generation to rely solely on the equivalent static load for analysis and design, especially for important bridges that are essential components of the United States infrastructure.
8) The assumption that the steel wire ropes lashing barges in adjacent rows will break during a collision is conditional. It is not appropriate to generate the

multi-barge flotilla impact forces only by one barge column. Conservatively, the impact force of a multi-barge flotilla should be generated by its whole mass and kinetic energy.

9) The impact time duration, mostly dependent on the kinetic impact energy and pier geometry, ranges from 0.3 to 8 seconds. The maximum forces occur at the very beginning of impact and usually last 0.1 to 0.3 seconds. The intensity of the barge impact on piers depends on both the impact forces and impact duration. A collision with small kinetic impact energy may produce a larger impact force peak value than a collision with large impact energy. However, a collision with small kinetic energy corresponds to shorter time duration.

In summary, through this research a better understanding of impact mechanics has been achieved. Although physical barge-pier impact tests are not carried out to verify the accuracy of the simulations, a variety of exercises have been conducted to provide confidence in the analysis results. These exercises included mesh refinement studies, energy balance audits, impulse/momentum conservation checks, monitoring of hourglass control energy during the simulations, and comparison of pertinent results to data from actual ship-ship collision tests.

11.3 Future Work

Future research needs may be classified into two broad categories: loading time history and the bridge dynamic response. The following suggestions for future research are presented in order of importance:

1) More parametric studies and validations are required. Although computer simulation has proven to be a useful research tool, it cannot replace the impact

testing. At present, little actual collision data of sufficient detail is available for method validation.

2) In order to ensure that all bridge elements exposed to barge collision are designed to certain strength and robustness, local point or area loadings, and localized yielding or cracking of structures should be investigated.
3) Studies of arbitrary angle impacts are necessary. Since a small change in collision angle may cause a dramatic difference in barge penetration and impact forces, a comprehensive 3-D analytical model is needed to accurately predict the impact forces for some circumstances.
4) Hydrodynamic forces generated by the surrounding water deserve further investigation.
5) Dynamic vessel-pier-soil interaction during a barge collision event is also an important topic, since seventy percent or more of vessel impact loading is transferred directly to the foundation (not superstructure) [52]. Specifically, the load transfer to the piles and the surrounding soil mass is deserves further study.

Bibliography

[1] Brezosky L. Four killed in collapse of Padre Island Bridge. Amarillo Globe-News, Sep. 16, 2001.

[2] Peters ME. Safety recommendation. Federal Highway Administration, Washington, D.C., Sep. 9, 2004.

[3] Anderson M. At least 7 killed in Oklahoma bridge collapse. http://www.disasterrelief.org/, Oct. 8, 2004.

[4] http://www.caria.org/waterway_facts.html. Oct. 18, 2004.

[5] Carter R. A mission for the future: the McAlpine Locks Project. The Lane Report, Kentucky Transportation Cabinet, December 1999.

[6] Viegas J. Heavyweight challenge: barge vs. bridge. Discovery News, Mar. 4, 2004.

[7] Knott MA, Pruca Z. Vessel collision design of bridges. CRC Press, 2002.

[8] Larsen OD. Ship collision with bridges. Structural Engineering Documents No. 4, International Association for Bridge and Structural Engineering, IABSE Switzerland, 1993.

[9] American Association of State Highway and Transportation Officials (AASHTO). Guide specification and commentary for vessel collision design of highway bridges. Volume I, final report. Washington, DC, 1991.

[10] Whitney MW, Harik IE. Analysis and design of bridges susceptible to barge impact. Research Rep. KTC-97-2, Kentucky Transportation Center, College of Engineering, Univ. of Kentucky, Lexington, KY40506, 1997.

[11] Meir-Dornberg KE. Ship collision safety zones, and loading assumptions for structures on inland waterways. VDI-Berichte No. 496, pp 1-9, 1983.

[12] Pedersen PT, et al. Ship Impacts: bow collisions. International Journal of Impact Engineering, Vol. 13, No. 2, pp. 163-187, 1993.

[13] Consolazio GR, et al. Barge impacting test of the St. George Island Causeway Bridge phase I: feasibility study. Report No: BC354 RPWO#23, 2002.

[14] Livermore Software Technology Corporation (LSTC). LS-DYNA user's manual. Version 970, 2003.

[15] MSC.Software Corporation. MSC.Dytran Release Guide. Version 2002 r2, 2002.

[16] Hallquist JO. LS-DYNA theoretical manual. LSTC, May, 1998.

[17] Consolazio GR, Cowan DR. Nonlinear analysis of barge crush behavior and its relationship to impact resisting bridge design". Computer and Structures 81(2003)547-557.

[18] Consolazio GR, et al. Dynamic finite element analysis of vessel-pier-soil interaction during barge impact events. Journal of the Transportation Research Board, Washington, D.C., 2003.

[19] Patev RC, Barker BC, and Koestler III LV. Prototype barge impact experiments, Allegheny Lock and Dam 2, Pittsburgh, Pennsylvania. US Army Corps of Engineers, 2003.

[20] Minorsky VU. An analysis of ship collisions with reference to protection of nuclear power plants". Journal of Ship Research, Vol. 3, No. 1, pp. 1-4, 1959.

[21] Reardon P, Sprung JL. Validation of Minorsky's ship collision model and use of the model to estimate the probability of damaging a radioactive material transportation cask during a ship collision. Proceedings of the International 98 Conference on Design and Methodologies for Collision and Grounding Protection of Ships, San Francisco, August 1996.

[22] Chen D. Simplified ship collision model. Ms. Thesis, Virginia Polytechnic Institute and State University, 2002.

[23] Giannotti, JG, Johns N, Genalis P and Van Mater PR. Critical evaluations of low-energy ship collision Vol. I - damage theories and design methodologies". Ship Structure Committee Report No. SSC-284, 1979.

[24] Woisin G. Design against collision. International Symposium on Advances in Marine Technology, Trondheim, Norway, June 1979.

[25] Hutchison BL. Barge collisions, rammings and groundings - an engineering assessment of the potential for damage to radioactive material transport casks. Report No. SAND85-7165 TTC-05212, 1986.

[26] Crake K. Probabilistic evaluations of tanker ship damage in grounding events. Naval Engineer Thesis, MIT, 1995.

[27] Woisin G. The collision test of the GKSS. Jahrbuch der Schiffbautechnischen

Gesellschaft, Volume 70, pp. 465-487, Berlin, 1976.

[28] Woisin G, Gerlach W. On the estimation of forces developed in collisions between ships and offshore lighthouses. International Conference on the Lighthouses and Other Aids to Navigation, Stockholm, 1970.

[29] Woisin G. Design against collision. International Symposium on Advances in Marine Technology, Trondheim, Norway, June 1979.

[30] Pedersen PT, et al. Ship impacts—bow collisions. 3rd International Symposium on Structural Crashworthiness and Failure, Liverpool, April 1993.

[31] Knott MA, Bonyun D. Ship collision against the sunshine skyway bridge. IABSE Colloquium on Ship Collision with Bridges and Offshore Structures, Copenhagen, 1983.

[32] Norwegian Public Roads Administration. Load regulations for bridges and ferry ramps in the public road system (in Norwegian). Preliminary Edition, Olso, 1986.

[33] Frandsen AG, Olsen D, Fujii Y, and Spangenberg S. Ship collision studies for the Great Belt East Bridge, Denmak", IABSE Symposium on Bridges – Interaction between Construction Technology and Design, Leningrad,1991.

[34] ANSYS, Inc. ANSYS8.1 user's manual, 2004.

[35] Nurick G, Brebbia A. Advances in dynamics and impact mechanics. ISBN: 1853129283, WIT Press (UK), October, 2002.

[36] Frandsen AG, LangsØ H. Ship collision problems. International Association for Bridge and Structural Engineering, Proceedings, P-31(2):81-101, 1991.

[37] Livermore Software Technology Corporation (LSTC). LS-PRE/POST user's manual. Version 1.0, 2002.

[38] Sanlo Manufacturing Co., Inc. Product catalogue. Michigan City, IN46360, USA, 2004.

[39] The Mathworks, Inc. MATLAB User's manual, version 6.5, 2003.

[40] Griffiths, JB. The theory of classical dynamics. Cambridge University Press, 1985.

[41] Tedesco JW, et al. Structural Dynamics. Addison-Wesley Longman, Inc., 1999.

[42] Modjeski & Masters, Consulting Engineers. Criteria for: the design of bridge piers with respect to vessel collision in Louisiana waterways. New Orleans, July, 1985.

[43] Consolazio GR, et al. Barge impacting test of the St. George Island Causeway Bridge phase II: design of instrumentation systems. Report No: BC354 RPWO#56, 2003.

[44] Frieze PA. Dartford Crossing: An assessment of the likely forces involved and extent of overrun arising from ship collision with a main pier. Report to T H Engineering Services Ltd, Croydon, 1988.

[45] Amdahl J. Energy absorption in ship-platform Impacts. Report No. UR-83-84, the Norwegian Institute of Technology, Trondheim, 1983.

[46] Nagasawa H, Arita K, Tani M, and Oka S. A study on the collapse of ship structure in collision with bridge piers. Naval Architecture and Ocean Engineering, Society of Naval Architects, Japan, Vol. 19, 1981.

[47] Olnhausen WV. Ship collision with bridge piers (in Swedish), Teknisk Tidskrift, No. 17, Stockholm, 1966.

[48] Jagannathan S, Gray D. An analytical model for barge collisions with rigid structures. 1995 OMAE.

[49] Ghosn M, et al. Design of highway bridges for extreme events. NCHRP Report 489, 2003.

The End

This page intentionally left blank